TECHNISCHE UNIVERSITÄT WIEN

DIPLOMARBEIT

Predictive driver model for speed control in the presence of road obstacles

Vorausschauendes Fahrermodell zur Geschwindigkeitsregelung vor Fahrbahnhindernissen unter Berücksichtigung der Längs- und Vertikaldynamik

ausgeführt zum Zwecke der Erlangung des akademischen Grades eines
Diplom-Ingenieurs
eingereicht an der Technischen Universität Wien
Fakultät für Maschinenwesen und Betriebswissenschaften

von

Philipp Mandl
Matrikelnummer 01529135

unter der Leitung von

Senior Lecturer Dipl.-Ing. Dr.techn. Florian Klinger

Assistant Prof. Dipl.-Ing. Dr.techn. Christoph Hametner

Institut für Mechanik und Mechatronik

Wien, im Oktober 2021

Die approbierte gedruckte Originalversion dieser Diplomarbeit ist an der TU Wien Bibliothek verfügbar
The approved original version of this thesis is available in print at TU Wien Bibliothek.
TU Bibliothek Your knowledge hub WIEN

Eidesstattliche Erklärung

Ich habe zur Kenntnis genommen, dass ich zur Drucklegung meiner Arbeit unter der Bezeichnung Diplomarbeit nur mit Bewilligung der Prüfungskommission berechtigt bin. Ich erkläre weiters an Eides statt, dass ich meine Diplomarbeit nach den anerkannten Grundsätzen für wissenschaftliche Abhandlungen selbstständig ausgeführt habe und alle verwendeten Hilfsmittel, insbesondere die zugrunde gelegte Literatur, genannt habe. Weiters erkläre ich, dass ich dieses Diplomarbeitsthema bisher weder im In- noch Ausland (einer Beurteilerin/einem Beurteiler zur Begutachtung) in irgendeiner Form als Prüfungsarbeit vorgelegt habe und dass diese Arbeit mit der vom Begutachter beurteilten Arbeit übereinstimmt.

Wien, im Oktober 2021

Philipp Mandl

Die approbierte gedruckte Originalversion dieser Diplomarbeit ist an der TU Wien Bibliothek verfügbar
The approved original version of this thesis is available in print at TU Wien Bibliothek.
TU Bibliothek Your knowledge hub WIEN

Kurzfassung

Seit einigen Jahren vollzieht sich in der Fahrzeugindustrie ein Umbruch hin zur Automatisierung von Fahraufgaben sowohl in Quer- als auch in Längsrichtung. Der Trend zum teil- oder vollautonomen Fahren wird immer deutlicher. Damit einher geht das Potenzial, die Verkehrssicherheit und den Komfort der Insassen deutlich zu erhöhen. Die Automatisierung verschiedener Fahraufgaben ist eng mit der Fahrermodellierung verknüpft, da menschliches Fahrverhalten sowohl aus Komfort- als auch aus Sicherheitsgründen erwünscht ist.

Diese Arbeit soll dazu beitragen, indem der Frage nachgegangen wird, wie ein Fahrer bzw. eine Fahrerin die Fahrzeuggeschwindigkeit beim Überfahren eines Fahrbahnhindernisses wählt und wie dies mit einem Fahrermodell dargestellt werden kann, insbesondere im Hinblick auf das Verzögern des Fahrzeugs in Annäherung an das Hindernis, das Überfahren des Hindernisses und das Beschleunigen des Fahrzeuges beim Verlassen desselben. Auf dem Gebiet des Hindernisüberfahrens wurde in Bezug auf die Fahrwerksabstimmung (passive, semi- und aktive Radaufhängung) bereits viel geforscht, allerdings oft unter der Annahme einer konstanten Fahrzeuggeschwindigkeit. In dieser Arbeit hingegen soll nun untersucht werden, wie Straßenhindernisse nur durch eine Geschwindigkeitsplanung „optimal“ überwunden werden können. Zu diesem Zweck wurde ein Fahrermodell auf der Grundlage einer modellprädiktiven Regelung (MPC) entwickelt. Das Fahrermodell kann eine Geschwindigkeits- bzw. Beschleunigungstrajektorie unter Berücksichtigung von Straßeninformationen, wie z.B. Hindernissen und gesetzlich vorgegebenen Maximalgeschwindigkeiten, generieren. Basierend auf einem Gütefunktional, welches einen Kompromiss aus einem komfortablen und jedoch zügigen Überfahren des Hindernisses ermöglichen soll, und einem internen Fahrzeugmodell plant der Regler für einen Vorschauhorizont die optimalen Trajektorien. Der MPC wird weiterhin dazu genutzt, um unterschiedliche Fahrertypen und -stile abzubilden und menschliche Reaktionszeiten in den Planungshorizont einfließen zu lassen. Es wird gezeigt, dass das Fahrermodell gängige Straßenhindernisse im Stadtverkehr robust überfahren kann. Zur Darstellung des Einflusses des internen Fahrzeugmodells in der Trajektoriengenerierung des Fahrermodells werden ein Viertel- und ein Halbfahrzeugmodell gegenübergestellt.

Die approbierte gedruckte Originalversion dieser Diplomarbeit ist an der TU Wien Bibliothek verfügbar
The approved original version of this thesis is available in print at TU Wien Bibliothek.
TU Bibliothek Your knowledge hub WIEN

Abstract

For some years now, the automotive industry has been undergoing a change toward the automation of driving tasks in both lateral and longitudinal directions. The trend toward partially or fully autonomous driving is obvious. This is accompanied by the potential to significantly increase road safety and passenger comfort. The automation of various driving tasks is closely related to driver modeling, as human driving behavior is desirable for both comfort and safety reasons.

This work aims to contribute by addressing the question of how a driver chooses the speed of the vehicle when driving over a road obstacle, and how this can be represented with a driver model, particularly with respect to the deceleration of the vehicle when approaching the obstacle, passing the obstacle, and the acceleration of the vehicle when departing the obstacle. Much research effort has been done in the field of obstacle crossing with respect to suspension tuning (passive, semi-active and active suspension), but most often under the assumption of constant vehicle speed. In this work, however, the aim is now to investigate how road obstacles can be overcome in a "optimal" fashion by speed planning only. For this purpose, a model predictive control (MPC) based on a quarter-car and a half-car model has been developed. The driver model can generate a speed and acceleration trajectory considering road information such as obstacles and legal speed limits. Based on a cost function, which should enable a compromise of comfortable but quick crossing of the obstacle, and an internal vehicle model, the controller plans the optimal trajectories for a preview horizon. The MPC is further utilized to represent different driving types and styles and to incorporate human reaction times into the planning horizon. It is shown that the driver model can robustly negotiate typical obstacles in urban roads. To illustrate the influence of the internal vehicle model in the trajectory generation of the driver model, a quarter- and half-car model are compared.

Die approbierte gedruckte Originalversion dieser Diplomarbeit ist an der TU Wien Bibliothek verfügbar
The approved original version of this thesis is available in print at TU Wien Bibliothek.
TU Bibliothek Your knowledge hub WIEN

Acknowledgement

I would like to express my deep appreciation to Florian Klinger, the main supervisor of this thesis, who accompanied me throughout the project, enabled me to carry out this project, and supported me with his suggestions and availability. I wish to acknowledge Prof. Christoph Hametner for his support, professionalism and friendship over the past years during my work at the Institute of Mechanics and Mechatronics and for his support during the preparation of this thesis. I would as well like to thank Prof. Johannes Edelmann for his very interesting suggestions and proposals during the numerous discussions that occurred during the preparation of the thesis.

I would especially like to thank my greatest supporters, my parents Ernestine and Rupert, and my brother Alexander, who made so many sacrifices and made it possible for me to achieve my ambitions. Throughout the long period of my studies, they always supported me, put up with me, and stood by me emotionally, helping me to become the person I am today.

I would also like to thank my good friend Maximilian. We not only studied side by side, but also experienced a lot together, which has shaped me – in a positive sense.

Die approbierte gedruckte Originalversion dieser Diplomarbeit ist an der TU Wien Bibliothek verfügbar
The approved original version of this thesis is available in print at TU Wien Bibliothek.
TU Bibliothek Your knowledge hub WIEN

Contents

Die approbierte gedruckte Originalversion dieser Diplomarbeit ist an der TU Wien Bibliothek verfügbar
The approved original version of this thesis is available in print at TU Wien Bibliothek.
TU Bibliothek Your knowledge hub WIEN

Die approbierte gedruckte Originalversion dieser Diplomarbeit ist an der TU Wien Bibliothek verfügbar
The approved original version of this thesis is available in print at TU Wien Bibliothek.
TU Bibliothek Your knowledge hub WIEN

1 Introduction

The main objective of this work is to model human driving behavior with respect to vehicle speed when approaching, passing, and departing various road obstacles. The scenario considered in this thesis consists of a road vehicle crossing an obstacle, e.g. a speed bump or a pedestrian crosswalk. When considering the scenario at hand, the question naturally arises as to why or to what extent a human driver would reduce the forward speed of the vehicle when passing the obstacle. There are a number of reasons: The most important reason is perhaps that the driver aims to maintain the level of driving comfort when passing the obstacle, thus reducing the vertical movement of the vehicle. In extreme cases, the driver might also be concerned that too high vehicle speeds could cause damage to the vehicle. In addition, the style in which the driver brakes and accelerates the vehicle contributes to the perceived driving comfort. On the other hand, the driver does not want to lose too much speed or time when driving over the obstacle. So the answer to the question of how and why a driver slows down when approaching an obstacle is quite complicated, and mapping this behavior is even more challenging.

The following sections are intended to provide a motivating example of why such research is important in today's world. In addition, the goal of this thesis is outlined, respective research questions are defined, and the approach of the thesis is stated.

1.1 Motivation

The recent trend towards automation of various driving functions is aimed at increasing the safety of road vehicles as well as the comfort of drivers and passengers. This development is strongly driven by road safety reports that highlight the problem of traffic fatalities, e.g. in a World Health Organization (WHO) report in [1], for the U.S. in [2], or in a European Commission (EC) report in [3]. However, this trend is also being propelled by established companies such as Daimler, Audi, etc., or newer players like Tesla, Mobileye and Waymo, which are trying to bring fully autonomous driving to market and be the first to realize a fully self-driving vehicle. In an effort in recent decades to improve safety, several key technologies have emerged in form of advanced driver assistance

Die approbierte gedruckte Originalversion dieser Diplomarbeit ist an der TU Wien Bibliothek verfügbar
The approved original version of this thesis is available in print at TU Wien Bibliothek.
TU Bibliothek Your knowledge hub WIEN

[TABLE 1] ADASs GROUPED BY LONGITUDINAL CONTROL, LATERAL CONTROL, AND ANGULAR RATE CONTROL, RESPECTIVELY.

	ACTUATOR				PRIMARY SENSORS				
SYSTEM	BRAKE	ACC.	STEERING	DRIVER	SPEED	IMU	DME	WHEEL SPEED	VISION
ANTILOCKING BRAKE SYSTEMS (ABS)	X	—	—	—	X	—	—	X	—
BRAKE ASSISTANCE SYSTEMS (BAS)	X	—	—	—	—	—	—	X	—
CRUISE CONTROL	—	X	—	—	X	—	—	—	—
ADAPTIVE CRUISE CONTROL (ACC)	—	X	—	—	X	—	X	—	—
STOP AND GO	X	X	—	—	X	—	X	—	—
ANTISPIN CONTROL ($V < 20$ KM/H)	X	–	—	—	X	—	—	—	—
TRACTION CONTROL ($V > 20$ KM/H)	—	X	—	—	X	—	—	—	—
FORWARD COLLISION WARNING (FCW)	—	—	—	X	X	—	X	—	—
FORWARD COLLISION MITIGATION (FCM)	—	—	—	—	X	—	X	—	—
PARKING AID SYSTEMS	—	—	X	X	—	—	X	—	X
FORWARD COLLISION AVOIDANCE (FCA)	X	—	X	—	X	—	X	—	—
LANE-KEEPING AID SYSTEMS (LKA)	—	—	(X)	X	X	—	X	—	X
LANE-CHANGE AID SYSTEMS	—	—	—	X	—	—	X	—	X
ADAPTIVE STEERING	—	—	X	—	X	—	—	—	—
YAW CONTROL (ESP)	X	X	(X)	—	X	X	—	—	—
ROLL STABILITY CONTROL	X	—	—	—	X	X	—	—	—
ROLLOVER DETECTION (AIRBAG)	—	—	—	—	X	X	—	—	—

Table 1.1: ADAS grouped by longitudinal control, lateral control, and angular rate control, respectively. Table taken from [4]. A wide range of sensory information is required to control vehicle dynamics.

systems (ADAS), as shown in Tab. 1.1.

The goal of ADAS is to compensate to some extent for human error in avoiding traffic accidents by taking over some primary vehicle control functions, e.g., steering or braking, to reduce the consequences of an accident, but as well to reduce the work load of the driver and to improve the ride quality and comfort of the passengers [5]. Main objectives are to reduce the number and severity of accidents, improve handling and comfort by controlling the longitudinal, lateral, and vertical motions of a vehicle. Although most of the systems introduced in recent decades are designed to improve safety, they have also significantly improved driving comfort. There are only a few systems whose purpose is solely to increase comfort, such as Parking Aid Systems (PAS), Cruise Control (CC) or Adaptive Cruise Control (ACC). In [4], a comprehensive overview of the recent state of the art in automotive safety systems is given.

Many of the systems listed in Tab. 1.1 are already standard today or may become mandatory by legislative means in the coming years. There are, for example, new legislative measures and political ambitions, such as the European Commission's ambitious plan to have zero traffic fatalities by 2050 [6], [7]. This plan is called "Vision Zero". To achieve such an ambitious goal, legislators are mandating a host of new vehicle safety systems starting in 2022: This standard mandates new features such as Automated Emergency Braking (AEB) and overridable Intelligent Speed Assistance (ISA) as standard for newly sold vehicles [8]. These systems are aiming to control the longitudinal motion of the vehicle or vehicle speed in order to improve road safety. Similarly, in this

Die approbierte gedruckte Originalversion dieser Diplomarbeit ist an der TU Wien Bibliothek verfügbar
The approved original version of this thesis is available in print at TU Wien Bibliothek.
TU Bibliothek Your knowledge hub WIEN

thesis, a method for longitudinal control is developed that can improve driving comfort by planning speed trajectories for the vehicle to pass road obstacles.

Expanding on the rapid development of automotive safety systems and the drive to achieve fully autonomous driving, the International Society of Automotive Engineers (SAE) has developed the SAE J3016 standard [9]. This standard provides detailed definitions for six levels of driving automation, see Fig. 1.1. The stages define how the task of operating a vehicle is divided between a human and a driving automation system. When the human performs the entire Dynamic Driving Task (DDT), the SAE standard classifies this as Level 0 (No Driving Automation). At Level 5 (Full Driving Automation), the DDT is executed entirely by the automated driving system.

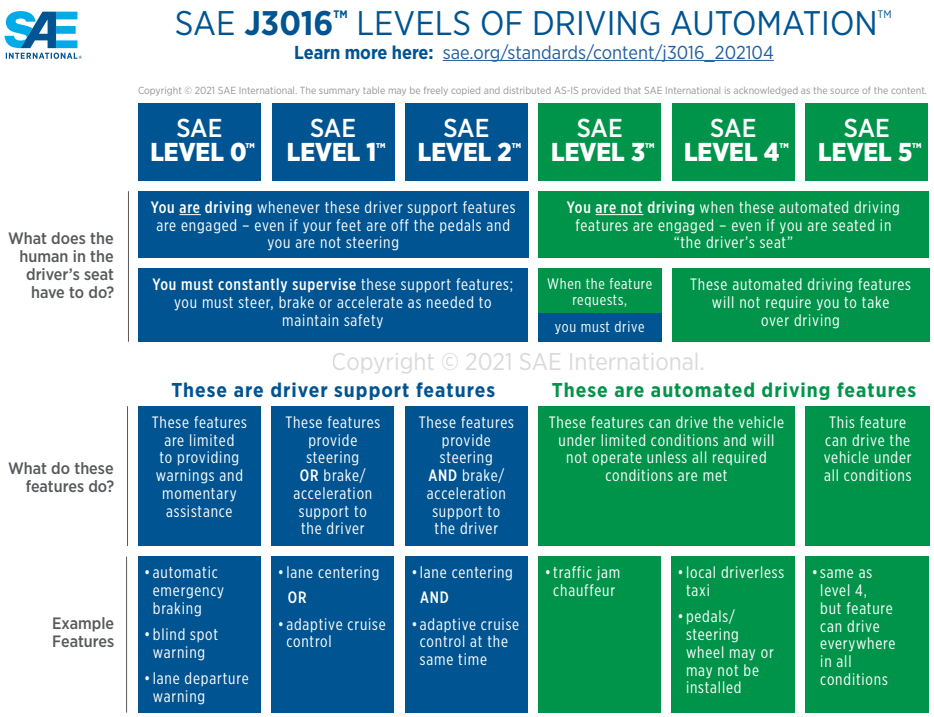

Figure 1.1: Levels of driving automation as defined by the SAE J3016 standard. Figure taken from [9].

Referring to the issues of increasing traffic safety and passenger comfort, promoting the use of self-driving cars could be a possible solution to reduce traffic accidents and the socioeconomic burden of traffic fatalities [7], but also to increase passenger comfort by relieving them of the task of driving in traffic. In [10], the potential cost savings from

Die approbierte gedruckte Originalversion dieser Diplomarbeit ist an der TU Wien Bibliothek verfügbar
The approved original version of this thesis is available in print at TU Wien Bibliothek.
TU Bibliothek Your knowledge hub WIEN

the introduction of automated driving systems (SAE Level 5) were calculated. Under an optimistic scenario, accidents are estimated to decrease by 90%, resulting in savings of 1.6 trillion dollars in the period as in the conservative case.

Before there can be widespread use and acceptance of autonomous driving vehicles, driverless vehicles must demonstrate that they are capable of reliably performing the DDT in order to gain social acceptance. This means not only that the vehicle can drive from point A to point B, but also that it does so in a way that makes passengers feel safe and comfortable with giving up control of a vehicle. Passengers will only accept and rely on ADAS or autonomous vehicles if they feel comfortable and therefore will not urge them to take control of the vehicle. One approach to strengthen trust in the systems could be to control the vehicle as if it were being driven by a human driver. Another option would be to make the intentions and actions of the automated driving system more transparent, for example by providing information via displays and audio about what the car is doing and plans to do in the future [11].

How can this thesis contribute to solve this problem in the presence of road obstacles such as speed bumps and pedestrian crossings? Providing information alone may not be enough to give people a complete sense of security and trust. It may be that the human passenger perceives the actions of the vehicle as unnatural or not human-like and therefore disapproves of how the vehicle is being driven as unsafe. At a road obstacle, rapid deceleration/acceleration could cause the passenger to feel uncomfortable and loose trust in the underlying system. To cope with this problem, a human driver model is incorporated into the system which assesses actions as humanly as possible.

If the focus is now shifted from real-world driving applications to a more economic consideration, a human driver model that resembles human driving behavior in the presence of obstacles may also be relevant in vehicle development, traffic flow studies, and research where the combined overall human-vehicle system is studied [12]. In vehicle development, capturing the behavior of a human driver in form of a driver model can help reduce development costs by shifting costly experimental road tests to a simulator.

Model Predictive Control (MPC) can be used here to incorporate human driving behavior and create a driver model that plans speed trajectories in the presence of obstacles on the road with the goal of driving as comfortably and human-like as possible. With the MPC it is even possible to map different driver characteristics, e.g., reaction times, or to map completely different drivers, e.g., an aggressive or a conservative driving style.

Die approbierte gedruckte Originalversion dieser Diplomarbeit ist an der TU Wien Bibliothek verfügbar
The approved original version of this thesis is available in print at TU Wien Bibliothek.
TU Bibliothek Your knowledge hub WIEN

1.2 Aim of the Thesis

To summarize the motivation, a suitable representation of the human driver specifically for speed control in the presence of road bumps can be helpful to improve passenger comfort and thus help in autonomous applications as well as in automotive development. In this thesis, a novel predictive driver model for speed control in the presence of road obstacles should be developed:

- A comprehensive cost function is developed that enables human-like acceleration and/or speed trajectories in the presence of road obstacles.
- A simple vehicle model is introduced that captures relevant effects of the longitudinal and vertical motions of a vehicle.
- Based on a cost function and vehicle model, a model predictive controller (MPC) is introduced which performs a trajectory optimization problem and solves for the optimal speed and/or acceleration trajectory.
- Analysis of speed profiles from a human point of view for approaching, passing and departing different road obstacles (speed bumps, crosswalks, ...).

Summary: Aim of the Thesis

The aim of this work is to represent human vehicle speed control using a model predictive controller (MPC) in the presence of road obstacles. The objective is to design a cost function and optimization problem with emphasis on human driving style and generate robust speed and/or acceleration trajectories. The vertical and longitudinal motions of the vehicle are to be captured by a simple model and are taken into account by a comfort criterion.

Research Questions Proceeding from the aim of this thesis to design a predictive driver model for longitudinal vehicle control based on a model predictive control approach, the following research questions are formulated.

Die approbierte gedruckte Originalversion dieser Diplomarbeit ist an der TU Wien Bibliothek verfügbar
The approved original version of this thesis is available in print at TU Wien Bibliothek.
TU Bibliothek Your knowledge hub WIEN

Research Questions

1. How can human longitudinal vehicle control be modeled with a model predictive controller?
2. How to determine suitable driving speed profiles from a human point of view for approaching, passing and departing different road obstacles (speed bumps, crosswalks, ...)?
3. How can human properties such as dexterity, skill, driving style and reaction time be incorporated into the driver model?

1.3 Structure of the Thesis

The remaining parts of the thesis are structured as follows.

In Chapter 2, background information is given on related work, vehicle models, driver modeling, and control theory, especially model predictive control (MPC).

In Chapter 3, the underlying system dynamics representation of the human driver model is formulated. Therein, models for the internal representation of the vehicle in the driver model are formulated and investigated. A simulation environment is developed for the vehicle–road system in which the driver model can be tested. The simulation model is based on common vehicle models used in vehicle dynamics literature under respective assumptions. Two models are used in this work: The quarter-car model, which captures the vertical motion of one corner of the vehicle, and the half-car model, which additionally captures the pitching motion of the vehicle. Therefore, the latter model should reflect the real driving scenario more accurately.

In Chapter 4, a nonlinear model predictive control method for trajectory planning is proposed, which forms the basis for the novel predictive driver model. This section provides the context for answering the research question stated in Section 1.2. Therein, the driver model is initially based on the assumption that the driver has only a limited understanding of the movements that occur when passing an obstacle. For this purpose, a predictive driver model is designed on the basis of a simple quarter-car model. The cost function of the MPC – which defines the optimization objective – is regressed on various comfort measures, and a suitable choice thereof is made with respect to human driving

Die approbierte gedruckte Originalversion dieser Diplomarbeit ist an der TU Wien Bibliothek verfügbar
The approved original version of this thesis is available in print at TU Wien Bibliothek.
TU Bibliothek Your knowledge hub WIEN

behavior. Afterwards, it is assumed that an experienced driver also has knowledge about the pitching motion of the vehicle. For this purpose, the MPC is further developed to take into account pitching motion via the half-car model.

In Chapter 5, the proposed predictive driver model is demonstrated with some examples such as potholes, bumps of different length and height and pedestrian crossings, which in turn are used to validate the methods and control schemes proposed in Chapter 4. The driver model, either with the quarter-car or with the half-car as internal model, are subjected to be tested on different road obstacles and their performance is evaluated in the simulation environment.

The final Chapter 6 concludes with answering the research questions and proposing possible directions for future work.

Die approbierte gedruckte Originalversion dieser Diplomarbeit ist an der TU Wien Bibliothek verfügbar
The approved original version of this thesis is available in print at TU Wien Bibliothek.
TU Bibliothek Your knowledge hub WIEN

2 Literature Review and Background

This chapter is intended to provide a brief overview of previous research related to this thesis. First, literature with focus on increasing ride comfort in the context of vehicle speed in the presence of road bumps is discussed. Subsequently, the focus of this chapter is shifted to research work on active and semiactive suspension in the context of comfort optimization for uneven road surfaces. Therein, different vehicle models are discussed, which are also applicable to the posed problem in the thesis. Several commonly used road profiles in research are also covered. The next section shifts the focus to human driver modeling, and the remainder of the section specifically explains why model predictive control (MPC) is particularly of use to create a driver model. In the last section, a brief and general introduction to MPC itself is given.

2.1 Longitudinal Control with Respect to Comfort

Few publications were found that directly address the adjustment of vehicle speed near a speed bump to improve experienced passenger comfort.

A publication that seeks to improve vehicle comfort by adjusting vehicle speed near elevation was published by Wu [13]. Therein, perceived passenger comfort is optimized in two ways: First, global road data, including upcoming obstacle information, is used to optimize the speed profile through dynamic programming. Second, a MPC is used for a nonlinear semiactive suspension system. Therefore, not only the comfort is improved by actively modifying the suspension, but as well by adjusting the vehicle speed. For the suspension control, a hybrid MPC with varying preview horizon as a function of vehicle speed is used and shows large improvements in ride comfort compared to a Skyhook system and several other MPCs, e.g. a MPC with fixed preview time. One drawback of the proposed method is that the global road information has to be available for the speed planing, which in many cases cannot be guaranteed. Additionally, the underlying dynamic programming problem only allows the vehicle speed to increment in predefined increments and therefore restricts the solution to a set of trajectories.

In [14], a model predictive control of engine torque and braking in the presence of road

Die approbierte gedruckte Originalversion dieser Diplomarbeit ist an der TU Wien Bibliothek verfügbar
The approved original version of this thesis is available in print at TU Wien Bibliothek.
TU Bibliothek Your knowledge hub WIEN

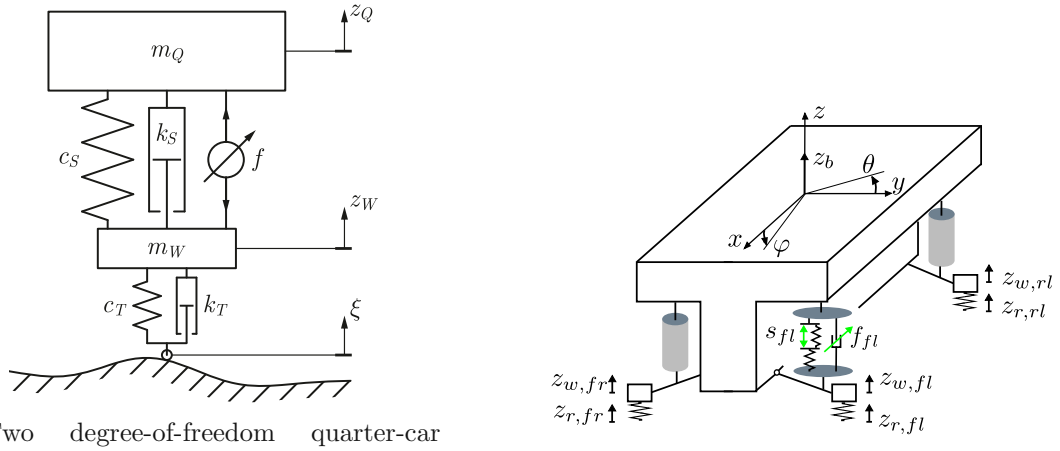

(a) Two degree-of-freedom quarter-car model taken from [15].

(b) Full-vehicle model taken from [16].

Figure 2.1: Depending on the problem, different complex models are required to capture the desired motions. A simple quarter-car model (a) can be sufficient to capture ride comfort. More complex model (b) can be necessary when lateral, longitudinal and vertical motions are investigated.

bumps is presented. In this paper, the authors investigated to improve the behavior of the vehicle when passing two obstacles at very low speeds: A stepped obstacle resembling a curb on a sidewalk and a cable bridge were chosen. The focus of this work is more on achieving a constant vehicle acceleration in the longitudinal direction to smoothly negotiate the obstacle at low speeds, for example, than on planning the vehicle speed directly. The idea in the paper is that the vehicle comes to a stop before the obstacle and the obstacle should be climbed comfortably with a constant longitudinal acceleration. The MPC in this work does not consider the comfort in the vertical vehicle direction, but rather tries to reduce the inconvenience of passing over the obstacle by following a given vehicle acceleration in the longitudinal direction – thus improving the ride comfort in the longitudinal direction.

2.2 Suspension Control with Respect to Comfort

Control of active or semi-active suspension systems in the presence of road obstacles has attracted considerable interest from researchers. Since many of the applied vehicle models, control methods, and so forth also apply to the application considered here in the thesis, these will now be discussed.

Die approbierte gedruckte Originalversion dieser Diplomarbeit ist an der TU Wien Bibliothek verfügbar
The approved original version of this thesis is available in print at TU Wien Bibliothek.
TU Bibliothek Your knowledge hub WIEN

Vehicle Model The choice of the vehicle model is dependent on the application and the dynamics to be captured. In cases where ride comfort in the presence of uneven roads or road obstacles are investigated, it is a common approach to model only the vertical motion of a vehicle with a quarter-car model [17]–[21]. The quarter-car model – though quite simple – reasonably reproduces the vertical motion of a vehicle. If more than one axle or additional vehicle motions are to be captured, such as pitching or lateral motions, more detailed models, such as the half-car or full-vehicle models are required [17], [22]–[24]. The choice of the model depends on the particular problem and thus also on the dynamics of interest.

Fig. 2.1 shows two vehicle models representing these examples: The quarter-car model at the left-hand captures only the vertical motion, while the full-vehicle model at right-hand allows to capture the lateral and longitudinal motions as well.

A good example of the use of different complex models is given in [25]. Here, a vehicle with a Fully Active Suspension (FAS) is investigated in the presence of cosine-shaped road bumps and potholes of different heights and lengths. The vehicle dynamics are modeled with both a quarter-car model and a 10-degree-of-freedom model, and the potential for cooperative control of the front and rear FAS actuators are investigated.

Control Methods Optimal control theory has been widely applied to automotive applications. For a comprehensive overview, please refer to the article by Sharp [26]. A broad spectrum of modern control theory finds application especially in the field of suspension control for comfort optimization:

1. Linear Quadratic Regulator (LQR) in [27].
2. Model Predictive Control (MPC) in [16], [19], [20], [22], [24], [28].
3. Explicit MPC where a multi-parametric problem is solved to find a piece wise affine solution as in [18], [21].
4. Explicit MPC-based Gaussian radial basis function neural networks (RBF-NN) [18].
5. Robust control theory for example in the form of H_∞-control as found in [29].

In addition to the wide application of various control methods, MPC is becoming increasingly popular in the automotive industry, according to [30]. MPC has several inherent advantages over other methods: It not only allows to find an optimal solution for the underlying control problem, but it also allows arbitrary constraints to be satisfied,

Die approbierte gedruckte Originalversion dieser Diplomarbeit ist an der TU Wien Bibliothek verfügbar
The approved original version of this thesis is available in print at TU Wien Bibliothek.
TU Bibliothek Your knowledge hub WIEN

such as an anti-wheel-hop constraint for speed bumps in [25], non-linear constraints on the damper characteristics in [16], or soft constraints on the tire load, pitch and roll of the vehicle in [17] to enhance the handling performance. One of the biggest advantages is that a model predictive controller is able to predict future system states, thus being able to react proactively and prepare for future excitations or disturbances on the system.

However, the work in [18] addresses one of the major drawbacks of model predictive controllers: computation time. Therein, a model predictive controller was devised in combination with a Kalman-Filter to estimate non-measured states for a quarter-car model. As mentioned in the paper, a major drawback of solving an optimal control problem online is the computational cost. One solution to this problem entails finding the explicit solution to this optimal problem, as is done in [21]. However, the explicit solution scales very poorly with the size of the optimization problem and the computational advantage can turn into a disadvantage quite quickly. Therefore, in [18] the explicitly solved MPC was approximated by a Gaussian neural network with radial basis function to speed up the online computation.

Cost Function: Comfort Criterion Most of the control methods mentioned have a cost function in common, via which a control input is to be optimized. The cost function takes on an essential position here, as it can be used to tailor the problem specifically to the application. The cost functions are designed to achieve specific objectives, such as minimizing sprung mass acceleration to increase ride comfort or minimize tire load variations to support vehicle handling. To improve ride comfort, the cost function typically incorporates the sprung mass acceleration as a measure of discomfort, additionally some measure again for the tire load variations and cost for actuator forces in case of semi-active or active suspension systems [17], [18], [20]. In cases with higher degrees of freedom models where multiple modes of the vehicle are captured, it is also common to include, for example, pitching motion in the cost function to penalize severe vehicle nodding when going over bumps.

Road Profiles Particularly in the effort to improve ride comfort, the road irregularities and obstacles which excite the vehicle when driving through a road section are of importance. Here, several profiles have distinguished themselves in the literature as a testing ground for comfort-seeking control methods:

1. Stochastic road excitations [15], [16], [18].
2. Speed bumps and potholes with cosine shape [25] or triangular shape [24].

Die approbierte gedruckte Originalversion dieser Diplomarbeit ist an der TU Wien Bibliothek verfügbar
The approved original version of this thesis is available in print at TU Wien Bibliothek.
TU Bibliothek Your knowledge hub WIEN

It should also be mentioned in this context that all publications mentioned so far assume a constant speed of the vehicle when driving over uneven road surfaces and can therefore assume a constant preview horizon or a constant preview duration. This assumption allows to know in advance when the vehicle will experience the road obstacle or disturbance.

2.3 Human Driver Modeling

The previous section focused exclusively on the vehicle as a dynamic system. Yet, it has always been of interest to researchers to investigate the role of the human driver as the primary control element within the traditional driver-vehicle system. The systematic study of automobile vehicle dynamics was initiated in the early 1940s and shortly thereafter, in the mid-1950s, the influence of the driver in the context of vehicle dynamics began to gain research interest [12]. A suitable driver model and understanding of the vehicle-driver-road system is not only interesting from a scientific point of view, but can also help to reduce the time and cost of vehicle development by mathematically simulating the driving conditions rather than relying on costly field test [31], [32].

Control Tasks Among others, the driver has two control tasks to perform in a vehicle: longitudinal control and lateral control. From these control tasks, several subtasks can be derived for a human driver model, e.g., keeping the vehicle on the road, following other vehicles, road pursuit, collision avoidance, lane keeping, and many more [33]. Modeling the full capabilities of a human driver using only "if-then" expressions would contain about 10 000-50 000 rules [33]. Thus, mathematical modeling of the human driver has been a heavily researched topic for many decades. Comprehensive reviews and overviews of driver modeling are provided by Plöchl and Edelmann [12], Macadam [34], Delice and Ertugrul [33], and most recently, Cole [31].

Characteristics of a Human Driver The model of a human driver should consider various human features, such as the physical limitations and control behavior of a human. Macadam [34] states that a model of a human driver should have some essential properties and characteristics of a human driver such as:

- the integration of a transport time delay or reaction time of the driver,
- the use of preview information by the driver to detect upcoming lateral and longitudinal control demands,

Die approbierte gedruckte Originalversion dieser Diplomarbeit ist an der TU Wien Bibliothek verfügbar
The approved original version of this thesis is available in print at TU Wien Bibliothek.
TU Bibliothek Your knowledge hub WIEN

- the driver's ability to adapt to changing vehicle dynamics and operating conditions and
- the use of an internal vehicle model to estimate future vehicle behavior.

Macadam [34], Plöchl and Edelmann [12] elaborate on the human driver model further and state, that an advanced driver model should try to capture not only the essential characteristics but also:

- visual, vestibular, tactile, auditory information reception,
- a pipline for perception and processing of perceived information,
- neuromuscular dynamics with thresholds, time delays and limitations,
- planning capabilities for path and speed,
- adaption/learning of the human driver and
- the ability to adjust to specific types of driving styles based on, e.g.:
  - age,
  - experience/skill,
  - willingness to take risks,
  - different levels of concentration,
  - tiredness,
  - stress and
  - emotions.

Driver Models The task of driving and steering a vehicle is often divided into two, three, or four levels of control. More recently, predictive control has also been used as a method to view driving tasks holistically rather than separately at different levels.

In the simplest case of a two-level driver model, the control structure consists of an anticipatory open-loop (feedforward) and a compensatory closed-loop (feedback) control, see Fig. 2.2. In the case of controlling the steering input of a vehicle, the anticipatory loop may be associated with the generation of a drivable trajectory through a curve [35]–[37]. For example, the trajectory generation may be based on an experiential knowledge between steering input and road curvature. The task of the compensatory loop is to

Die approbierte gedruckte Originalversion dieser Diplomarbeit ist an der TU Wien Bibliothek verfügbar
The approved original version of this thesis is available in print at TU Wien Bibliothek.
TU Bibliothek Your knowledge hub WIEN

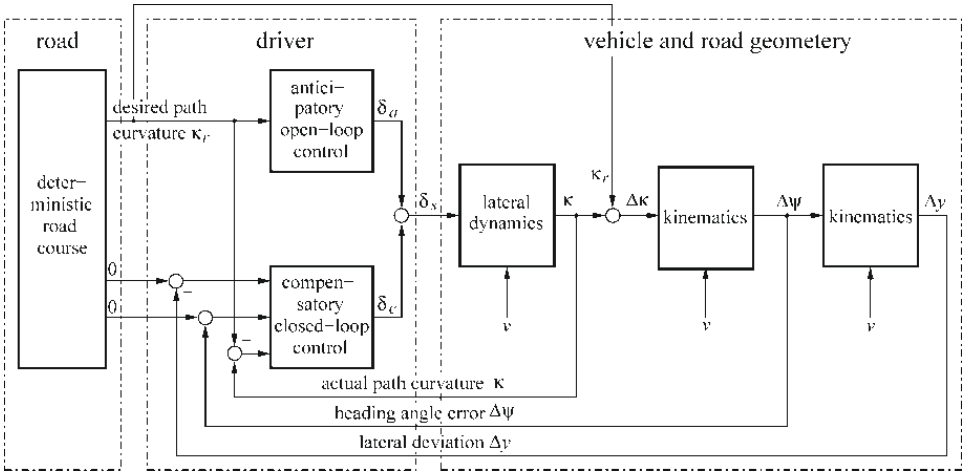

Figure 2.2: Two-level driver model for steering control, taken from [37]. The driver model consists of an anticipatory open-loop and compensatory closed-loop control.

ensure that the vehicle can follow the anticipated trajectory and to correct internal and external disturbances.

The two-level model can be extended to a third level, which takes large local deviations into account [12], [32]. In the case of local deviations, large feedback compensations can arise and lead to undesired driving behavior. Therefore, in [32] a three-level driver is introduced which in cases of large local disturbances tries to smoothly transition back to the road trajectory. Preview steering tasks (anticipatory loop) will be of minor importance during this maneuver. Therefore, in critical situations, the third level controller is activated and the others deactivated.

In [12], a method is described in which "steering by experience" is introduced as a fourth level of control. The idea is based on the adaptation of the driver model in difficult but recurring driving scenarios. Thus, the driver model is not static, but adapts dynamically to the situation.

More recently, the focus of research has shifted to the application of model predictive control to model the driver. Based on a model, controllers are able to consider future travel paths, predict trajectories and calculate an optimal control sequence [38]. Thus, MPC is a natural choice to represent the cognitive thought process of a human driver, as it is based on the assumption that a human makes predictions based on an internal representation of the situation [31]. MPC can be used for predictive control by generating optimal speed and steering trajectories, for example. The model predictive controller combines the anticipatory and feedback tasks, as the control scheme can be executed in

Die approbierte gedruckte Originalversion dieser Diplomarbeit ist an der TU Wien Bibliothek verfügbar
The approved original version of this thesis is available in print at TU Wien Bibliothek.
TU Bibliothek Your knowledge hub WIEN

a feedback loop.

For a detailed consideration of driver models, the extensive review by Plöchl and Edelmann [12] is recommended.

2.4 Model Predictive Control

This section gives a general introduction to model predictive control. A model predictive controller calculates an optimal control input for a given dynamical system – the model – in order to minimize a specified cost criterion. Thus, an optimization problem arises. The cost criterion can be used to perform a specific task like reference tracking, minimizing actuator input, suppress or shape certain dynamics. The controller can be enhanced to include constraints on states, input and output of the system in an optimal fashion. MPC is not limited to linear system dynamics compared to Linear Quadratic Regulator (LQR) or simple feedback control. The control method is intuitive as the decision making process for finding the current control input also considers its future influence on the system. This "planning" or prediction is intuitive for controlling, for example, a vehicle.

Model The optimal control problem can be defined for either a continuous- or a discrete-time system. In general, a discrete-time approach is preferred when working with complex, higher-dimensional and nonlinear systems, since the available solvers in many cases outperform the solvers for the continuous case. In Fig. 2.3, the prediction step for a discrete MPC is illustrated. The state trajectories are planned until a certain horizon is reached, and an optimal input trajectory that minimizes a given cost function is planned for the same duration.

This thesis focuses on the discrete-time formulation of an MPC. Therefore, only the discrete-time MPC will be considered from this point on. A detailed consideration of both continuous and discrete-time MPC can be found in [39]. It is assumed that a given control problem is governed by the following difference equation with scalar input:

$$\mathbf{x}_{k+1} = \mathbf{f}(\mathbf{x}_k, u_k)\,, \tag{2.1}$$

where the time step index $k \in \{0, 1, 2, \ldots\}$ defines a time lattice $t_k = kT_s$ with sampling time $T_s \in \mathbb{R}_{>0}$. The states of the system $\mathbf{x}_k \in \mathcal{X}$ and control input $u_k \in \mathcal{U}$ for $\forall k$ with the dynamics $\mathbf{f}(\cdot)$ define the difference equation. For the set $\mathcal{X}$ of permissible states and the set $\mathcal{U}$ of permissible inputs

$$\{\mathbf{0}\} \subset \mathcal{X} \subseteq \mathbb{R}^m\,, \quad \{\mathbf{0}\} \subset \mathcal{U} \subseteq \mathbb{R} \tag{2.2}$$

Die approbierte gedruckte Originalversion dieser Diplomarbeit ist an der TU Wien Bibliothek verfügbar
The approved original version of this thesis is available in print at TU Wien Bibliothek.
TU Bibliothek Your knowledge hub WIEN

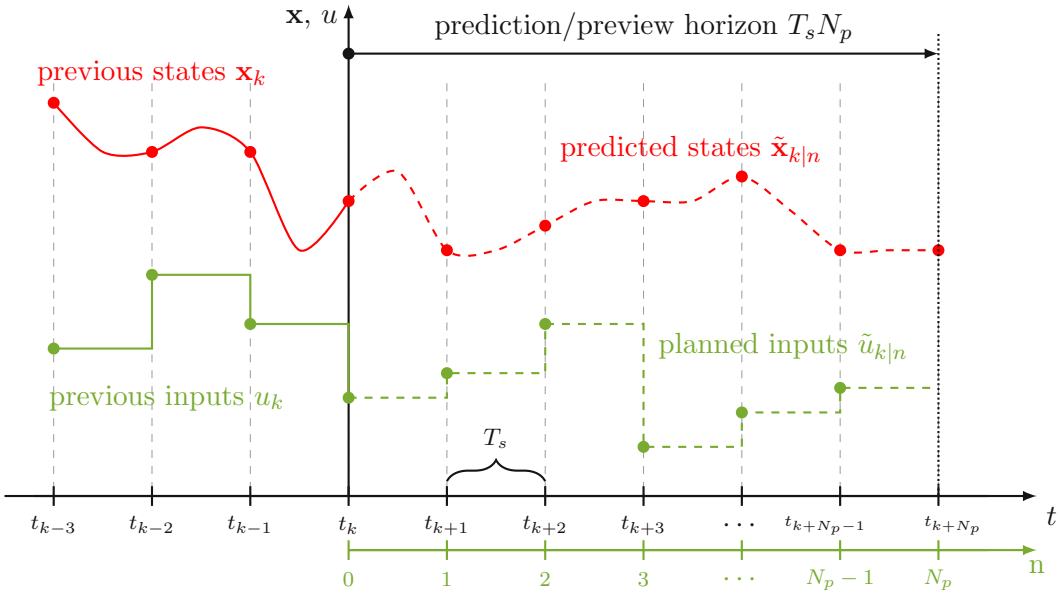

Figure 2.3: Concept of MPC: Predicted and passed states, planned and applied inputs schematically sketched at time step t_k. Figure adapt from [39], [40] for discrete-time.

must hold, where m is the number of states. For the MPC formulation, a second, local prediction time grid with $N_p \in \mathbb{Z}_{>0}$ sampling intervals, $n \in \{0, 1, 2, \ldots, N_p\}$ as local index is introduced so that the beginning of the grid at $n = 0$ is equal to t_k. Note that the sampling time T_s is the same for the local and global grids.

Optimal Control Problem (OCP) With the given difference equation (2.1) and the admissible sets (2.2), the model predictive optimization problem can be written as follows:

$$\tilde{\mathbf{U}}_k^* = \arg\min_{\tilde{\mathbf{U}}_k} \quad J(k, \mathbf{x}_k, \tilde{\mathbf{U}}_k) \tag{2.3a}$$

$$\text{s.t.} \quad \tilde{\mathbf{x}}_{k|n+1} = \mathbf{f}(\tilde{\mathbf{x}}_{k|n}, \tilde{u}_{k|n}), \quad \tilde{\mathbf{x}}_{k|0} = \mathbf{x}_k, \tag{2.3b}$$

$$\tilde{\mathbf{x}}_{k|n} \in \mathcal{X}, \quad \tilde{u}_{k|n} \in \mathcal{U}, \quad \forall n = 0, 1, \ldots, N_p - 1 \tag{2.3c}$$

$$\tilde{\mathbf{x}}_{k|N_p} \in \mathcal{X}_T, \tag{2.3d}$$

where $\mathbf{x}_k$ is given as the starting point for the prediction, $\tilde{\mathbf{x}}_{k|n}$ are predicted states, $\tilde{u}_{k|n}$ are planned inputs and yield the planned input sequence $\tilde{\mathbf{U}}_k = \left[\tilde{u}_{k|0}, \tilde{u}_{k|1}, \ldots, \tilde{u}_{k|N_p-1}\right]$. $J(\cdot)$ is the scalar optimization criterion or cost function. The cost function is generally a

Die approbierte gedruckte Originalversion dieser Diplomarbeit ist an der TU Wien Bibliothek verfügbar
The approved original version of this thesis is available in print at TU Wien Bibliothek.
TU Bibliothek Your knowledge hub WIEN

summation over the prediction grid. The constraints of states and inputs are contained in the definition of the sets $\mathcal{X}$ and $\mathcal{U}$ in (2.2). Sometimes it may be useful to add terminal conditions at the end of the prediction horizon $\tilde{\mathbf{x}}_{k|N_p}$, as seen in (2.3d). For the terminal set $\mathcal{X}_T$, the condition $\{0\} \subseteq \mathcal{X}_T \subseteq \mathcal{X}$ must hold. The optimization problem (2.3) is solved in a receding horizon fashion in every time step k, i.e. the first planned input $\tilde{u}^*_{k|0}$ of the optimal input sequence $\tilde{\mathbf{U}}^*_k$ is applied to the system. Then the OCP is solved again at the next time $k+1$.

Solving the OCP Solving the OCP in (2.3) can be a complex undertaking, depending on the cost function, the system dynamics and the constraints. In the generalized case of a nonlinear optimization problem, the problem is categorized as a static optimization problem that can be either constrained or unconstrained. For the unconstrained case, there are various methods, e.g., steepest descent method, conjugate gradient method, Newton method, Quasi-Newton method or Gauss-Newton method [41], [42]. When constraints are introduced, the whole problem becomes more sophisticated as one has to check whether certain constraints are active and should be considered or not. A minimum in a static optimization problem with equality and inequality constraints is defined by the Karush-Kuhn-Tucker (KKT) condition. Various solvers such as sequential quadratic-programming (SQP), the interior-point algorithm (IP) or the active-set (AS) method have been developed to solve such a problem and are contained in the FMINCON-Algorithm provided in MATLAB [43]. For a neat list of solvers, see [42, pp. 30–32]. For a short introduction to model predictive control and nonlinear programming, the overview [26] is recommended which focuses on the automotive application. For a deeper understanding, the online available lecture notes by Prof. Steinböck [41] and [39] may be considered. As a simple introduction to model predictive control, an example is given in Appx. B.

Die approbierte gedruckte Originalversion dieser Diplomarbeit ist an der TU Wien Bibliothek verfügbar
The approved original version of this thesis is available in print at TU Wien Bibliothek.
TU Bibliothek Your knowledge hub WIEN

3 Vehicle Model

Before directly addressing the predictive driver model for speed control in the presence of road obstacles, it is first necessary to deal with the representation of the vehicle in the driver's mind – the internal model of the car. This internal model is designed to give the driver a precise idea of the excitation of the vehicle by the road, and thus of the vehicle's response and movements and the impact on the perceived comfort. Based on this model, the driver decides from experience how best to behave – either keeping the speed constant, accelerating or braking the vehicle.

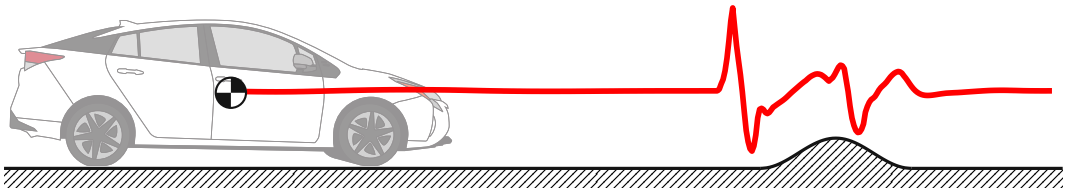

Figure 3.1: Given vehicle[1]and road obstacle, the driver uses a representation (model) of the scenario to assess how the road will affect the experienced comfort. This assessment of the observed situation leads to an adjustment of the driving speed and affects, for example, the vertical body acceleration – shown here in red – which is commonly seen as a comfort measure. The experienced comfort is therefore mainly influenced by vehicle dynamics, road obstacle and vehicle speed.

To arrive at a dynamic model, some levels of abstraction must first be discussed. The question naturally arises as how detailed the vehicle model in the driver's mind generally is. Does it take into account the drivetrain dynamics, brake dynamics, aerodynamics or to what extent does the driver take into account the chassis? Of course, it depends very much on a driver's skills, experience, and the extent to which he or she is familiar with the vehicle. This work attempts to represent the driver's planning process for a comfortable speed profile for a given road excitation in form of a MPC. Therefore, one wants to keep the model rather simple in order to make the subsequent MPC not too complex. Hence, it is a useful assumption to concentrate only on the chassis and

[1]Vehicle graphic from vecteezy.com

Die approbierte gedruckte Originalversion dieser Diplomarbeit ist an der TU Wien Bibliothek verfügbar
The approved original version of this thesis is available in print at TU Wien Bibliothek.

to neglect most other dynamics. In this work, the chassis model is considered as the abstraction limit and no other components are taken into account. As already shown in the introduction, there are considerable differences in the chassis models, especially concerning the order and complexity of the model.

For the most general case of an uneven road, still a detailed car model is required to represent the interactions between the left and right side of the vehicle (roll motion), the front and rear (pitch motion and yaw motion) and lift motion of the vehicle as shown in Fig. 2.1b. With some assumptions, the modeling process can be drastically simplified to produce simple models that represent the vertical motions that are essentially responsible for perceived passenger comfort:

Assumption 1 (Road Assumptions) *The following assumptions are chosen for the driver's internal vehicle model:*

Asm. A: *The road excitation of the left and right lanes are identical and the vehicle is symmetrical about its longitudinal axis. Thus, the vehicle movements are reduced to planar motions.*

Asm. B: *The road contact with the vehicle is approximated by a single point. Since the tire contact patch is concentrated into one point, a sufficiently large curvature of the road can be considered only.*

For a complete and detailed description of the complex interrelationships of the various chassis components and their modeling, reference should be made here to Mitschke's standard textbook [44]. Since this book is only available in German, reference should also be made here to the work by Jazar [45].

In this thesis, two vehicle models are investigated. First, the quarter-car model is presented. As shown in the literature section, the quarter-car model has found wide application in the field of comfort optimization and vehicle control in general. This is mainly due to its simplicity. A main limitation of the quarter-car is that it only captures the dynamics of one axle and cannot represent the pitching motion of the vehicle when passing over a road obstacle. Therefore, the half-car model is presented, which models two axles and should better reflect the real driving scenario.

In the following, equations of motion in state-space representation are sought to predict the state of the vehicle. These models form the basis for the subsequent formulation of the trajectory optimization problem in form of a MPC. A model is given as follows:

$$\dot{\mathbf{x}} = \mathbf{f}(\mathbf{x}, u, \mathbf{z})\,. \tag{3.1}$$

Die approbierte gedruckte Originalversion dieser Diplomarbeit ist an der TU Wien Bibliothek verfügbar
The approved original version of this thesis is available in print at TU Wien Bibliothek.
TU Bibliothek Your knowledge hub WIEN

Here $\mathbf{x} \in \mathbb{R}^n$ is a state vector, the input is given by $u \in \mathbb{R}$, and the disturbance, in this case the road excitations, are given by $\mathbf{z} \in \mathbb{R}^p$. The number of states n and disturbances p depend on the underlying vehicle model. The dynamics of the vehicle are delegated by the mapping $\mathbf{f} : \mathbb{R}^n \times \mathbb{R} \times \mathbb{R}^p \to \mathbb{R}^n$.

In the remaining sections of this chapter, the quarter-car is presented in Sec. 3.1 and the half-car in Sec. 3.2 – with a special look at suspension modeling in Sec. 3.3 and Sec. 3.4. The final state-space equations for both models are given in Sec. 3.5. This chapter is concluded by a brief look at individual road elevations in Sec. 3.6 which are used in this work.

3.1 Quarter-Car: Two-Mass Model

The quarter-car model, as shown in Fig. 3.2, consists of two masses: The body mass m_B and wheel mass m_W. The suspension consists of a nonlinear progressive spring and a damper with nonlinear damping characteristics. The individual suspension components are covered in separate sections later in this chapter. The tire is modeled by a linear spring and damper. In addition to the Asm. 1, the following applies:

Assumption 2 (Quarter-Car Assumptions) *The following assumptions are chosen in addition to the Asm. 1 for the driver's internal vehicle model:*

Asm. A: *The elastic properties of the tire are approximated by a simple damper spring model. The tire force is presumed to always act vertically.*

Asm. B: *The suspension and tire masses are part of either the sprung mass m_B (body) or the unsprung mass m_W (wheel).*

Asm. C: *The sprung and unsprung mass experience the same longitudinal velocity and longitudinal acceleration. No rotations of the masses are allowed.*

Asm. D: *The "drive-train" force F_D is presumed to act as external force on the sprung mass.*

Equations of Motion Based on the free-body diagram in Fig. 3.2b, the governing equations for the longitudinal and vertical directions are derived. Since the vehicle model is rigid in the longitudinal direction and no rotation of the sprung and unsprung masses is possible, the equation of motion in the longitudinal direction simply reads:

$$(m_B + m_W)\ddot{s} = F_D \,. \tag{3.2}$$

Die approbierte gedruckte Originalversion dieser Diplomarbeit ist an der TU Wien Bibliothek verfügbar
The approved original version of this thesis is available in print at TU Wien Bibliothek.
TU Bibliothek Your knowledge hub WIEN

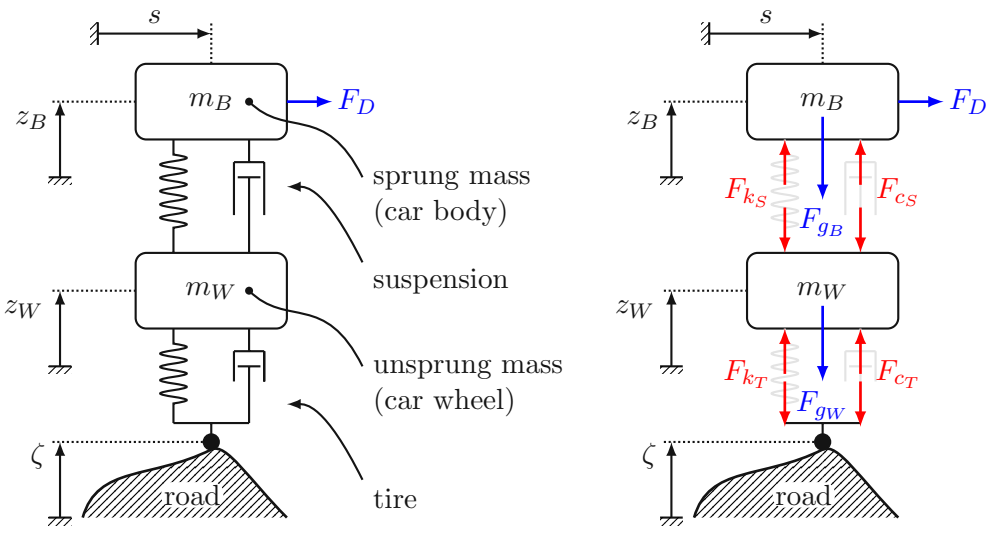

(a) Quarter-car model.

(b) Free-body diagram.

Figure 3.2: Quarter-car model: Mass m_B represents the (quarter of) the vehicle body, mass m_W represents one wheel. The horizontal force F_D may be understood as a "drive-train" force. Depending on the sign of F_D, the vehicle is either accelerated or decelerated. The vehicle is excited from the road via the road elevation ζ. The movement of the wheel mass is measured from the static equilibrium via z_W. The movement of the body mass is measured from the static equilibrium via z_B.

Here m_B is the sprung mass (car body), m_W is the unsprung mass (car wheel), F_D is the "drive-train" force responsible for braking and accelerating the vehicle and s is the distance traveled on the road and $\ddot{s}$ the vehicle acceleration, respectively. The equations of motion in vertical direction are given by:

$$m_B \ddot{z}_B = -F_{g_B} + F_{k_S} + F_{c_S}\,, \tag{3.3}$$

$$m_W \ddot{z}_W = -F_{g_W} - F_{k_S} - F_{c_S} + F_{k_T} + F_{c_T}\,, \tag{3.4}$$

with the suspension spring force F_{k_S} which is modeled in detail in Sec. 3.3, the suspension damper force F_{c_S} given by a piece-wise affine (PWA) law in Sec. 3.4, gravitational forces F_{g_B} and F_{g_W} and linear tire forces F_{k_T} and F_{c_T}. The model is further developed into a state-space description in Sec. 3.5.

Die approbierte gedruckte Originalversion dieser Diplomarbeit ist an der TU Wien Bibliothek verfügbar
The approved original version of this thesis is available in print at TU Wien Bibliothek.
TU Bibliothek Your knowledge hub WIEN

3.2 Half-Car: Two-Axle Model

The previous vehicle model represented only one quarter and one axle of a vehicle and therefore could not capture the pitching motion. The half-car shown in the Fig. 3.3 captures not only the vertical motion but also the pitching of the vehicle. The front and rear axle of the vehicle share a combined sprung mass (body). As with the quarter-car, further assumptions are made:

Assumption 3 (Half-Car Assumptions) *The following are required in addition to Asm. 1, Asm. 2.A, Asm. 2.B and Asm. 2.C:*

Asm. A: *The pitch angle φ_B remains small. The pitching motion is linearized[2] for small pitch angles $\varphi_B \ll 1$ around the static equilibrium, e.g. $\varphi_B = 0$.*

Asm. B: *The rear wheel travels in the same track as the front wheel and thus experience the same excitation from the road. The excitations at the front and rear axle are time delayed, which depends on the wheelbase $L = l_r + l_f$ and the driving speed v.*

Asm. C: *No rotation of the unsprung masses are allowed.*

Asm. D: *The "drive-train" force is decomposed into a braking force F_B and driving force F_T which act as external forces on a massless rod connected to the sprung mass.*

The half-car model in Fig. 3.3 composes of the front and rear wheel mass $m_{W,f}$ and $m_{W,r}$ and the body (mass m_B, pitch moment of inertia I_B w.r.t. the center of mass). The models for suspension spring and damper as well as for the tires are the same at the front and rear axle, but a different parameterization of the front and rear is used. The representation of the driving force F_D has been replaced by a braking force F_B and driving force F_T. Under real conditions, the drive and braking forces act in the tire contact patches and would lead to pitching during braking or acceleration, depending on the chassis geometry and drivetrain layout. To account for this, a massless rod with different leverage lengths is introduced at the center of mass. Depending on whether the vehicle is braked or accelerated, the point of application of the force changes, as shown in the Fig. 3.3a. With the variable set of lengths $h_i \in \{h_T, h_B\}$, the forces induce different pitching moments.

[2] This simplification is justified by the fact that no larger pitch angles from $5° \approx 0.09$ rad are expected in sharp braking and acceleration maneuvers, see [44] and Chapter 5.

Die approbierte gedruckte Originalversion dieser Diplomarbeit ist an der TU Wien Bibliothek verfügbar
The approved original version of this thesis is available in print at TU Wien Bibliothek.
TU Bibliothek Your knowledge hub WIEN

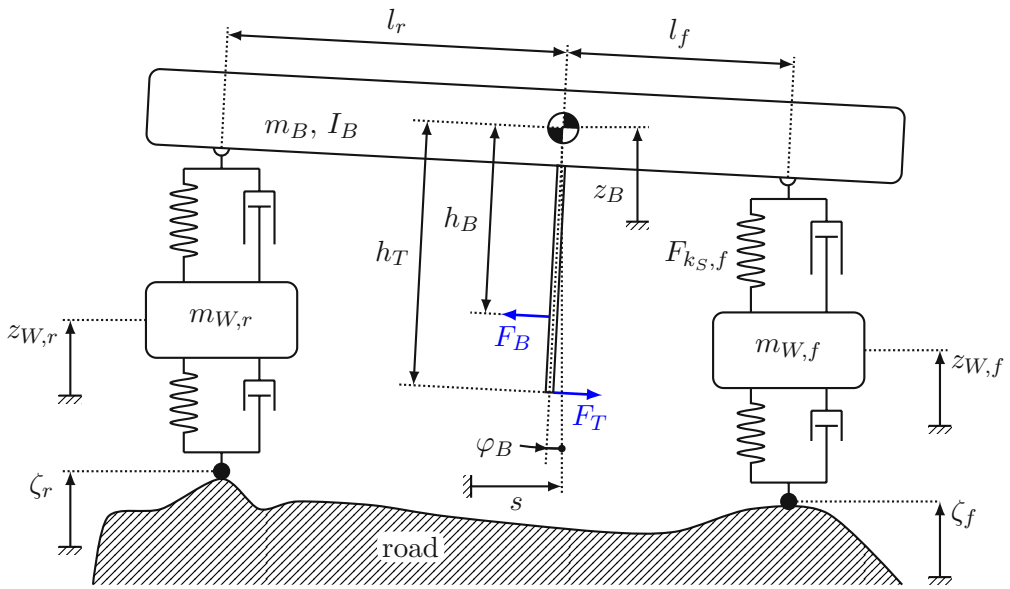

(a) Half-car model.

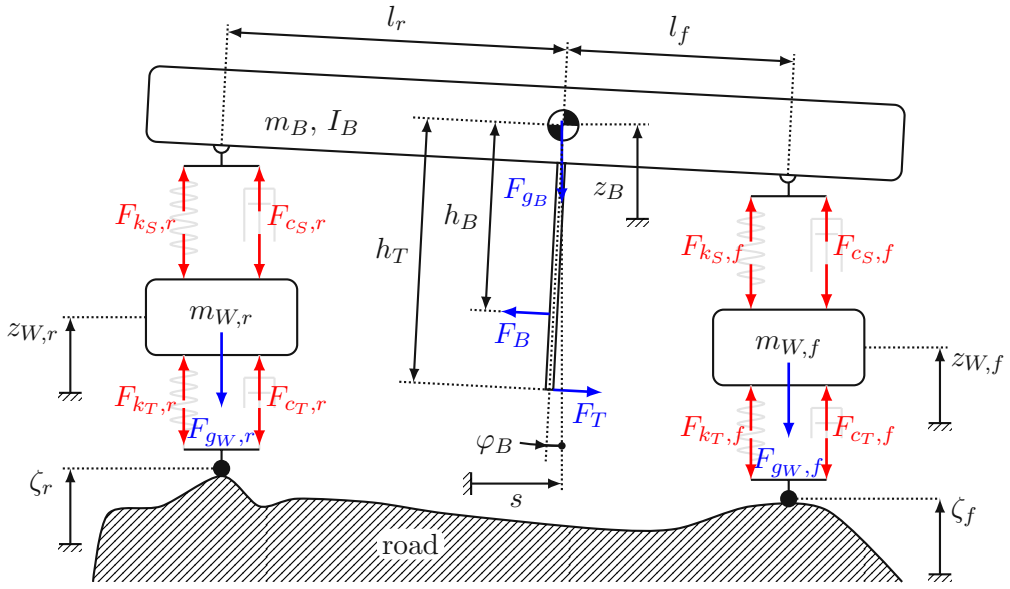

(b) Free-body diagram.

Figure 3.3: Half-car model: F_B is the braking and F_T is the driving force. Depending on F_B and F_T different leverage lengths are used to induce different pitching moments. The vehicle is excited from the road via the road elevation ζ_r on the rear and ζ_f on the front. All movements are measured in relation to the static equilibrium position.

Die approbierte gedruckte Originalversion dieser Diplomarbeit ist an der TU Wien Bibliothek verfügbar
The approved original version of this thesis is available in print at TU Wien Bibliothek.
TU Bibliothek Your knowledge hub WIEN

Equations of Motion Based on the free-body diagram in Fig. 3.3b, the governing equations for the longitudinal and vertical directions are derived. The equation of motion in the longitudinal direction is simple:

$$(m_B + m_{W,r} + m_{W,f})\ddot{s} = \underbrace{F_T - F_B}_{F_D} . \tag{3.5}$$

Here m_B is the sprung mass (car body), $m_{W,r}$ and $m_{W,f}$ are the unsprung masses for the rear and front wheels, respectively. F_B and F_T are the forces for braking and accelerating the vehicle and combined similar to the driving force F_D in the quarter-car. The vertical equations of motion for the sprung mass m_B is given by (3.6). The pitching motion is given by (3.7). The lifting motion of the rear and front wheels are given by (3.8) with the index $i \in \{r, f\}$ referring either to the rear or front suspension:

$$m_B \ddot{z}_B = -F_{g_B} + F_{k_S,r} + F_{c_S,r} + F_{k_S,f} + F_{c_S,f} , \tag{3.6}$$

$$I_B \ddot{\varphi}_B = F_B h_B - F_T h_T + F_{k_S,r} l_r + F_{c_S,r} l_r - F_{k_S,f} l_f - F_{c_S,f} l_f , \tag{3.7}$$

$$m_{W,i} \ddot{z}_{W,i} = -F_{g_W,i} - F_{k_S,i} - F_{c_S,i} + F_{k_T,i} + F_{c_T,i} , \tag{3.8}$$

where $F_{k_S,i}$ is mapped according to the same model as for the quarter-car in Sec. 3.3. The suspension damper force $F_{c_S,i}$ is given by a PWA law in Sec. 3.4. l_f and l_r are the distances from the front and rear axle to the center of mass (CoM).

3.3 Suspension Spring Model

In this work, a nonlinear spring model is chosen for the chassis. Usually, the human driver is aware of the fact that the vehicle suspension has a limited suspension travel, as at a certain point the spring is completely compressed. There is also a limited deflection when the suspension is released. However, before the end of the suspension travel in both directions is reached, progressive behavior sets in before this. In Fig. 3.4a, the chosen spring model is sketched. The spring curve consists of a linear range around the static rest position. After a certain amount of clearance Δz_{cmp}, a gentle progression occurs during compression. In the opposite direction, after a slightly larger clearance Δz_{rbd}, a strong progression occurs during rebound.

As seen from the figure, the spring curve is split into a static, linear and nonlinear

Die approbierte gedruckte Originalversion dieser Diplomarbeit ist an der TU Wien Bibliothek verfügbar
The approved original version of this thesis is available in print at TU Wien Bibliothek.
TU Bibliothek Your knowledge hub WIEN

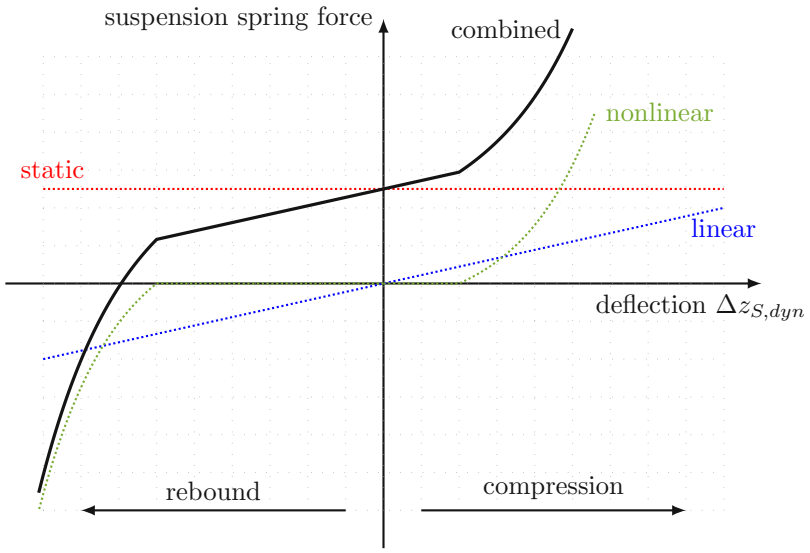

(a) Static, linear and nonlinear components of suspension spring force.

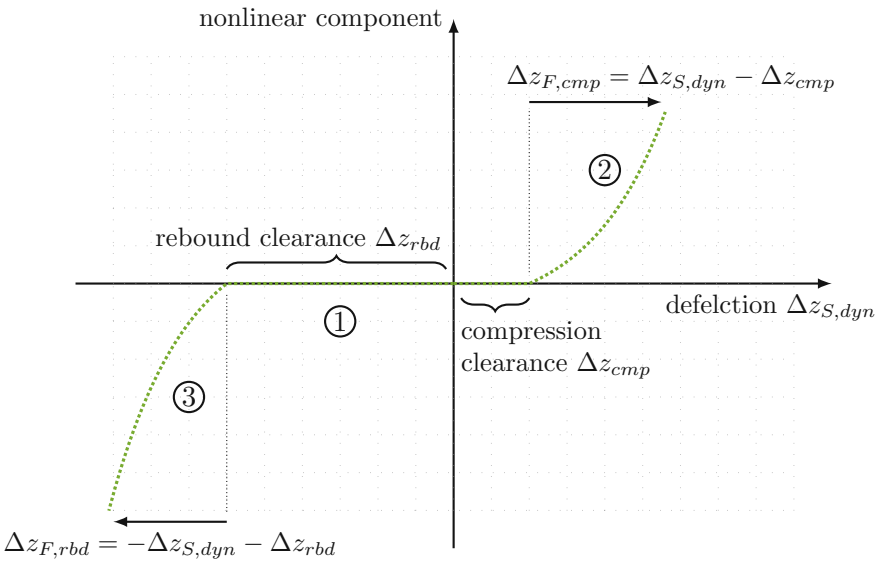

(b) Nonlinear component of suspension spring model.

Figure 3.4: Suspension spring: In (a) the suspension spring force-deflection relationship is sketched. In (b) the nonlinear part is solely plotted. Suspension force is given over suspension deflection $\Delta z_{S,dyn}$ from static equilibrium position $\Delta z_{S,stat}$. Total deflection: $\Delta z_S = \Delta z_{S,stat} + \Delta z_{S,dyn}$. In case of the quarter-car, $\Delta z_{S,dyn}$ is defined as $z_W - z_B$. For the half-car, the rear deflection $\Delta z_{S,dyn,r}$ is given by $z_{W,r} - \varphi_B l_r - z_B$ and the front deflection $\Delta z_{S,dyn,f}$ by $z_{W,f} + \varphi_B l_f - z_B$.

Die approbierte gedruckte Originalversion dieser Diplomarbeit ist an der TU Wien Bibliothek verfügbar
The approved original version of this thesis is available in print at TU Wien Bibliothek.
TU Bibliothek Your knowledge hub WIEN

component[3]:

$$F_{k_S} = F_{k_S,stat} + F_{k_S,lin} + F_{k_S,nonlin}\,.$$

The static and linear parts of the suspension model are straightforward and provided in Sec. 3.5 in combination with the full state-space model. The nonlinear part is further developed starting from a progressive spring characteristic for a constant natural frequency under varying loading condition as derived in [44], [46]. The progressive model is extended with additional parameters to allow fine tuning and to include clearance until the onset of the progression. The nonlinear component of the total spring characteristic in the compression (cmp) section – case (2) in Fig. 3.4b – is given as

$$F_{k_S,cmp}\left(\Delta z_{F,cmp}\right) = k_S\left[\Delta z_{S,stat} f_{1,cmp}\left(e^{f_{2,cmp}\frac{\Delta z_{F,cmp}}{\Delta z_{S,stat}}} - 1\right) - \Delta z_{F,cmp}\right]. \tag{3.9}$$

For the rebound (rbd) section – case (3) in Fig. 3.4b – the nonlinear force is defined as

$$F_{k_S,rbd}\left(\Delta z_{F,rbd}\right) = -k_S\left[\Delta z_{S,stat} f_{1,rbd}\left(e^{\frac{\Delta z_{F,rbd}}{\Delta z_{S,stat}} f_{2,rbd}} - 1\right) - \Delta z_{F,rbd}\right]. \tag{3.10}$$

The deflection in the progressive section is $\Delta z_{F,cmp}$ for the compression stage and $\Delta z_{F,rbd}$ for the rebound stage which are defined in Fig. 3.4b. $\Delta z_{S,stat}$ is the static equilibrium deflection and k_S is the linear spring stiffness. The parameter f_1 is used to scale the overall progression[4] and f_2 scales the curvature[4] of the progressive rise. Note that in the case of the half-car, for each axle exist different static equilibrium points $\Delta z_{S,stat}$ as well as that the parameters f_1 and f_2 vary between the front and rear. The delay until the progressive part is active is given by Δz_{cmp} or Δz_{rbd}, compare Fig. 3.4b. Since the progressive nonlinear component is basically unlimited and its force can increase exponentially, this naturally leads to a limitation of the suspension travel. This knowledge of the vehicle's limited suspension travel may be expected from a skilled driver. The full equation for the nonlinear part of the suspension force results to:

$$F_{k_S,nonlin}\left(\Delta z_{S,dyn}\right) = \begin{cases} F_{k_S,cmp}, & \text{case (2) for } \Delta z_{S,dyn} > \Delta z_{cmp} \\ F_{k_S,rbd}, & \text{case (3) for } \Delta z_{S,dyn} < -\Delta z_{rbd} \\ 0. & \text{else case (1)} \end{cases} \tag{3.11}$$

[3] For better readability, the equation is given without the subscript i, which in the case of the half-car denotes the front or rear axle.

[4] For the sake of simplicity, the indexing for rebound, compression and axle was omitted.

Die approbierte gedruckte Originalversion dieser Diplomarbeit ist an der TU Wien Bibliothek verfügbar
The approved original version of this thesis is available in print at TU Wien Bibliothek.
TU Bibliothek Your knowledge hub WIEN

The necessary nature of such a complex model will be discussed later when some results are considered and compared with a linear approach in Sec. 5.2.1.

3.4 Suspension Damper Model

The vehicle damper force-stroke relationship is approximated by a piece-wise linear damper characteristic, similar to the models used in textbooks by Mitschke [44], Richter [46] or in the publication [47]. The damper characteristics, as shown in Fig. 3.5, consists of four linear sections: ① low speed compression, ② low speed rebound, ③ high speed compression and ④ high speed rebound.

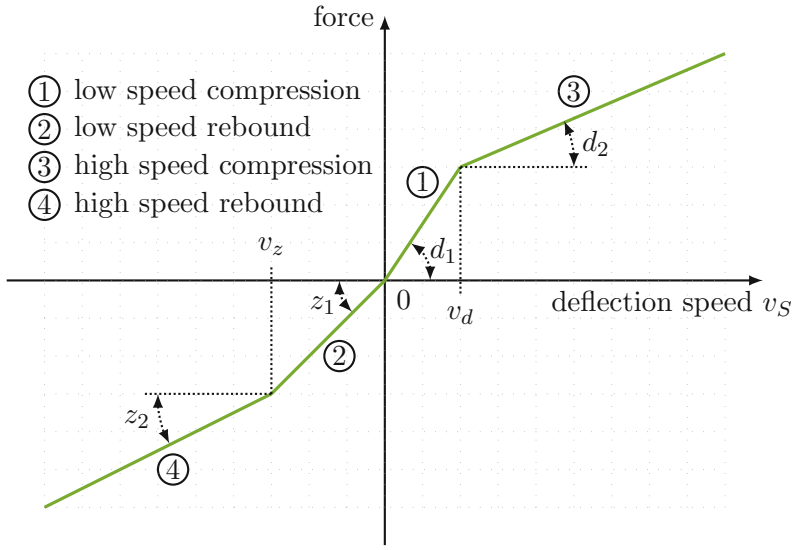

Figure 3.5: Suspension damper: The damper force-stroke relationship is split into low and high speed compression and rebound sections. The transition velocities v_z and v_d define the switch from low/high speed damping. Slopes z_1, z_2, d_1 and d_2 define the behavior of the damper in the respective sections. The deflection speed v_S is given for the quarter-car as $\dot{z}_W - \dot{z}_B$. For the half-car, the deflection speed of the rear $v_{S,r}$ is given by $\dot{z}_{W,r} - \dot{\varphi}_B l_r - \dot{z}_B$ and for the front damper the speed $v_{S,f}$ by $\dot{z}_{W,f} + \dot{\varphi}_B l_f - \dot{z}_B$. The model is primarily based on [47].

Die approbierte gedruckte Originalversion dieser Diplomarbeit ist an der TU Wien Bibliothek verfügbar
The approved original version of this thesis is available in print at TU Wien Bibliothek.
TU Bibliothek Your knowledge hub WIEN

The function that determines the damper's final behavior is given as:

$$F_{c_S}(v_S) = \begin{cases} d_1 v_S\,, & \text{case } \textcircled{1} \text{ for } v_d > v_S > 0 \\ z_1 v_S\,, & \text{case } \textcircled{2} \text{ for } v_z < v_S < 0 \\ d_2\,(v_S - v_d) + d_1 v_d\,, & \text{case } \textcircled{3} \text{ for } v_S \geq v_d \\ z_2\,(v_S - v_z) + z_1 v_z\,, & \text{case } \textcircled{4} \text{ for } v_S \leq -v_z \end{cases} \tag{3.12}$$

where v_d and v_z are the transition velocities from the low to the high speed of the compression and rebound stages, respectively. The deflection velocity v_S is given in the caption of Fig. 3.5. d_1 and d_2 are the slopes of the compression stage and analogously z_1 and z_2 are the slopes for the rebound stage. Similar to the suspension spring model, the slopes and transition velocities may vary in the case of the half-car between the front and rear axle. Similarly to the spring model, the necessity of such a complex model will be discussed later when looking at some results and be compared to a linear approach as well.

3.5 State-Space Models

In this section, the final state-space equations are derived by inserting the previously derived spring model of Sec. 3.3 and the damper model of Sec. 3.4 into the vehicle models of Sec. 3.1 and Sec. 3.2, respectively. In addition, the static displacement/equilibrium point of the vehicle suspension and tire is derived and vehicle control input is briefly discussed.

3.5.1 Quarter-Car

Starting from the equations in the vertical direction of the quarter-car model in (3.3) and (3.4), the equations of motion are extended by inserting the gravitational forces and the suspension spring model with the split into static, linear and nonlinear components:

$$\begin{aligned} m_B \ddot{z}_B &= -F_{g_B} + F_{k_S} + F_{c_S} \\ &= -m_B g + \underbrace{F_{k_S,stat} + F_{k_S,lin} + F_{k_S,nonlin}}_{F_{k_S}} + F_{c_S}\,, \end{aligned} \tag{3.13}$$

Die approbierte gedruckte Originalversion dieser Diplomarbeit ist an der TU Wien Bibliothek verfügbar
The approved original version of this thesis is available in print at TU Wien Bibliothek.
TU Bibliothek Your knowledge hub WIEN

$$\begin{aligned} m_W \ddot{z}_W &= -F_{g_W} - F_{k_S} - F_{c_S} + F_{k_T} + F_{c_T} \\ &= -m_W g - \underbrace{F_{k_S,stat} - F_{k_S,lin} - F_{k_S,nonlin}}_{F_{k_S}} - F_{c_S} + \underbrace{F_{k_T,stat} + F_{k_T,lin}}_{F_{k_T}} + F_{c_T} \,. \end{aligned} \tag{3.14}$$

The nonlinear suspension component $F_{k_S,nonlin}$ is governed by (3.11). The damper force F_{c_S} is given by (3.12). The remaining forces are yielded by the linear laws:

$$\text{static suspension spring force:} \quad F_{k_S,stat} = k_S \Delta z_{S,stat} \,, \tag{3.15a}$$

$$\text{linear suspension spring force:} \quad F_{k_S,lin} = k_S(z_W - z_B) = k_S \Delta z_{S,dyn} \,, \tag{3.15b}$$

$$\text{static tire spring force:} \quad F_{k_T,stat} = k_T \Delta z_{T,stat} \,, \tag{3.15c}$$

$$\text{linear tire spring force:} \quad F_{k_T,lin} = k_T(\zeta - z_W) = k_T \Delta z_{T,dyn} \,, \tag{3.15d}$$

$$\text{linear tire damping force:} \quad F_{c_T} = c_T(\dot{\zeta} - \dot{z}_W) = c_T \Delta \dot{z}_T \,, \tag{3.15e}$$

with the linear suspension spring stiffness k_S, linear tire stiffness k_T and linear tire damping coefficient c_T. $\Delta z_{S,stat}$, $\Delta z_{T,stat}$ and $\Delta z_{S,dyn}$, $\Delta z_{T,dyn}$ are the static and dynamic deflections of suspension or tire.

Control Input The longitudinal motion is dictated by the drivetrain force F_D in (3.2). The equation is rearranged such that the vehicle acceleration is used as the new input on the right hand side of the equation:

$$\ddot{s} = \dot{v} = \frac{F_D}{m_B + m_W} = a \,. \tag{3.16}$$

Static Displacement The total spring/tire travel is composed of a static and a dynamic component [44]:

$$\Delta z_S(t) = \Delta z_{S,stat} + \Delta z_{S,dyn}(t) \,, \tag{3.17}$$

$$\Delta z_T(t) = \Delta z_{T,stat} + \Delta z_{T,dyn}(t) \,. \tag{3.18}$$

From the vertical equation of motions in (3.13) and (3.14), the static displacement is calculated by setting the time-dependent parts such as the velocities, accelerations, and damping forces to zero. With the results from (3.15a) and (3.15c), the static displacement

Die approbierte gedruckte Originalversion dieser Diplomarbeit ist an der TU Wien Bibliothek verfügbar
The approved original version of this thesis is available in print at TU Wien Bibliothek.
TU Bibliothek Your knowledge hub WIEN

of the suspension and tire is calculated as:

$$\begin{aligned} 0 &= -F_{g_B} + F_{k_S,stat} \\ &= -m_B g + k_S \Delta z_{S,stat} \quad \longrightarrow \quad \Delta z_{S,stat} = \frac{m_B g}{k_S} \,, \end{aligned} \tag{3.19}$$

$$\begin{aligned} 0 &= -F_{g_W} - F_{k_S,stat} + F_{k_T,stat} \,, \\ &= -m_W g - m_B g + k_T \Delta z_{T,stat} \quad \longrightarrow \quad \Delta z_{T,stat} = \frac{(m_B + m_W)\, g}{k_T} \,. \end{aligned} \tag{3.20}$$

Finally, the dynamic equations in (3.2) - (3.4) are simplified with the static displacement in (3.19, 3.20) and the new input from (3.16) to yield the final set of equations:

$$\ddot{z}_B = \frac{1}{m_B} \left(F_{k_S,lin} + F_{k_S,nonlin} + F_{c_S} \right) \,, \tag{3.21a}$$

$$\ddot{z}_W = \frac{1}{m_W} \left(-F_{k_S,lin} - F_{k_S,nonlin} - F_{c_S} + F_{k_T,lin} + F_{c_T} \right) \,, \tag{3.21b}$$

$$\ddot{s} = a \,. \tag{3.21c}$$

State-Space Model The set of Eqs. (3.21) can be transformed into a state-space model by introducing the following state vector $\mathbf{x}_q$, input u_q and disturbance/road excitation z_q with the index q denoting the quarter-car model:

$$\mathbf{x}_q = \begin{bmatrix} x_{q,1} \\ x_{q,2} \\ x_{q,3} \\ x_{q,4} \\ x_{q,5} \end{bmatrix} = \begin{bmatrix} \zeta - z_W \\ \dot{z}_W \\ z_W - z_B \\ \dot{z}_B \\ v \end{bmatrix} \,, \quad \dot{\mathbf{x}}_q = \frac{d\mathbf{x}_q}{dt} = \begin{bmatrix} \dot{\zeta} - x_{q,2} \\ \ddot{z}_W \\ x_{q,2} - x_{q,4} \\ \ddot{z}_B \\ \dot{v} \end{bmatrix} \,, \quad u_q = a \,, \quad z_q = \dot{\zeta} \,. \tag{3.22}$$

The governing equations are further simplified by splitting them into a linear and a nonlinear part by introducing a common linear system dynamics matrix $\mathbf{A}_{q,1} \in \mathbb{R}^{5\times5}$, as is standard in linear system control theory, and a nonlinear vector $\mathbf{A}_{q,2} \in \mathbb{R}^{5\times1}$ which maps the nonlinear state dynamics. Inserting the linear force equations from (3.15) and

Die approbierte gedruckte Originalversion dieser Diplomarbeit ist an der TU Wien Bibliothek verfügbar
The approved original version of this thesis is available in print at TU Wien Bibliothek.
TU Bibliothek Your knowledge hub WIEN

defining the input u_q as the vehicle acceleration a, the state space model is obtained as:

$$\begin{aligned}\dot{\mathbf{x}}_q = &\underbrace{\begin{bmatrix} 0 & -1 & 0 & 0 & 0 \\ \frac{k_T}{m_W} & -\frac{c_T}{m_W} & -\frac{k_S}{m_W} & 0 & 0 \\ 0 & 1 & 0 & -1 & 0 \\ 0 & 0 & \frac{k_S}{m_B} & 0 & 0 \\ 0 & 0 & 0 & 0 & 0 \end{bmatrix}}_{\mathbf{A}_{q,1}} \mathbf{x}_q + \underbrace{\begin{bmatrix} 0 \\ 0 \\ 0 \\ 0 \\ 1 \end{bmatrix}}_{\mathbf{B}_q} u_q + \underbrace{\begin{bmatrix} 1 \\ \frac{c_T}{m_W} \\ 0 \\ 0 \\ 0 \end{bmatrix}}_{\mathbf{E}q} z_q \\ &+ \underbrace{\begin{bmatrix} 0 \\ -\frac{1}{m_W} \\ 0 \\ \frac{1}{m_B} \\ 0 \end{bmatrix}}_{\mathbf{A}_{q,2}} F_{k_S,nonlin}(x_{q,3}) + \underbrace{\begin{bmatrix} 0 \\ -\frac{1}{m_W} \\ 0 \\ \frac{1}{m_B} \\ 0 \end{bmatrix}}_{\mathbf{A}_{q,2}} F_{c_S}(x_{q,2} - x_{q,4}) = \mathbf{f}_q\left(\mathbf{x}_q, u_q, \mathbf{z}_q\right) ,\end{aligned} \tag{3.23}$$

where $\mathbf{B}_q \in \mathbb{R}^{5\times 1}$ is the input vector and $\mathbf{E}_q \in \mathbb{R}^{5\times 1}$ the road excitation disturbance vector. Last, in a more readable form, the state space equation with linear and nonlinear dynamics:

$$\dot{\mathbf{x}}_q = \underbrace{\mathbf{A}_{q,1}\mathbf{x}_q}_{\text{linear dynamics}} + \underbrace{\mathbf{B}_q u_q}_{\text{input}} + \underbrace{\mathbf{E}_q z_q}_{\text{road excitation}} + \underbrace{\mathbf{A}_{q,2}\left(F_{k_S,nonlin}(x_{q,3}) + F_{c_S}(x_{q,2} - x_{q,4})\right)}_{\text{nonlinear dynamics}} . \tag{3.24}$$

The two degrees-of-freedom state-space model obtained herewith captures the lifting motions of a vehicle driving on a road. The parameters used for the simulation study are given in Appx. A.1.

3.5.2 Half-Car

Based on the equations of motion (3.6), (3.7) and (3.8), the following equations are obtained by substituting gravitational, suspension and tire forces:

$$\begin{aligned} m_B\ddot{z}_B &= -F_{g_B} + F_{k_S,r} + F_{c_S,r} + F_{k_S,f} + F_{c_S,f} \\ &= -m_B g + \underbrace{F_{k_S,stat,r} + F_{k_S,lin,r} + F_{k_S,nonlin,r}}_{F_{k_S,r}} + F_{c_S,r} \\ &\quad + \underbrace{F_{k_S,stat,f} + F_{k_S,lin,f} + F_{k_S,nonlin,f}}_{F_{k_S,f}} + F_{c_S,f} \end{aligned} \tag{3.25}$$

Die approbierte gedruckte Originalversion dieser Diplomarbeit ist an der TU Wien Bibliothek verfügbar
The approved original version of this thesis is available in print at TU Wien Bibliothek.
TU Bibliothek Your knowledge hub WIEN

$$\begin{aligned} I_B\ddot{\varphi}_B &= F_B h_B - F_T h_T + F_{k_S,r} l_r + F_{c_S,r} l_r - F_{k_S,f} l_f - F_{c_S,f} l_f \\ &= F_B h_B - F_T h_T + \underbrace{(F_{k_S,stat,r} + F_{k_S,lin,r} + F_{k_S,nonlin,r})}_{F_{k_S,r}} l_r + F_{c_S,r} l_r \\ &\quad - \underbrace{(F_{k_S,stat,f} + F_{k_S,lin,f} + F_{k_S,nonlin,f})}_{F_{k_S,f}} l_f - F_{c_S,f} l_f \end{aligned} \tag{3.26}$$

$$\begin{aligned} m_{W,i}\ddot{z}_{W,i} &= -F_{g_W,i} - F_{k_S,i} - F_{c_S,i} + F_{k_T,i} + F_{c_T,i} \\ &= -m_{W,i} g - \underbrace{F_{k_S,stat,i} - F_{k_S,lin,i} - F_{k_S,nonlin,i}}_{F_{k_S,i}} - F_{c_S,i} \\ &\quad + \underbrace{F_{k_T,stat,i} + F_{k_T,lin,i}}_{F_{k_T,i}} + F_{c_T,i} \end{aligned} \tag{3.27}$$

Note that the nonlinear terms $F_{k_S,nonlin,r}$ and $F_{k_S,nonlin,f}$ for the rear and front suspensions are governed by (3.11), but differently parameterized. The dampers determined by (3.12) are also parameterized differently for the rear and front axles. The index $i \in \{r, f\}$ in (3.27) denotes the axle. Remaining forces are further defined as:

$$\text{static suspension force:} \quad F_{k_S,stat,i} = k_{S,i} \Delta z_{S,stat,i} \,, \tag{3.28a}$$

$$\text{linear suspension spring force:} \quad F_{k_S,lin,i} = k_{S,i} \Delta z_{S,dyn,i} \,, \tag{3.28b}$$

$$\text{static tire spring force:} \quad F_{k_T,stat,i} = k_{T,i} \Delta z_{T,stat,i} \,, \tag{3.28c}$$

$$\text{linear tire spring force:} \quad F_{k_T,lin,i} = k_{T,i}(\zeta_i - z_{W,i}) = k_{T,i} \Delta z_{T,dyn,i} \,, \tag{3.28d}$$

$$\text{linear tire damping force:} \quad F_{c_T,i} = c_{T,i}(\dot{\zeta}_i - \dot{z}_{W,i}) = c_{T,i} \Delta \dot{z}_{T,i} \,. \tag{3.28e}$$

with the linear constants for suspension $k_{S,i}$, tire stiffness $k_{T,i}$ and tire damping coefficient $c_{T,i}$. The dynamic suspension deflection $\Delta z_{S,dyn,i}$ is not as straight forward as in the quarter-car case as the deflection of the spring is linked to the pitch angle of the vehicle. The spring deflection for the front axle is given by $\Delta z_{S,dyn,f} = z_{W,f} + \varphi_B l_f - z_B$ and for the rear axle as $\Delta z_{S,dyn,r} = z_{W,r} - \varphi_B l_r - z_B$.

Control Input The longitudinal motion is dictated by the braking and acceleration forces F_B and F_T, respectively, in (3.5). Similar to the quarter-car, the equation is

Die approbierte gedruckte Originalversion dieser Diplomarbeit ist an der TU Wien Bibliothek verfügbar
The approved original version of this thesis is available in print at TU Wien Bibliothek.
TU Bibliothek Your knowledge hub WIEN

rearranged such that the vehicle acceleration emerges as the new input:

$$\ddot{s} = \dot{v} = \frac{\overbrace{F_T - F_B}^{F_D}}{\underbrace{m_B + m_{W,r} + m_{W,f}}_{m_{\text{total}}}} = a \tag{3.29}$$

Compared with the quarter-car, the drive forces occur not only in the longitudinal equations of motion but as well in the pitching equations. Hence, it is necessary to rewrite the input $(F_B h_B - F_T h_T)$ in (3.7) so that the vehicle acceleration is retained as input:

$$F_B h_B - F_T h_T = -p_h\left(F_D\right) F_D = -p_h\left(a\right) m_{\text{total}} a\,, \tag{3.30}$$

where the nonlinear function $p_h\left(\cdot\right)$ switches between the braking or accelerating leverage arm lengths through

$$p_h\left(\cdot\right) = \begin{cases} h_T & \text{for } F_D > 0 \text{ or } a > 0\,, \\ h_B & \text{for } F_D < 0 \text{ or } a < 0\,. \end{cases} \tag{3.31}$$

It is further assumed that F_B and F_T cannot occur simultaneously; no simultaneous braking or acceleration.

Static Displacement Similar to the quarter-car, the static deflections for tire and suspension springs are determined as follows: From the given set of Eqs. (3.25) to (3.27) four static deflections are to be calculated by setting the time-dependent parts to zero. The static deflection of the rear and front suspension are calculated from the conservation of momentum and impulse of the body. The static deflection of the body springs is thus yielded by:

$$F_{k_S,stat,r} = k_{S,r}\Delta z_{S,stat,r} = F_{g_B}\frac{l_f}{l_f + l_r} \quad \longrightarrow \quad \Delta z_{S,stat,r} = \frac{m_B g}{k_{S,r}}\frac{l_f}{l_f + l_r}\,, \tag{3.32}$$

$$F_{k_S,stat,f} = k_{S,f}\Delta z_{S,stat,f} = F_{g_B}\frac{l_r}{l_f + l_r} \quad \longrightarrow \quad \Delta z_{S,stat,f} = \frac{m_B g}{k_{S,f}}\frac{l_r}{l_f + l_r}\,. \tag{3.33}$$

The remaining static deflections of the tires are evaluated by substituting the previously found deflections into the vertical equations of motion of the rear and front wheels:

$$\begin{aligned} F_{k_T,stat,r} &= k_{T,r}\Delta z_{T,stat,r} \\ &= F_{g_T,r} + F_{k_S,stat,r} \quad \longrightarrow \quad \Delta z_{T,stat,r} = \frac{g}{k_{T,r}}\left(m_{W,r} + m_B\frac{l_f}{l_f + l_r}\right)\,, \end{aligned} \tag{3.34}$$

Die approbierte gedruckte Originalversion dieser Diplomarbeit ist an der TU Wien Bibliothek verfügbar
The approved original version of this thesis is available in print at TU Wien Bibliothek.
TU Bibliothek Your knowledge hub WIEN

$$
\begin{aligned}
F_{k_T,stat,f} &= k_{T,f}\Delta z_{T,stat,f} \\
&= F_{g_T,f} + F_{k_S,stat,f} \quad \longrightarrow \quad \Delta z_{T,stat,f} = \frac{g}{k_{T,f}}\left(m_{W,f} + m_B\frac{l_f}{l_f+l_r}\right) .
\end{aligned} \tag{3.35}
$$

The equations of motion in (3.25) to (3.27) are combined with the definition of the static displacement obtained before and the new input to gain the final set of equations:

$$\ddot{z}_{W,r} = \frac{1}{m_{W,r}}\left(-F_{k_S,lin,r} - F_{k_S,nonlin,r} - F_{c_S,r} + F_{k_T,lin,r} + F_{c_T,r}\right) , \tag{3.36a}$$

$$\ddot{z}_{W,f} = \frac{1}{m_{W,f}}\left(-F_{k_S,lin,f} - F_{k_S,nonlin,f} - F_{c_S,f} + F_{k_T,lin,f} + F_{c_T,f}\right) , \tag{3.36b}$$

$$\ddot{z}_B = \frac{1}{m_B}\left(F_{k_S,lin,r} + F_{k_S,nonlin,r} + F_{c_S,r} + F_{k_S,lin,f} + F_{k_S,nonlin,f} + F_{c_S,f}\right) , \tag{3.36c}$$

$$
\begin{aligned}
\ddot{\varphi}_B = \frac{1}{I_B}\big(&- p_h(a) m_{tot} a + F_{c_S,r} l_r - F_{c_S,f} l_f \\
&- \left(F_{k_S,lin,f} + F_{k_S,nonlin,f}\right) l_f + \left(F_{k_S,lin,r} + F_{k_S,nonlin,r}\right) l_r\big)
\end{aligned} \quad , \tag{3.36d}
$$

$$\ddot{s} = a\,. \tag{3.36e}$$

The equations thus obtained represent a four degree-of-freedom vehicle model capable of capturing the pitch and vertical motions of a vehicle.

State Space Model The set of Eqs. (3.36) is transformed into a state space model by introducing the following state vector $\mathbf{x}_h$, input u_h and disturbances vector $\mathbf{z}_h$, which is composed of the road excitation of the front and rear axle, with the index h for the half-car:

$$
\mathbf{x}_h = \begin{bmatrix} x_{h,1} \\ x_{h,2} \\ x_{h,3} \\ x_{h,4} \\ x_{h,5} \\ x_{h,6} \\ x_{h,7} \\ x_{h,8} \\ x_{h,9} \end{bmatrix} = \begin{bmatrix} \zeta_r - z_{W,r} \\ \dot{z}_{W,r} \\ \zeta_f - z_{W,f} \\ \dot{z}_{W,f} \\ z_{W,r} - \varphi_B l_r - z_B \\ \dot{z}_B \\ z_{W,f} + \varphi_B l_f - z_B \\ \dot{\varphi}_B \\ v \end{bmatrix} , \quad \dot{\mathbf{x}}_h = \begin{bmatrix} \dot{\zeta}_r - x_{h,2} \\ \ddot{z}_{W,r} \\ \dot{\zeta}_f - x_{h,4} \\ \ddot{z}_{W,f} \\ x_{h,2} - x_{h,8} l_r - x_{h,6} \\ \ddot{z}_B \\ x_{h,4} + x_{h,8} l_f - x_{h,6} \\ \ddot{\varphi}_B \\ \dot{v} \end{bmatrix} , \quad u_h = a, \quad \mathbf{z}_h = \begin{bmatrix} \dot{\zeta}_r \\ \dot{\zeta}_f \end{bmatrix} . \tag{3.37}
$$

Similar to the quarter-car, the state space equation is set up by substituting the set of Eqs. (3.36a) - (3.36e) into the time derivatives in (3.37). The final state space system is

Die approbierte gedruckte Originalversion dieser Diplomarbeit ist an der TU Wien Bibliothek verfügbar
The approved original version of this thesis is available in print at TU Wien Bibliothek.
TU Bibliothek Your knowledge hub WIEN

decomposed into a linear system dynamic with the matrix $\mathbf{A}_{h,1} \in \mathbb{R}^{9\times9}$ and a nonlinear part with the vector $\mathbf{A}_{h,2} \in \mathbb{R}^{9\times1}$. Inserting the definitions of linear forces from (3.28) as well yields:

Die approbierte gedruckte Originalversion dieser Diplomarbeit ist an der TU Wien Bibliothek verfügbar
The approved original version of this thesis is available in print at TU Wien Bibliothek.
TU Bibliothek Your knowledge hub WIEN

Die approbierte gedruckte Originalversion dieser Diplomarbeit ist an der TU Wien Bibliothek verfügbar
The approved original version of this thesis is available in print at TU Wien Bibliothek.

$$\dot{\mathbf{x}}_h = \underbrace{\begin{bmatrix} 0 & -1 & 0 & 0 & 0 & 0 & 0 & 0 & 0 \\ \frac{k_{T,r}}{m_{W,r}} & -\frac{c_{T,r}}{m_{W,r}} & 0 & 0 & -\frac{k_{S,r}}{m_{W,r}} & 0 & 0 & 0 & 0 \\ 0 & 0 & 0 & -1 & 0 & 0 & 0 & 0 & 0 \\ 0 & 0 & \frac{k_{T,f}}{m_{W,f}} & -\frac{c_{T,f}}{m_{W,f}} & 0 & 0 & -\frac{k_{S,f}}{m_{W,f}} & 0 & 0 \\ 0 & 1 & 0 & 0 & 0 & -1 & 0 & -l_r & 0 \\ 0 & 0 & 0 & 0 & \frac{k_{S,r}}{m_B} & 0 & \frac{k_{S,f}}{m_B} & 0 & 0 \\ 0 & 0 & 0 & 1 & 0 & -1 & 0 & l_f & 0 \\ 0 & 0 & 0 & 0 & \frac{l_r k_{S,r}}{I_B} & 0 & -\frac{l_f k_{S,f}}{I_B} & 0 & 0 \\ 0 & 0 & 0 & 0 & 0 & 0 & 0 & 0 & 0 \end{bmatrix}}_{\mathbf{A}_{h,1}} \mathbf{x}_h + \underbrace{\begin{bmatrix} 0 \\ 0 \\ 0 \\ 0 \\ 0 \\ 0 \\ 0 \\ -\frac{m_B}{I_B} p_h(u_h) \\ 1 \end{bmatrix}}_{\mathbf{B}_h(u_h)} u_h + \underbrace{\begin{bmatrix} 1 & 0 \\ \frac{c_{T,r}}{m_{T,r}} & 0 \\ 0 & 1 \\ 0 & \frac{c_{T,f}}{m_{W,f}} \\ 0 & 0 \\ 0 & 0 \\ 0 & 0 \\ 0 & 0 \\ 0 & 0 \end{bmatrix}}_{\mathbf{E}_h} \mathbf{z}_h \tag{3.38}$$

$$+ \underbrace{\begin{bmatrix} 0 & 0 \\ -\frac{1}{m_{W,r}} & 0 \\ 0 & 0 \\ 0 & -\frac{1}{m_{W,f}} \\ 0 & 0 \\ \frac{1}{m_B} & \frac{1}{m_B} \\ 0 & 0 \\ \frac{l_r}{I_B} & -\frac{l_f}{I_B} \end{bmatrix}}_{\mathbf{A}_{h,2}} \underbrace{\begin{bmatrix} F_{k_S,nonlin,r}(x_{h,5}) \\ F_{k_S,nonlin,f}(x_{h,7}) \end{bmatrix}}_{\mathbf{F}_{k_S,nonlin}(\mathbf{x}_h)} + \underbrace{\begin{bmatrix} 0 & 0 \\ -\frac{1}{m_{W,r}} & 0 \\ 0 & 0 \\ 0 & -\frac{1}{m_{W,f}} \\ 0 & 0 \\ \frac{1}{m_B} & \frac{1}{m_B} \\ 0 & 0 \\ \frac{l_r}{I_B} & -\frac{l_f}{I_B} \end{bmatrix}}_{\mathbf{A}_2} \underbrace{\begin{bmatrix} F_{c_S,r}(x_{h,2} - x_{h,8} b - x_{h,6}) \\ F_{c_S,f}(x_{h,4} + x_{h,8} a - x_{h,6}) \end{bmatrix}}_{\mathbf{F}_{c_S}(\mathbf{x}_h)} = \mathbf{f}_h\left(\mathbf{x}_h, u_h, \mathbf{z}_h\right) ,$$

where $\mathbf{B}_h(u_h) \in \mathbb{R}^{9\times 1}$ is the nonlinear input vector and $\mathbf{E}_h \in \mathbb{R}^{9\times 2}$ the linear disturbance matrix. In a more readable form, the state space equation with linear and nonlinear dynamics is as follows:

$$\dot{\mathbf{x}}_h = \underbrace{\mathbf{A}_{h,1}\mathbf{x}_h}_{\text{linear dynamics}} + \underbrace{\mathbf{B}_h(u_h)u_h}_{\text{input}} + \underbrace{\mathbf{E}_h\mathbf{z}_h}_{\text{road excitation}} + \underbrace{\mathbf{A}_{h,2}\left(\mathbf{F}_{k_S,nonlin}(\mathbf{x}_h) + \mathbf{F}_{c_S}(\mathbf{x}_h)\right)}_{\text{nonlinear dynamics}} . \tag{3.39}$$

Later in this thesis, it becomes necessary to consider the jerk $j = \frac{da}{dt}$ as input to the system instead of the vehicle acceleration a. For this purpose, an integrator ($x_{h,10} = a$, $\dot{x}_{h,10} = j$, $u_h = j$) is added to the system. The final state space equation[5] with linear system matrix $\mathbf{A}_{h,1} \in \mathbb{R}^{10\times 10}$, input vector $\mathbf{B}_h \in \mathbb{R}^{10\times 1}$, disturbance input $\mathbf{E}_h \in \mathbb{R}^{10\times 2}$, nonlinear dynamics vectors $\mathbf{A}_{h,2} \in \mathbb{R}^{10\times 1}$ and $\mathbf{A}_{h,3} \in \mathbb{R}^{10\times 1}$ read

$$\begin{aligned}\dot{\mathbf{x}}_h = \underbrace{\mathbf{A}_{h,1}\mathbf{x}_h}_{\text{linear dynamics}} + \underbrace{\mathbf{B}_h u_h}_{\text{input}} + \underbrace{\mathbf{E}_h\mathbf{z}_h}_{\text{road excitation}} \\ + \underbrace{\mathbf{A}_{h,2}\left(\mathbf{F}_{k_S,nonlin}(\mathbf{x}_h) + \mathbf{F}_{c_S}(\mathbf{x}_h)\right) + \mathbf{A}_{h,3}p_h(x_{h,10})x_{h,10}}_{\text{nonlinear dynamics}} .\end{aligned} \tag{3.40}$$

The parameters used for the simulation study are given in Appx. A.2.

3.6 Road-Excitation

So far, only the vehicle has been treated, but as shown in Fig. 3.1, the road itself has to be considered as well. Since this work focuses on a simulation-based approach, it is assumed that the road information is accurately known. In the literature, there are many bumps based on cosine approaches, stochastic[6] road excitations and some specialized bumps such as potholes, road crossings, or triangle shaped ones. Some of those bumps were already briefly introduced in the literature review in Ch. 2.

Cosine Bumps The cosine approach is probably one of the most widely used, e.g. [13], [25]. The function is continuously differentiable and the requirement for the tire contact

[5] The matrices are given in Appendix A.3.

[6] These are not of interest in this application because the magnitude of these excitations are not significant. Stochastic excitations are a frequently used excitation in semi-active and active wheel suspension, respectively [16].

Die approbierte gedruckte Originalversion dieser Diplomarbeit ist an der TU Wien Bibliothek verfügbar
The approved original version of this thesis is available in print at TU Wien Bibliothek.
TU Bibliothek Your knowledge hub WIEN

area is not violated[7]. The bump is given by:

$$\zeta(l) = \begin{cases} \frac{H_b}{2}\left[1 - \cos\left(\frac{2\pi}{W_b}(l - l_b)\right)\right], & \text{for } l_b \leq l \leq l_b + W_b \\ 0\,. & \text{otherwise} \end{cases} \tag{3.41}$$

Common found cosine road bumps in literature approximately have widths W_b of 0.5 m

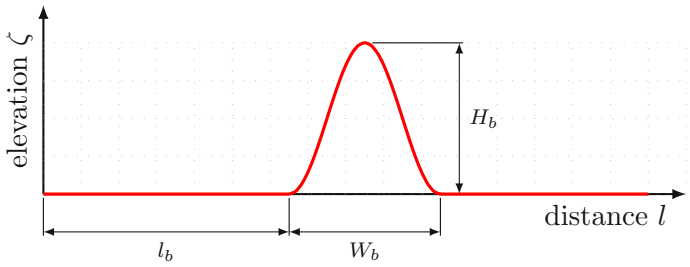

Figure 3.6: Geometric dimensions of a cosine bump.

to 1.5 m and heights H_b ranging from 5 cm to 15 cm. In this work, the length of the bump is designed to excite the vehicle with certain frequencies at a given driving speed.

Based on Frequency Analysis for Excitation of Resonant Frequencies Using the transfer function, which can be generated by applying a stochastic road excitation as described in [15], [44], [46], the amplitude spectrum of the vertical acceleration of the sprung mass of the quarter-car is shown in Fig. 3.7.

Especially the two resonant frequencies at about 1.17 Hz and 12.1 Hz are visible. Since the aim of this work is to generate a human driver model and behavior is very much influenced by sensation, the sensitivity of humans to vertical acceleration at about 5 Hz was also marked in the transfer function. With these frequencies, one can construct cosine bumps to directly excite these frequencies. Starting from (3.41), assuming a constant velocity v of the vehicle and rewriting in the time domain, the following is obtained:

$$\zeta(t) = \begin{cases} \frac{H_b}{2}\left[1 - \cos\left(2\pi\frac{v}{W_b}\left(t - \frac{l_b}{v}\right)\right)\right], & \text{for } \frac{l_b}{v} \leq t \leq \frac{l_b}{v} + \frac{W_b}{v} \\ 0\,. & \text{otherwise} \end{cases} \tag{3.42}$$

The frequency f_b of this cosine excitation is equal to $\frac{v}{W_b}$. For a given f_b, a bump length

[7] According to [44], for the use of the simplified tire model with a single-point excitation, the bump length should be at least four times the size of the tire contact patch (approx. 10–15 cm).

Die approbierte gedruckte Originalversion dieser Diplomarbeit ist an der TU Wien Bibliothek verfügbar
The approved original version of this thesis is available in print at TU Wien Bibliothek.
TU Bibliothek Your knowledge hub WIEN

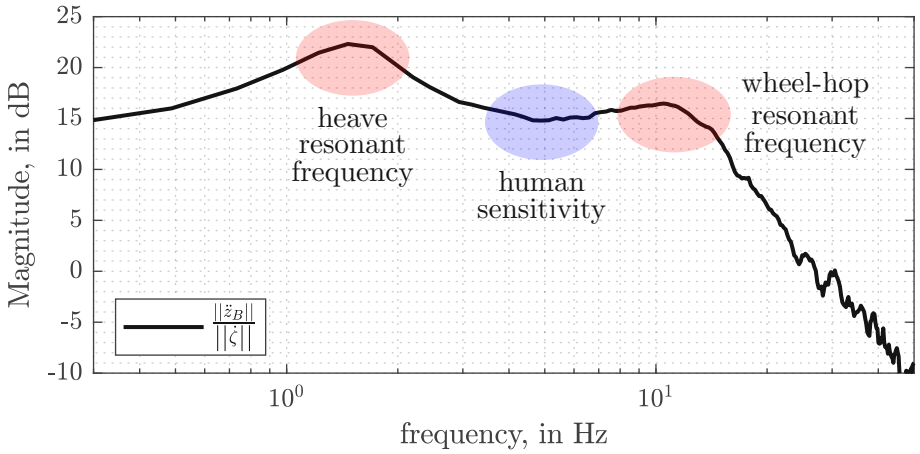

Figure 3.7: Transfer function from road input $\dot{\zeta}$ to sprung mass acceleration $\ddot{z}_B$ of the quarter-car model. Superimposed are regions of interest: The resonant frequency of the heave – around 1.17 Hz – the frequency of the wheel-hop around 12 Hz; in the range from 4–8 Hz humans are most sensitive to vertical accelerations [44].

W_b can be calculated to excite the desired frequency. The corresponding bump height H_b is chosen so that a "sensibly intense" excitation occurs. The frequencies from the transfer function of the quarter vehicle therefore result in Tab. 3.1.

bump name	f_b *in Hz*	W_b *in m*	H_B *in m*
long bump	1.17	9.50	0.1250
medium bump	5.00	2.22	0.0625
short bump	12.1	0.92	0.0250

Table 3.1: Calculated cosine bumps based on the resonant frequencies. Bumps calculated for given frequencies at $v = 40$ km/h. The height is chosen such to achieve a "sensibly intense" excitation of the vehicle.

Raised Crosswalk The raised crosswalk or road crossing, often found in low-traffic areas such as residential streets, is similar in design to the cosine approach except that it is much wider and has a flat section between the ramp-on and ramp-off. The ramps are designed with cosine functions to obtain a continuously differentiable road and not to violate the assumptions on the single-point excitation of the tire model.

The excitation is very interesting, especially for the half-car, because it can be used to excite the pitching motion to a greater extent.

Die approbierte gedruckte Originalversion dieser Diplomarbeit ist an der TU Wien Bibliothek verfügbar
The approved original version of this thesis is available in print at TU Wien Bibliothek.
TU Bibliothek Your knowledge hub WIEN

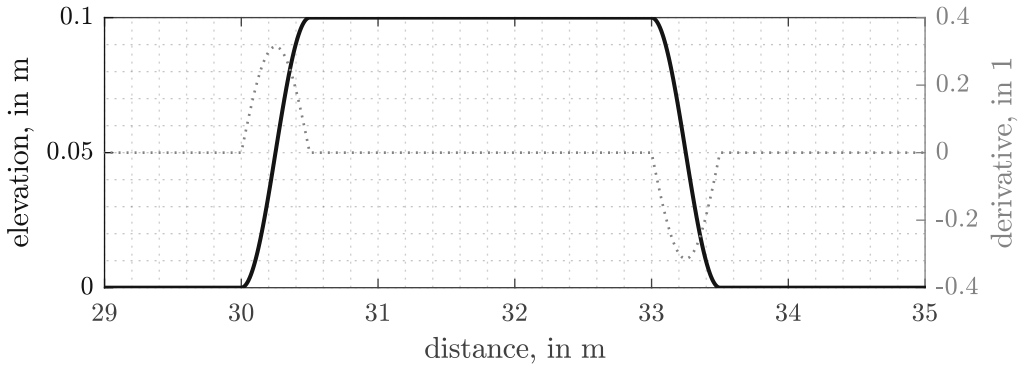

Figure 3.8: Raised crosswalk with half cosine ramps. The solid line shows the elevation $\zeta(l)$ of the raised crosswalk along the road l. The dashed line is the spatial derivative $\frac{d\zeta}{dl}$ of the crosswalk.

Potholes The pothole is a special case of cosine excitation or raised crosswalk, since it is a variant mirrored about the horizontal axis. Examples and illustrations can be found in Sec. 5.1.

Pavement Curb The curb is a special case of the raised crosswalk as it features only the ramp-on and then maintains the height. The ramp has a steeper slope. Examples and illustrations can be found in Sec. 5.1.

Road Excitation: Mathematical Formulation For the novel model predictive driver model, it has to be additionally considered that the underlying MPC operates in a discrete-time fashion. The road excitation cannot be considered continuously and is fed in discrete points to the driver model. This yields at time t a discrete point vector $\boldsymbol{Z}(t) \in \mathbb{R}^{N_s}$ with a constant sampling distance $\Delta l_s \in \mathbb{R}_{>0}$, see the top sketch in Fig. 3.9:

$$\boldsymbol{Z}(t) = \begin{bmatrix} \zeta_0(t) & \zeta_1(t) & \cdots & \zeta_{N_s-1}(t) \end{bmatrix}^T , \tag{3.43}$$

where the elements $\zeta_j(t)$ are the discrete points of the road with $j \in \{0, 1, \ldots, N_s - 1\}$, $N_s = \lfloor \frac{l_{prev}}{\Delta l_s} \rfloor \in \mathbb{Z}_+$ and the preview length $l_{prev} \in \mathbb{R}_{>0}$.

As can be seen in (3.24) and (3.39), the road is considered by the time derivative $z_q = \dot{\zeta}$ or $\mathbf{z}_h = \begin{bmatrix} \dot{\zeta}_r & \dot{\zeta}_f \end{bmatrix}^T$. In general, the derivative $\dot{\zeta}$ can be written as follows:

$$\dot{\zeta}(t) = \frac{d\zeta\left(l(t)\right)}{dt} = \frac{\partial \zeta}{\partial l}\frac{\partial l}{\partial t} = \zeta'(l)v(t)\,. \tag{3.44}$$

Die approbierte gedruckte Originalversion dieser Diplomarbeit ist an der TU Wien Bibliothek verfügbar
The approved original version of this thesis is available in print at TU Wien Bibliothek.
TU Bibliothek Your knowledge hub WIEN

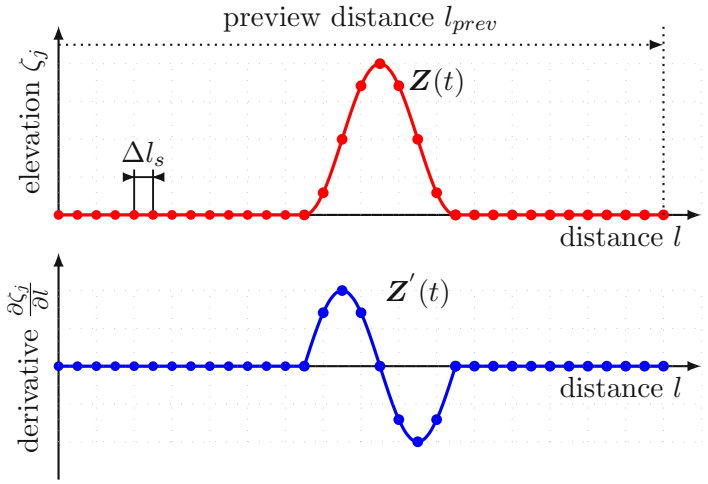

Figure 3.9: Road sampling with equidistant spacial intervals Δl_s. Upper sketch depicts the surface of the road $\mathbf{Z}(t)$ ahead of the vehicle at time t and the lower one is the computed spatial derivative $\mathbf{Z}'(t)$.

As can be seen in (3.44), the road input depends not only on the current spatial derivative at the vehicle's position, but also on the speed at which the vehicle is traveling. This means that for the same road obstacle, the excitation of the vehicle becomes more intense with increasing speed. Furthermore, in order to know the excitation at time t, the position of the vehicle must be known beforehand, but this depends on the vehicle's speed. Since the vehicle speed is not known a priori, the position and thus the excitation is also unknown. How this problem is tackled in this thesis will be explained again in more detail in the next chapter.

For the sake of completeness, the spatial derivative $\boldsymbol{Z}'(t)$ shall be defined similar as

$$\boldsymbol{Z}'(t) = \begin{bmatrix} \zeta_0'(t) & \zeta_1'(t) & \cdots & \zeta_{N_s-1}'(t) \end{bmatrix}^T . \tag{3.45}$$

Die approbierte gedruckte Originalversion dieser Diplomarbeit ist an der TU Wien Bibliothek verfügbar
The approved original version of this thesis is available in print at TU Wien Bibliothek.
TU Bibliothek Your knowledge hub WIEN

4 Driver Modeling

This chapter addresses the model predictive driver model to be used to generate human-like speed and acceleration trajectories for a vehicle in the presence of road obstacles. In Fig. 4.1 the underlying control problem is sketched. A vehicle is driven on a road. The driver observes with a constant distance – preview distance l_{prev} – the road in front. Information about the road and vehicle are fed into a trajectory generation MPC and an optimal velocity and/or acceleration trajectory is planned.

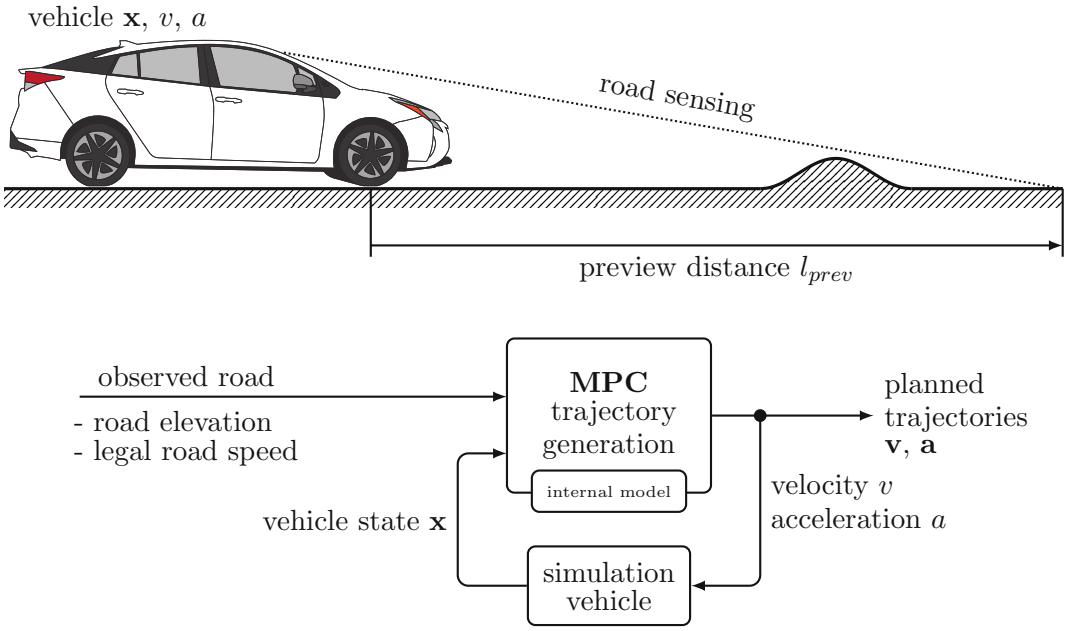

Figure 4.1: Trajectory optimization task for the vehicle–road problem.[1]Based on the current vehicle state $\mathbf{x}$ and the observed road, the predictive driver model plans the speed/acceleration trajectory for a preview distance l_{prev}. The MPC uses an internal vehicle model that maps the driving situation; internal model and simulation model are usually different.

The goal of the predictive driver model is to capture the planning behavior of humans when driving over irregularities of the road. The behavior is influenced by three objec-

[1]Vehicle graphic from vecteezy.com

Die approbierte gedruckte Originalversion dieser Diplomarbeit ist an der TU Wien Bibliothek verfügbar
The approved original version of this thesis is available in print at TU Wien Bibliothek.

tives that the driver tries to balance: First, and probably most important, the driver tries to increase the vertical comfort for passengers, which is affected by the movement of the vehicle excited by the obstacle on the road. For this purpose, the driver resorts to braking and acceleration maneuvers to reduce the intensity of the excitation caused by the road obstacle. Second, the driver attempts to improve comfort without performing inconvenient braking and acceleration maneuvers – therefore, longitudinal comfort is also taken into account. Third, the driver aims to pass the obstacle as quickly as possible and not lose too much time due to long periods of low driving speed. If possible, the vehicle should always drive close to the legal speed limit and the transition time should be kept as short as possible. To accommodate these objectives several factors like the sprung body acceleration, longitudinal vehicle acceleration, braking and longitudinal jerk need to be considered. The objectives are considered in form of a cost function in the subsequent trajectory optimization problem which is carried out by the MPC. The aim of this chapter is to analyze the impact of the design of the cost function and the weighting factors of the different objectives on the resulting trajectories. The resulting trajectories are examined in terms of human behavior on the basis of requirements set forth in this text, which have been derived from experience. It is also of interest to see how different driving styles can be represented in the cost function, e.g., an aggressive driver or a conservative driver.

The remainder of this chapter is structured as followed. The optimization problem for generating the trajectories, as depicted in Fig. 4.1, is formulated in Sec. 4.1. In Sec. 4.2 the differential equations of the internal vehicle model are rewritten from equations in time to equations in space. In the subsequent Sec. 4.3 the equations of motion are discretized for use in the predictive driver model. In Sec. 4.4, the cost function is set up meticulously and the various terms in the cost function are examined for the influence on the shape of the planned trajectory. The cost function is first developed for the quarter-car in Sec. 4.4.1 and later extended for the half-car in Sec. 4.4.2.

4.1 MPC based Trajectory Optimization

It is already known from Sec. 3.6 that the subsequent MPC requires the road information in discretely sampled form. Furthermore, it is understood from the vehicle models that the road does not directly excite the vehicle via the road height ζ, but via its spatial derivative or rising speed $\zeta' = \frac{d\zeta}{dl}$. Casting the problem depicted in the chapter introduction into more technical terms, the driver model in this situation is dealing

Die approbierte gedruckte Originalversion dieser Diplomarbeit ist an der TU Wien Bibliothek verfügbar
The approved original version of this thesis is available in print at TU Wien Bibliothek.
TU Bibliothek Your knowledge hub WIEN

with a trajectory optimization problem: Given the current vehicle[2] state vector $\boldsymbol{x}_k$ and the observed road segment $\boldsymbol{Z}_k^{'}$, which contains the spatial derivatives discretely sampled between the vehicle and the preview point, at time k, the driver model plans how to behave on the road segment based on the cost function and the model of the vehicle-road problem – the internal model. The outputs of the driver model are planned trajectories $\tilde{\mathbf{X}}_k$ for the vehicle states and $\tilde{\mathbf{U}}_k$ for the control input, e.g. longitudinal acceleration, along the preview horizon. The driver model applies the first control input of the planned trajectory and continuously updates the plan/trajectory for approaching and traversing the road obstacle – in control theory, this approach is called the *receding horizon principle*. In this text, the planned control input is applied directly to the simulation vehicle. In a real application, a lower level controller in the vehicle would try to follow the planned trajectory. The entire control structure is shown in Fig. 4.2.

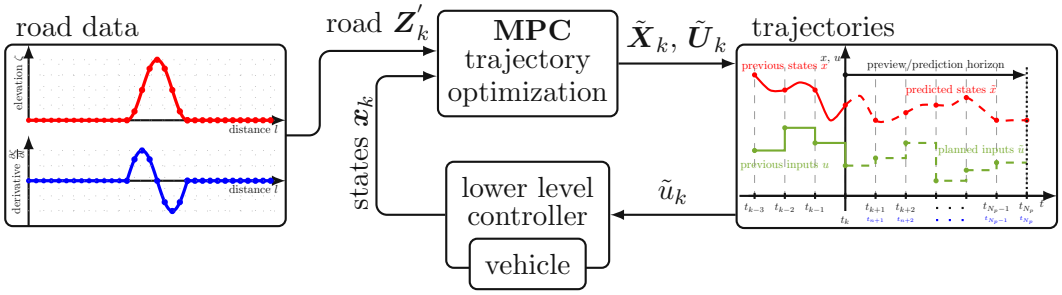

Figure 4.2: Trajectory optimization problem: Given the road information $\mathbf{Z}_k^{'}$ and vehicle state $\boldsymbol{x}_k$ at instant k the driver optimizes output trajectories $\tilde{\mathbf{X}}_k$ and $\tilde{\mathbf{U}}_k$ which are then applied to the underling system. In a real application, a lower level controller operates the vehicle and aims to follow the planned trajectory. In the present study, the planned accelerations/speeds are applied directly.

If this problem of trajectory optimization is now attempted to be captured mathematically, it can be done either in continuous or discrete form. In essence, optimization distinguishes between dynamic optimization or static optimization. While in the former a function space is optimized and thus results in a continuous trajectory, in the latter a finite dimensional, usually Euclidean space, is optimized and results in a discrete trajectory [41]. Dynamic optimization is a very popular method for trajectory optimization problems and is widely used here with e.g., Pontryagin's maximum principle. Unfortunately, in this optimization the treatment of state constraints is not as straightforward [41]. Due to the problems mentioned above, the trajectory optimization problem is solved using a MPC in discrete form and the first input is applied to the real system in

[2]For the sake of readability, the subscript for the quarter- and half-car are omitted.

Die approbierte gedruckte Originalversion dieser Diplomarbeit ist an der TU Wien Bibliothek verfügbar
The approved original version of this thesis is available in print at TU Wien Bibliothek.
TU Bibliothek Your knowledge hub WIEN

the receding horizon fashion.

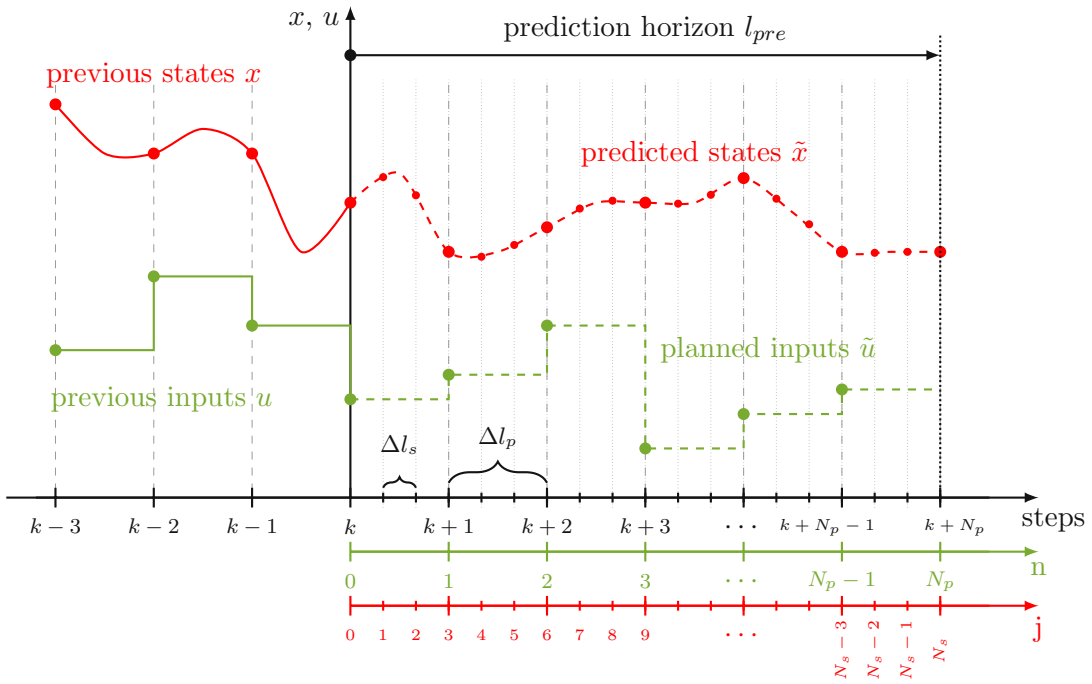

Figure 4.3: Predicted states $\tilde{\mathbf{x}}$ and passed states $\mathbf{x}$, planned inputs $\tilde{u}$ and applied inputs u schematically sketched at step k. Figure adapt from [39], [40] for discrete steps. Note that the step size between the planned inputs and the predicted states is different. Over several prediction steps, the inputs are kept constant or blocked. This allows for smaller prediction steps while keeping the overall optimization parameters – the inputs – small over the horizon.

The trajectory optimization problem shown in Fig. 4.2 and Fig. 4.3 given the vehicle state $\mathbf{x}_k$ and road data $\mathbf{Z}_k^{'}$ at instant k is stated as follows:

$$\tilde{\mathbf{U}}_k^* = \underset{\tilde{\mathbf{U}}_k}{\arg\min} \quad J(\tilde{\mathbf{X}}_k, \tilde{\mathbf{U}}_k, \mathbf{Z}_k^{'}) \tag{4.1a}$$

$$\text{s.t.} \quad \tilde{\mathbf{x}}_{k|j+1} = \mathbf{f}(\tilde{\mathbf{x}}_{k|j}, z_{k|j}, \tilde{u}_{k|n}), \quad \tilde{\mathbf{x}}_{k|0} = \mathbf{x}_k, \tag{4.1b}$$

$$\tilde{\mathbf{x}}_{k|j} \in \mathcal{X}, \quad \forall j = 0, 1, \ldots, N_s - 1 \tag{4.1c}$$

$$\tilde{u}_{k|n} \in \mathcal{U}, \quad \forall n = 0, 1, \ldots, N_p - 1 \tag{4.1d}$$

$$\tilde{\mathbf{x}}_{k|N_s} \in \mathcal{X}_T, \tag{4.1e}$$

where N_s is the number of prediction steps[3] and is given as $N_s = \lfloor \frac{l_{pre}}{\Delta l_s} \rfloor$, N_p is the number

[3]The floor function $\lfloor f \rfloor$ of a real number f gives the greatest integer less than or equal to f.

Die approbierte gedruckte Originalversion dieser Diplomarbeit ist an der TU Wien Bibliothek verfügbar
The approved original version of this thesis is available in print at TU Wien Bibliothek.
TU Bibliothek Your knowledge hub WIEN

of times the input can be modified in the preview horizon and is given by $N_P = \lfloor \frac{l_{pre}}{\Delta l_p} \rfloor$, Δl_s and Δl_p are the corresponding step sizes for state prediction and control variable, respectively, as shown in Fig. 4.3. Normally the step sizes are equal, but as will be discussed later, the step size Δl_s for the discrete system must be chosen rather small. To avoid that the number of optimization variables or control actions over the vehicle horizon become too large, a different step size Δl_p is introduced for this purpose. In control engineering this is also called *move blocking*, because the control variable is required to be constant over several prediction steps Δl_s – the action/move is blocked. The sets $\mathcal{X}, \mathcal{U}$ and $\mathcal{X}_T$ will be treated later and for the moment it shall be assumed that they are given. Analogously, let the scalar cost function $J(\cdot)$ be taken as given for the moment. The optimal solution to the optimization problem is denoted by $\tilde{\mathbf{U}}_k^*$ and the optimal cost as $J^*(\tilde{\mathbf{X}}_k, \tilde{\mathbf{U}}_k^*, \mathbf{Z}_k^{'})$. Whereby the trajectories are defined as

$$\mathbf{Z}_k^{'} = \begin{bmatrix} z_{k|0} & z_{k|1} & \dots & z_{k|N_s-2} & z_{k|N_s-1} \end{bmatrix}^T, \tag{4.2a}$$

$$\tilde{\mathbf{X}}_k = \begin{bmatrix} \tilde{\mathbf{x}}_{k|0} & \tilde{\mathbf{x}}_{k|1} & \dots & \tilde{\mathbf{x}}_{k|N_s-2} & \tilde{\mathbf{x}}_{k|N_s-1} \end{bmatrix}^T, \tag{4.2b}$$

$$\tilde{\mathbf{U}}_k = \begin{bmatrix} \tilde{u}_{k|0} & \tilde{u}_{k|1} & \dots & \tilde{u}_{k|N_p-2} & \tilde{u}_{k|N_p-1} \end{bmatrix}^T. \tag{4.2c}$$

Here for the quarter-car $\mathbf{Z}_k^{'} \in \mathbb{R}^{N_s}$, $\tilde{\mathbf{U}}_k \in \mathbb{R}^{N_p}$ and $\tilde{\mathbf{X}}_k \in \mathbb{R}^{N_s \times 5}$ and for the half-car $\mathbf{Z}_k^{'} \in \mathbb{R}^{N_s \times 2}$, $\tilde{\mathbf{U}}_k \in \mathbb{R}^{N_p}$ and $\tilde{\mathbf{X}}_k \in \mathbb{R}^{N_s \times 9}$. Note that the individual elements of the road $\mathbf{Z}_k^{'}$ given by (4.2a) are scalars for the quarter-car and vectors for the half-car.

4.2 From Time to Space

In this section, the state-space equations from the previous chapter are rewritten from a set of differential equations in time t to a set of differential equations depending on the road distance l, thus removing the dependence of velocity in the road excitation. One of the major problems with the current formulation of the MPC is that for temporal prediction, the predicted distance depends on the speed traveled and thus always varies. At low speeds, the predicted distance is short, while at high speeds it is long. This would mean that a previously visible obstacle could disappear in the next instant, as the speed decreases and the predicted distance reduces. A possible approach to circumvent this problem was shown by Wu in [13]: In that work, multiple MPCs were set up with different prediction times. However, in this work, to maintain a constant prediction distance, it was chosen to transform the state-space equations into the spatial domain.

The road input in the system equations for the quarter- or half-car is according

Die approbierte gedruckte Originalversion dieser Diplomarbeit ist an der TU Wien Bibliothek verfügbar
The approved original version of this thesis is available in print at TU Wien Bibliothek.
TU Bibliothek Your knowledge hub WIEN

to (3.44):

$$\dot{\zeta}(t) = \frac{\partial \zeta}{\partial l}\frac{\partial l}{\partial t} = \zeta'(l)v(t)\,,$$

which corresponds to the chain rule and gives the vehicle speed $v(t)$ times road excitation $\zeta'(l)$. Similarly, for the time derivative of the state vector $\dot{\mathbf{x}}$ holds $\dot{\mathbf{x}} = \mathbf{x}^{'}v$. By inserting the time derivatives for the state vector and road excitation with the chain rule, the equations of motion of the quarter- and half-car are transferred to the spatial domain.

Quarter-Car Inserting and dividing the set of differential equations by the vehicle speed $v = x_{q,5}$, the previous road input $z_q(t) = \dot{\zeta}(t)$ will now be $z_q(l) = \zeta^{'}(l)$ and the equations are

$$\mathbf{x}_q^{'} = \mathbf{f}_q(\mathbf{x}_q, z_q, u_q) = \frac{\mathbf{A}_{q,1}}{x_{q,5}}\mathbf{x}_q + \frac{\mathbf{B}_q}{x_{q,5}}u_q + \mathbf{E}_q z_q + \frac{\mathbf{A}_{q,2}}{x_{q,5}}\left(F_{k_S,nonlin}(x_{q,3}) + F_{c_S}(x_{q,2} - x_{q,4})\right)\,. \tag{4.3}$$

The equations now describe a dynamic system in the spatial domain and not in time, and thus for a prediction horizon the preview distance/horizon is always constant.

Half-Car Similarly, for the half-car, the road input is now $\mathbf{z}_h(l) = \begin{bmatrix}\zeta_r^{'}(l) & \zeta_f^{'}(l)\end{bmatrix}^T$, the velocity is given by $x_{h,9}$, and thus for the state-space model in (3.40) yield

$$\begin{aligned}\mathbf{x}_h^{'} = \mathbf{f}_h(\mathbf{x}_h, \mathbf{z}_h, u_h) = &\frac{\mathbf{A}_{h,1}}{x_{h,9}}\mathbf{x}_h + \frac{\mathbf{B}_h}{x_{h,9}}u_h + \mathbf{E}_h\mathbf{z}_h \\ &+ \frac{\mathbf{A}_{h,2}}{x_{h,9}}\left(\mathbf{F}_{k_S,nonlin}(\mathbf{x}_h) + \mathbf{F}_{c_S}(\mathbf{x}_h)\right) + \frac{\mathbf{A}_{h,3}}{x_{h,9}}f_h(x_{10})x_{10}\,.\end{aligned} \tag{4.4}$$

This transformation introduces the singularity $v \to 0$. To avoid a problem in solving the optimization task in (4.1), a state constraint is introduced later to always guarantee a positive velocity.

4.3 Discrete Model

The trajectory optimization is based on a discrete MPC problem and since it is known from the previous chapter that the system is nonlinear, it cannot be discretized exactly. To discretize the system, different forward time-stepping methods like the Forward-Euler, Runge-Kutta or other multistep methods are available. While the Forward-Euler is appealing for its simplicity, the accuracy, as will be shown later, is not sufficient for this application. The multistep methods are very costly in terms of computational effort and therefore were disregarded. Hence, in the following chapter, the nonlinear system

Die approbierte gedruckte Originalversion dieser Diplomarbeit ist an der TU Wien Bibliothek verfügbar
The approved original version of this thesis is available in print at TU Wien Bibliothek.
TU Bibliothek Your knowledge hub WIEN

is linearized and discretized along the trajectory. Then, the obtained discrete system is compared to an explicit Runge-Kutta formula [48] and the Forward-Euler.

4.3.1 Discrete Dynamics

The idea now is to linearize the spatial state-space equations in (4.3) and (4.4) along the points of the trajectory $\tilde{\mathbf{X}}_k$ and transform the system into a set of difference equations.

Quarter-Car: Linearized Equations Starting with linearizing the state space equation around an arbitrary operation point $\mathbf{x}_q^{0'}$, $\mathbf{x}_q^0$, u_q^0 and z_q^0:

$$\mathbf{F}(\mathbf{x}_q^{'},\, \mathbf{x}_q,\, z_q,\, u_q) = \mathbf{x}_q^{'} - \mathbf{f}_q(\mathbf{x}_q,\, z_q,\, u_q) = 0\,, \tag{4.5}$$

$$\begin{aligned}\mathbf{F}(\mathbf{x}_q^{'},\, \mathbf{x}_q,\, z_q,\, u_q) = \mathbf{x}_q^{'} &- \frac{\mathbf{A}_{q,1}}{x_{q,5}}\mathbf{x}_q - \frac{\mathbf{B}_q}{x_{q,5}}u_q - \mathbf{E}_q z_q \\ &- \frac{\mathbf{A}_{q,2}}{x_{q,5}}\left(F_{k_S,nonlin}(x_{q,3}) + F_{c_S}(x_{q,2} - x_{q,4})\right) = 0\,,\end{aligned} \tag{4.6}$$

and developing the intermediate function $\mathbf{F}(\cdot)$ into a Taylor series and breaking after the linear term yields

$$\begin{aligned}\mathbf{F}(\mathbf{x}_q^{'},\, \mathbf{x}_q,\, z,\, u) = \mathbf{F}^0 &+ \left.\frac{\partial \mathbf{F}}{\partial \mathbf{x}_q^{'}}\right|_0 (\mathbf{x}_q^{'} - \mathbf{x}_q^{0'}) + \left.\frac{\partial \mathbf{F}}{\partial \mathbf{x}_q}\right|_0 (\mathbf{x}_q - \mathbf{x}_q^0) \\ &+ \left.\frac{\partial \mathbf{F}}{\partial z_q}\right|_0 (z_q - z_q^0) + \left.\frac{\partial \mathbf{F}}{\partial u_q}\right|_0 (u_q - u_q^0) \\ &+ \text{h.o.t}\,,\end{aligned} \tag{4.7}$$

where the individual components are given through

$$\mathbf{F}^0 = \mathbf{x}_q^{'} - \mathbf{f}_q(\mathbf{x}_q^0,\, z_q^0,\, u_q^0) = \mathbf{0}\,, \tag{4.8a}$$

$$\left.\frac{\partial \mathbf{F}}{\partial \mathbf{x}_q^{'}}\right|_0 = 1\,, \tag{4.8b}$$

$$\begin{aligned}\left.\frac{\partial \mathbf{F}}{\partial \mathbf{x}_q}\right|_0 = &-\frac{\mathbf{A}_{q,1}}{x_{q,5}^0} - \frac{\mathbf{A}_{q,2}}{x_{q,5}^0}\left(\left.\frac{\partial F_{k_S,nonlin}}{\partial \mathbf{x}_q}\right|_0 + \left.\frac{\partial F_{c_S}}{\partial \mathbf{x}_q}\right|_0\right) \\ &+ [0\,0\,0\,0\,1]\left(\frac{\mathbf{A}_{q,1}}{x_{q,5}^{2,0}}\mathbf{x}_q^0 + \frac{\mathbf{B}_q}{x_{q,5}^{2,0}}u_q^0 + \frac{\mathbf{A}_{q,2}}{x_{q,5}^{2,0}}\left(F_{k_S,nonlin}^0 + F_{c_S}^0\right)\right)\,,\end{aligned} \tag{4.8c}$$

$$\left.\frac{\partial \mathbf{F}}{\partial z_q}\right|_0 = -\mathbf{E}_q\,, \tag{4.8d}$$

$$\left.\frac{\partial \mathbf{F}}{\partial u_q}\right|_0 = -\frac{\mathbf{B}_q}{x_{q,5}^0}\,. \tag{4.8e}$$

Die approbierte gedruckte Originalversion dieser Diplomarbeit ist an der TU Wien Bibliothek verfügbar
The approved original version of this thesis is available in print at TU Wien Bibliothek.
TU Bibliothek Your knowledge hub WIEN

Inserting (4.8) into (4.7), simplifying the equations, and recasting by the spatial derivative yields the linearized system equations:

$$\mathbf{x}_q^{'} \approx \tilde{\mathbf{A}}_q(\mathbf{x}_q^0, u_q^0)\mathbf{x}_q + \frac{\mathbf{B}_q}{x_{q,5}^0} u_q + \mathbf{E}_q z_q + \tilde{\mathbf{K}}(\mathbf{x}_q^0, u_q^0)\,, \tag{4.9}$$

where the linearized system dynamic matrix $\tilde{\mathbf{A}}_q(\cdot)$ and the constant vector $\tilde{\mathbf{K}}(\cdot)$ are given by

$$\begin{aligned}\tilde{\mathbf{A}}_q(\mathbf{x}_q^0, u_q^0) = \frac{\mathbf{A}_{q,1}}{x_{q,5}^0} + \frac{\mathbf{A}_{q,2}}{x_{q,5}^0}\left(\frac{\partial F_{k_S,nonlin}}{\partial \mathbf{x}_q}\bigg|_0 + \frac{\partial F_{c_S}}{\partial \mathbf{x}_q}\bigg|_0\right) \\ - [0\,0\,0\,0\,1]\left(\frac{\mathbf{A}_{q,1}}{x_{q,5}^{2,0}}\mathbf{x}_q^0 + \frac{\mathbf{B}_q}{x_{q,5}^{2,0}}u_q^0 + \frac{\mathbf{A}_{q,2}}{x_{q,5}^{2,0}}\left(F_{k_S,nonlin}^0 + F_{c_S}^0\right)\right)\,,\end{aligned} \tag{4.10}$$

$$\begin{aligned}\tilde{\mathbf{K}}(\mathbf{x}_q^0, u_q^0) = -\frac{\mathbf{A}_{q,2}}{x_{q,5}^0}\left(\frac{\partial F_{k_S,nonlin}}{\partial \mathbf{x}_q}\bigg|_0 + \frac{\partial F_{c_S}}{\partial \mathbf{x}_q}\bigg|_0\right) \\ + [0\,0\,0\,0\,1]\left(\frac{\mathbf{A}_{q,1}}{x_{q,5}^{2,0}}\mathbf{x}_q^0 + 2\frac{\mathbf{B}_q}{x_{q,5}^{2,0}}u_q^0 + \frac{\mathbf{A}_{q,2}}{x_{q,5}^{2,0}}\left(F_{k_S,nonlin}^0 + F_{c_S}^0\right)\right)\,.\end{aligned} \tag{4.11}$$

Quarter-Car: Difference Equations Similar as described in [49, p. 103], the continuous state equation is discretized with the sampling distance Δl_s. It is assumed that the input $u_{q,k}$, the road excitation $z_{q,k}$ and $\tilde{\mathbf{K}}(\cdot)$ have a constant value (zero-order hold) between two sampling instances. Considering the state $\mathbf{x}_{q,k} = \mathbf{x}_q(l_k)$, the successor state at $k+1$ is:

$$\mathbf{x}_{q,k+1} = e^{\tilde{\mathbf{A}}_q \Delta l_s}\mathbf{x}_{q,k} + \int_0^{\Delta l_s} e^{\tilde{\mathbf{A}}_q \mu}\left(\frac{\mathbf{B}_q}{x_{q,5}^0}u_{q,k} + \mathbf{E}_q z_{q,k} + \tilde{\mathbf{K}}\right) d\mu\,, \tag{4.12}$$

given that $\mathbf{x}_{q,k+1} = \mathbf{x}_q(l_{k+1}) = \mathbf{x}_q(l_k + \Delta l_s)$. For the linearization point holds $\mathbf{x}_q^0 = \mathbf{x}_{q,k}$, $u_q^0 = u_{q,k}$ and $z_q^0 = z_{q,k}$. After each successive iteration, the linearization point changes to the current state; the system is linearized along the trajectory. One problem remains in (4.12), namely that the matrix exponent is not analytically solvable. Therefore, the matrix exponent is approximated by inserting the Taylor series[4] such that the discretization step size Δl_s appears quadratic. Terminating the series for the homogeneous part of the equation after the second-order expansion and for the heterogeneous part of the

[4] From [49, p. 103], the matrix exponential of $\mathbf{A}t$, denoted by $e^{\mathbf{A}t}$, is the matrix given by the power series:

$$e^{\mathbf{A}t} = \mathbf{I} + \frac{t}{1!}\mathbf{A} + \frac{t^2}{2!}\mathbf{A}^2 + \frac{t^3}{3!}\mathbf{A}^3 + \cdots = \sum_{j=0}^{\infty}\frac{t^k}{k!}\mathbf{A}^k\,.$$

Die approbierte gedruckte Originalversion dieser Diplomarbeit ist an der TU Wien Bibliothek verfügbar
The approved original version of this thesis is available in print at TU Wien Bibliothek.
TU Bibliothek Your knowledge hub WIEN

equation after the first-order expansion results in

$$\mathbf{x}_{q,k+1} = \left(\mathbf{I} + \tilde{\mathbf{A}}_q \Delta l_s + \frac{1}{2}\tilde{\mathbf{A}}_q^2 \Delta l_s^2\right) \mathbf{x}_{q,k} + \Delta l_s \left(\mathbf{I} + \frac{1}{2}\tilde{\mathbf{A}}_q \Delta l_s\right) \left(\frac{\mathbf{B}_q}{x_{q,5}^0} u_{q,k} + \mathbf{E}_q z_{q,k} + \tilde{\mathbf{K}}\right) \tag{4.13}$$

where the discretization step size Δl_s appears quadratic. Simplifying further yields

$$\begin{aligned} \mathbf{x}_{q,k+1} = x_{q,k} &+ \Delta l_s \left(\tilde{\mathbf{A}}_q x_{q,k} + \frac{\mathbf{B}_q}{x_{q,5}^0} u_k + \mathbf{E}_q z_k + \tilde{\mathbf{K}}\right) \\ &+ \frac{1}{2}\tilde{\mathbf{A}}_q \Delta l_s^2 \left(\tilde{\mathbf{A}}_q x_{q,k} + \frac{\mathbf{B}_q}{x_{q,5}^0} u_k + \mathbf{E}_q z_k + \tilde{\mathbf{K}}\right), \end{aligned} \tag{4.14}$$

$$\mathbf{x}_{q,k+1} = \underbrace{x_{q,k} + \Delta l_s \mathbf{f}_q\left(\mathbf{x}_{q,k}, u_k, z_k\right)}_{\text{Forward-Euler}} + \frac{1}{2}\tilde{\mathbf{A}}_q \Delta l_s^2 \mathbf{f}_q\left(\mathbf{x}_{q,k}, u_k, z_k\right). \tag{4.15}$$

The Eq. (4.15) is a nonlinear difference equation and is composed of the Forward-Euler and an additional term.

Half-Car: Difference Equations Similar to the quarter-car, the difference equation is derived. The system is given only for the half-car model with longitudinal jerk as input, since the model with the longitudinal acceleration is almost identical to the quarter-car. Since the procedure is quite similar, only the final equations are given here:

$$\mathbf{x}_{h,k+1} = x_{h,k} + \Delta l_s \mathbf{f}_h\left(\mathbf{x}_{h,k}, u_{h,k}, \mathbf{z}_{h,k}\right) + \frac{1}{2}\tilde{\mathbf{A}}_h \Delta l_s^2 \mathbf{f}_h\left(\mathbf{x}_{h,k}, u_{h,k}, \mathbf{z}_{h,k}\right) \tag{4.16}$$

with

$$\begin{aligned} \tilde{\mathbf{A}}_h(\mathbf{x}_h^0, u_h^0) = &\frac{\mathbf{A}_{h,1}}{x_{h,9}^0} + \frac{\mathbf{A}_{h,2}}{x_{h,9}^0}\left(\left.\frac{\partial \mathbf{F}_{k_S,nonlin}}{\partial \mathbf{x}_h}\right|_0 + \left.\frac{\partial \mathbf{F}_{c_S}}{\partial \mathbf{x}_h}\right|_0\right) - [0\,0\,0\,0\,0\,0\,0\,0\,1\,0] \\ &\left(\frac{\mathbf{A}_{h,1}}{x_{h,9}^{2,0}}\mathbf{x}_h^0 + \frac{\mathbf{A}_{h,2}}{x_{h,9}^{2,0}}\left(\mathbf{F}_{k_S,nonlin}^0 + \mathbf{F}_{c_S}^0\right) + \frac{\mathbf{A}_{h,3}}{x_{h,9}^{2,0}} p_h(x_{h,10}^0) x_{h,10}^0 + \frac{\mathbf{B}_h}{x_{h,9}^{2,0}} u_h\right) \\ &+ [0\,0\,0\,0\,0\,0\,0\,0\,0\,1] \frac{\mathbf{A}_{3,h}}{x_{h,9}^{2,0}}\left(\left.\frac{\partial p_h}{\partial x_{h,10}}\right|_0 x_{h,10}^0 + p_h(x_{h,10}^0)\right). \end{aligned} \tag{4.17}$$

4.3.2 Comparison with Forward-Euler and ode45

In the following section, the difference equations of the two vehicle models are briefly compared against a classical Forward-Euler and ODE45 solver [48] from MATLAB. For

Die approbierte gedruckte Originalversion dieser Diplomarbeit ist an der TU Wien Bibliothek verfügbar
The approved original version of this thesis is available in print at TU Wien Bibliothek.
TU Bibliothek Your knowledge hub WIEN

this purpose, an cosine obstacle as described in Sec. 3.6 is traversed and the results are qualitatively examined. It should be noted here that this is by no means an accuracy and stability analysis of the discretization. It shall only be shown here that the obtained difference equation is more accurate than the Forward-Euler at larger step sizes and at the same time faster than the ODE solver of MATLAB.

In Fig. 4.4 a cosine bump, with a peak height of 10 cm and a total length of 1 m, is traversed. The simulation done by the MATLAB solver is used (denoted as *ODE45*) as reference. A classical Forward-Euler (denoted as *fwe.*) approach and the discretization (denoted as *dis.*) as described in the previous section are compared. For the sake of space over completeness in this thesis only the half-car is simulated. Shown is the the sprung body acceleration $\ddot{z}_B$, as this value plays a vital role in the following chapters.

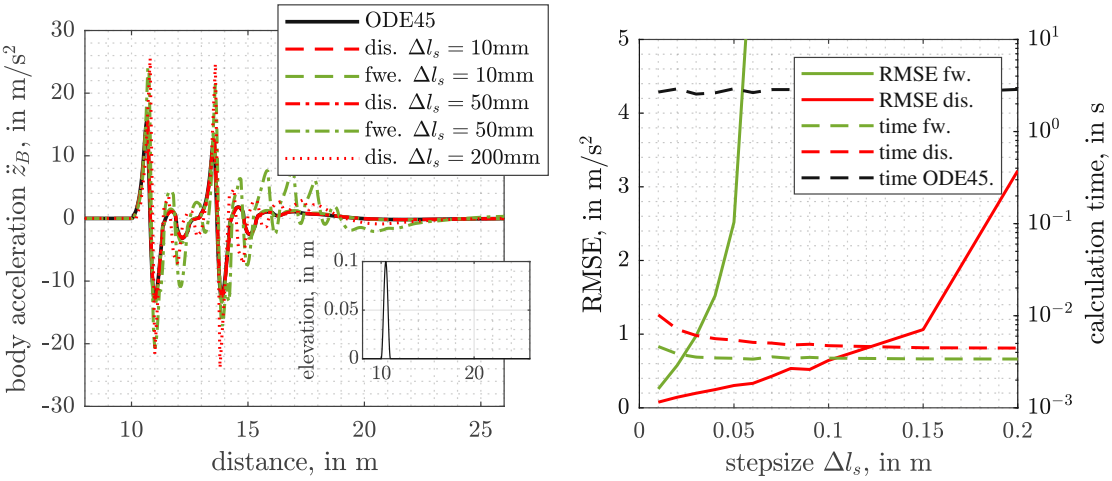

(a) Simulation results of different step sizes Δl_s over bump with height 0.1 m and length 1 m.

(b) Root-Mean-Square-Error (RMSE) as measured relative to the *ODE45* solution.

Figure 4.4: Benchmarking example of the half-car: Compared are a classical Forward-Euler (*fwe.*), the previously described discretization (*dis.*), and the solver (*ODE45*) as implemented in MATLAB. RMSE of $\ddot{z}_B$ with respect to *ODE45*.

In Fig. 4.4b the RMSE of $\ddot{z}_B$ in relation to the reference solution (*ODE45*) is given as a measure of accuracy over Δl_s. To give a rough indication of the algorithm's performance, the execution time was also measured. Clearly the discretization outperforms the built-in MATLAB solver in computational load and the Forward-Euler in terms of accuracy.

Die approbierte gedruckte Originalversion dieser Diplomarbeit ist an der TU Wien Bibliothek verfügbar
The approved original version of this thesis is available in print at TU Wien Bibliothek.
TU Bibliothek Your knowledge hub WIEN

4.4 Cost Function: The Key to Human-Like Trajectories

The previous sections dealt with the preparation of the underlying vehicle dynamics, which the driver is assumed to have knowledge of, and how this can be attributed to the optimization problem in (4.1). What is missing is how the human driver is mapped into this problem. The idea, as mentioned in the introductory section of this chapter, is to map the human driver behavior over bumps with a properly designed cost function $J(\cdot)$. But before the cost function can be defined, it is necessary to discuss about what constitutes a good acceleration/speed trajectory in first place, or rather how a human would navigate this problem. The answer to the question of human driving behavior could not be more subjective. It is challenging to represent or define human behavior mathematically. Rather, it sparked very interesting, detailed, and lengthy conversations between my supervisors and me, and ultimately led us to define some key factors that a human trajectory should exhibit. Based on experience and common agreements, the following key points were established, which are as well highlighted in the top right plot of Fig. 4.5:

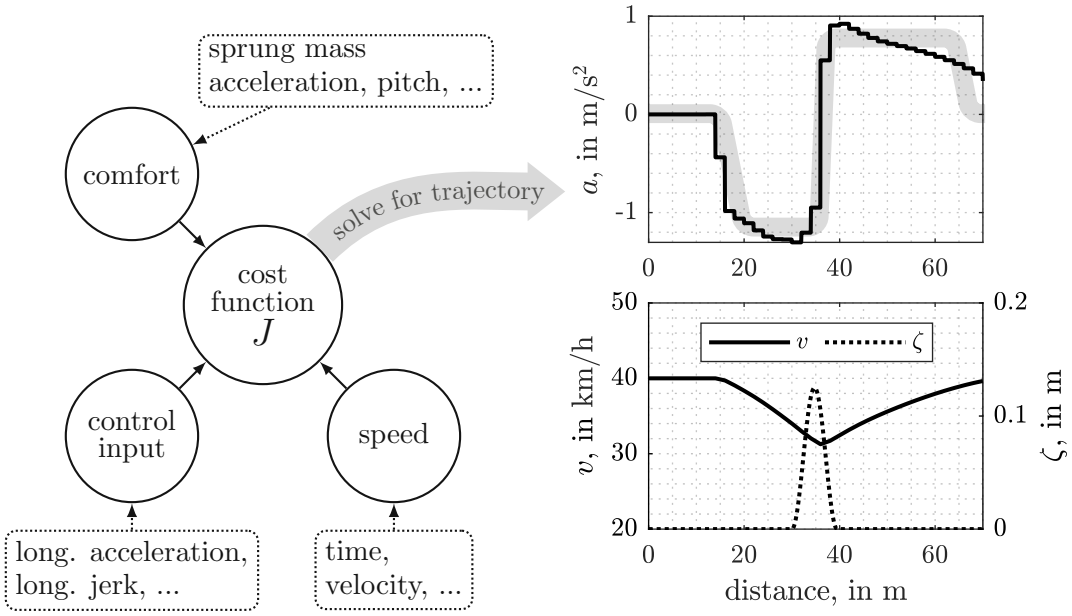

Figure 4.5: A cost function $J(\cdot)$ must be designed that balances comfort (vertical motion), speed, and control input (longitudinal motion). The design of the cost function influences the shape of the planned trajectories. By general consensus, a shape similar to the plots on the right is desired: Here, the vehicle passed through a cosine-shaped bump ζ and planned trajectories for longitudinal velocity v and acceleration a are shown.

Die approbierte gedruckte Originalversion dieser Diplomarbeit ist an der TU Wien Bibliothek verfügbar
The approved original version of this thesis is available in print at TU Wien Bibliothek.
TU Bibliothek Your knowledge hub WIEN

- The longitudinal acceleration trajectory should not be erratic. A smooth and steady acceleration is desired. Excessive jerking is not desirable.
- An initial rapid increase in deceleration should then be followed by an almost constant deceleration phase close to the obstacle.
- Similarly, after crossing the obstacle, the acceleration part should be fairly constant and gently drop to zero.
- The trajectories generated should aim to increase the experienced comfort of the passengers by, for example, reducing the movements of the sprung mass such as pitching and heaving.

As can be seen as gray area superimposed in Fig. 4.5, an approximately trapezoidal shape satisfies all of these requirements. It starts with a linear increase until it reaches a certain braking level and remains constant. Shortly after crossing the obstacle, the vehicle again accelerates at an almost constant rate. The question arises, why not just optimize a trapezoidal shape directly and have only a few optimization parameters? The idea is not to constrain the trajectory by specifying its shape, but to investigate how the choice of the cost function affects the planned trajectories and, along the way, to find one that meets the requirements set here. The novel approach is to design a certain cost function $J(\cdot)$ by essentially weighting three contributors (comfort, control input, speed) against each other. The aim of the following sections is to present a systematic investigation of these parts and to display how the trajectory can be shaped with them.

4.4.1 Quarter-Car

Before diving into the complex dynamics of the half-car, a basic cost function will first be developed for the quarter-car, since the number of influencing factors (states, accelerations, ...) is relatively manageable. The cost expected to result primarily in speed reduction is the comfort term, so this is considered first. Then the speed/time term is examined, followed by the vehicle control input. In summary, the cost function $J_0(\cdot)$ is composed as follows:

$$J_0(\tilde{\mathbf{X}}_k, \tilde{\mathbf{U}}_k) = \frac{1}{N_s} \sum_{j=0}^{N_s-1} J_{\text{comfort}}(\tilde{\mathbf{x}}_{k|j}) + J_{\text{speed}}(\tilde{\mathbf{x}}_{k|j}) + J_{\text{input}}(\tilde{u}_{k|j}), \tag{4.18}$$

Die approbierte gedruckte Originalversion dieser Diplomarbeit ist an der TU Wien Bibliothek verfügbar
The approved original version of this thesis is available in print at TU Wien Bibliothek.
TU Bibliothek Your knowledge hub WIEN

The cost $J_0(\cdot)$ has now to establish the balancing between the contributors comfort, speed and input[5]. The individual parts of the function are examined below. In the further course, in addition to the three main factors, other factors are also taken into account, resulting in the final cost function $J(\cdot)$.

Ride Comfort: Vertical Motion The comfort term plays a vital role in the trajectory planning problem as without it, solving the optimization problem yields a trivial velocity trajectory as the intention for decreasing the vehicle speed is absent. Before any criteria can be defined, it must be understood how people perceive comfort in the vehicle. In the models described, it is assumed that the driver is rigidly connected to the vehicle body. Since the driver perceives the movements of the vehicle body, the comfort perceived by the driver depends on the vertical motion of the sprung mass. Many authors [15], [18], [20], [25] chose sprung mass acceleration $\ddot{z}_B$ as the measure of comfort, and so will this text. The cost associated with experienced comfort $J_{\text{comfort}}(\tilde{\mathbf{x}}_{k|j}) \geq 0$ for all $\tilde{\mathbf{x}}_{k|j} \in \mathcal{X}$ must be a positive definite function, so that an increase in sprung mass acceleration is always associated with an increase in cost. This is usually achieved by choosing the comfort term such that the acceleration of the sprung mass appears as a quadratic function, e.g., a (root) mean square (RMS) function or some other positive definite function, e.g., a (root) mean quartic (RMQ) function or a mean absolute (MA) function. Before deciding on a function, a simulation study is carried out and the costs are calculated for various evaluation functions. For this purpose, a simple cosine bump was traversed at different speeds in Fig. 4.6 and the corresponding RMS and RMQ values are evaluated for the section.

A trend is evident in the simulation study: For a quadratic cost term, the minimum of the evaluation function is around 40 km/h, while the minimum in the quartic case is found at lower speeds. Since the ride comfort term is intended to force the driver model to reduce speed near irregularities on the road to small values, the quartic term is chosen. The figure, however, highlights an inherent problem. At high speeds, the RMS and RMQ values start to decrease slightly again, which will be subject to discussion

[5]The cost $J_0(\cdot)$ can as well be split into two summations: One over the prediction grid for spacing Δl_s and one for the control input with spacing Δl_p:

$$J_0(\tilde{\mathbf{X}}_k, \tilde{\mathbf{U}}_k) = \frac{1}{N_p} \sum_{n=0}^{N_p-1} J_{\text{input}}(\tilde{u}_{k|n}) + \frac{1}{N_s} \sum_{j=0}^{N_s-1} J_{\text{comfort}}(\tilde{\mathbf{x}}_{k|j}) + J_{\text{speed}}(\tilde{\mathbf{x}}_{k|j}) \,. \tag{4.19}$$

Die approbierte gedruckte Originalversion dieser Diplomarbeit ist an der TU Wien Bibliothek verfügbar
The approved original version of this thesis is available in print at TU Wien Bibliothek.
TU Bibliothek Your knowledge hub WIEN

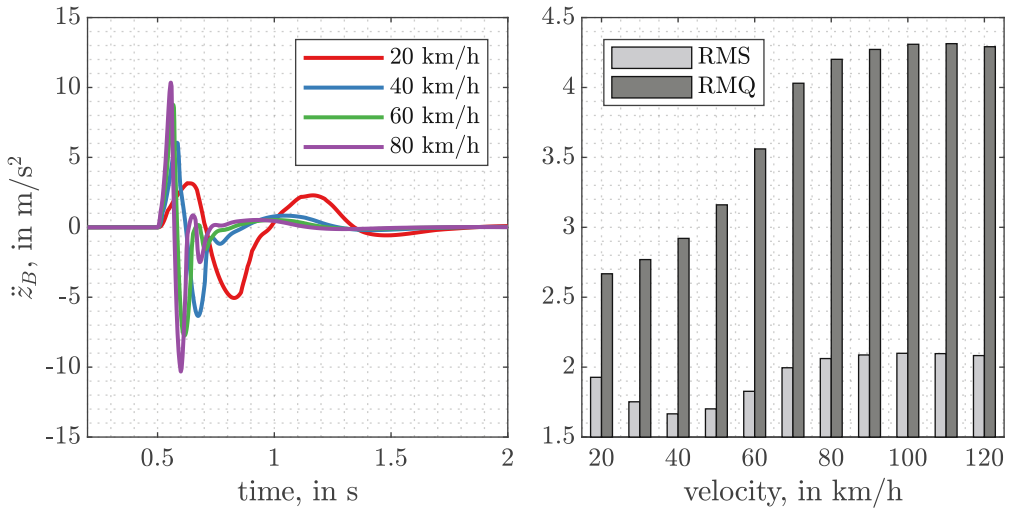

Figure 4.6: Investigation of RMS and RMQ values over a cosine bump with length of 2 m and height of 6.5 cm. It is clearly visible that the global optimum for this bump would be to traverse it with 40 km/h in the RMS case and with the lowest possible velocity in the RMQ case.

later. The final cost of comfort for the quarter-car results in:

$$J_{\text{comfort}}(\tilde{\mathbf{x}}_{k|j}) = Q_c f^4_{q,4}(\tilde{\mathbf{x}}_{k|j}) = Q_c \ddot{z}^4_{B,k|j} \,, \tag{4.20}$$

where the value $Q_c \in \mathbb{R}_{>0}$ is a weight to tune the impact on the total cost and $f^4_{q,4}(\tilde{\mathbf{x}}_{k|j})$ is the dynamic equation for the sprung body mass acceleration $\ddot{z}_{B,k|j}$ of the quarter-car.

Driving Speed Up to now the solution of the optimization problem is only shaped by the comfort term. As shown in Fig. 4.6, the optimal trajectory would bring the vehicle towards lower speeds. However, after passing over the bump – if the vehicle does not come to a stop before the bump – the driver would not have the intention to increase speed again. Thus, a term will be added that penalizes the driver model if too much time is required for passing the obstacle or if the velocity drops too much, respectively. The driver model now tries to reach a balance between the comfort and speed terms that allows some speed reduction but still ensures a fast passage through the preview horizon.

Consider how the cost of $J_{\text{speed}}(\tilde{\mathbf{x}}_{k|j})$ can be designed to achieve a balance between comfort and speed. A simple, but not yet satisfying approach would be to discount the travel time directly. This would have been a easy choice if the system was not

Die approbierte gedruckte Originalversion dieser Diplomarbeit ist an der TU Wien Bibliothek verfügbar
The approved original version of this thesis is available in print at TU Wien Bibliothek.
TU Bibliothek Your knowledge hub WIEN

transformed from a difference equation in time to one in space[6]. For the presented case in the spacial domain the time step $\Delta t_{k|j}$ is not given directly and is depending approximately on the velocity between two instants by $\frac{\Delta l_s}{v_{k|j}}$. Preferable, the speed term should not depend on time directly but rather on the velocity. This is achievable by penalizing the velocity deviation from a given reference point. This is called *reference point tracking*. The reference in this case will be a velocity v_{ref} which can for example be the legal road speed or a velocity specified by the driver. The cost $J_{\text{speed}}(\tilde{\mathbf{x}}_{k|j})$ is then to ensure in case of an increase in the comfort level due to a speed reduction, the speed drop is limited and the velocity returns to the reference after the bump.

Similarly, $J_{\text{speed}}(\tilde{\mathbf{x}}_{k|j})$ should be positive definite, therefore $J_{\text{speed}}(\tilde{\mathbf{x}}_{k|j}) \geq 0$ for all $\tilde{\mathbf{x}}_{k|j} \in \mathcal{X}$. Here, too, it must be decided whether it should be weighted absolute, quadratic, or even higher. In short, for higher order functions, velocity dips, as shown in Fig. 4.5, are penalized severely more than smaller and constant deviations. In fact, a velocity dip above the bump is readily accepted because the main goal of the velocity term is to provide slow but gradual reference tracking of v_{ref}, which is of paramount importance after the bump. Therefore, higher order penalty functions are not chosen, since they would penalize such peaks. Based on this consideration, two approaches for the speed term are considered:

$$\text{absolute cost term:} \quad J_{\text{speed}}(\tilde{\mathbf{x}}_{k|j}) = Q_v \left| v_{ref} - \tilde{x}_{5,k|j} \right| = Q_v \left| v_{ref} - v_j \right| , \tag{4.21a}$$

$$\text{squared cost term:} \quad J_{\text{speed}}(\tilde{\mathbf{x}}_{k|j}) = Q_v (v_{ref} - \tilde{x}_{5,k|j})^2 = Q_v (v_{ref} - v_j)^2 , \tag{4.21b}$$

where is $Q_v \in \mathbb{R}_{>0}$ is the corresponding weight factor for the speed term. In Fig. 4.7, a cosine bump is traversed with a combined cost function for speed and ride comfort.

Vehicle Input: Longitudinal Comfort If the optimization problem in (4.1) is solved taking into account solely the combined costs of comfort and speed, the optimal trajectory would be to wait until the last moment of the bump, then to brake enormously hard and then accelerate immensely hard again, as shown Fig. 4.7. Therefore, large longitudinal accelerations should be penalized as well. Compared to the comfort and speed terms, which are designed to ensure that the driver model detects road bumps, reduces speed, and accelerates back to a given target speed, the vehicle input probably plays the most critical role in shaping the trajectory.

As mentioned at the beginning of this chapter, a fairly sharp rise followed by a constant

[6] From the perspective of a human driver, taking travel time into account would also make little sense, since a human driver uses a speedometer as a guide while driving.

Die approbierte gedruckte Originalversion dieser Diplomarbeit ist an der TU Wien Bibliothek verfügbar
The approved original version of this thesis is available in print at TU Wien Bibliothek.
TU Bibliothek Your knowledge hub WIEN

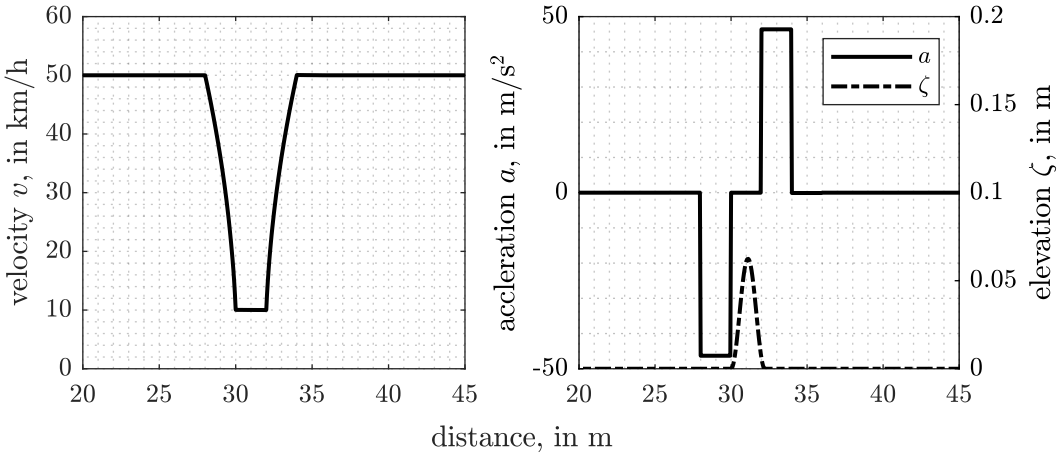

Figure 4.7: Illustrative example for a cosine bump with the combined costs of comfort and speed. This example was computed with an quadratic penalization for the speed, however, similar results are expected with an absolute one. Constraint at $v = 10\,\mathrm{km/h}$ active to accomplish computation. Configuration: $Q_v = 0.7$, $Q_c = 0.3$, $\Delta l_s = 0.05\,\mathrm{m}$, $\Delta l_p = 2\,\mathrm{m}$, $l_{prev} = 25\,\mathrm{m}$.

negative longitudinal acceleration is desirable. After the obstacle, the acceleration of the vehicle should also be constant again and gradually go to zero. Thus, similar to the vertical comfort term, the primary concern is to penalize large acceleration values, not constant accelerations. On closer inspection, the input term can be understood as a comfort in itself, but not in the vertical but in the longitudinal direction. The fact that the term vehicle input is used here is only to make it clear which quantity is optimized in the MPC. Once again, a positive definite cost term $J_{\text{input}}(\tilde{u}_{k|j}) \geq 0$ for all $\tilde{u}_{k|j} \in \mathcal{U}$ is necessary, the simple quadratic and quartic cost functions are favored and benchmarked against each other in Fig. 4.8:

$$\text{squared cost term:} \quad J_{\text{input}}(\tilde{u}_{k|j}) = Q_u \tilde{u}_{k|j}^2 = Q_u a_j^2\,, \tag{4.22a}$$

$$\text{quartic cost term:} \quad J_{\text{input}}(\tilde{u}_{k|j}) = Q_u \tilde{u}_{k|j}^4 = Q_u a_j^4\,, \tag{4.22b}$$

where $Q_u \in \mathbb{R}_{>0}$ is the input cost term weight.

In Fig. 4.8 all four combinations of the speed and input terms were simulated with the same cosine disturbance as in Fig. 4.7. The generated velocity profiles look quite similar for all cases. Larger differences are seen when looking at the planned acceleration trajectory. In the deceleration phase, all combinations look quite similar, with a rapid increase in negative acceleration and a fairly constant deceleration to the hill at 30 m. Where differences become visible is after passing the cosine bump. Here, the quadratic

Die approbierte gedruckte Originalversion dieser Diplomarbeit ist an der TU Wien Bibliothek verfügbar
The approved original version of this thesis is available in print at TU Wien Bibliothek.

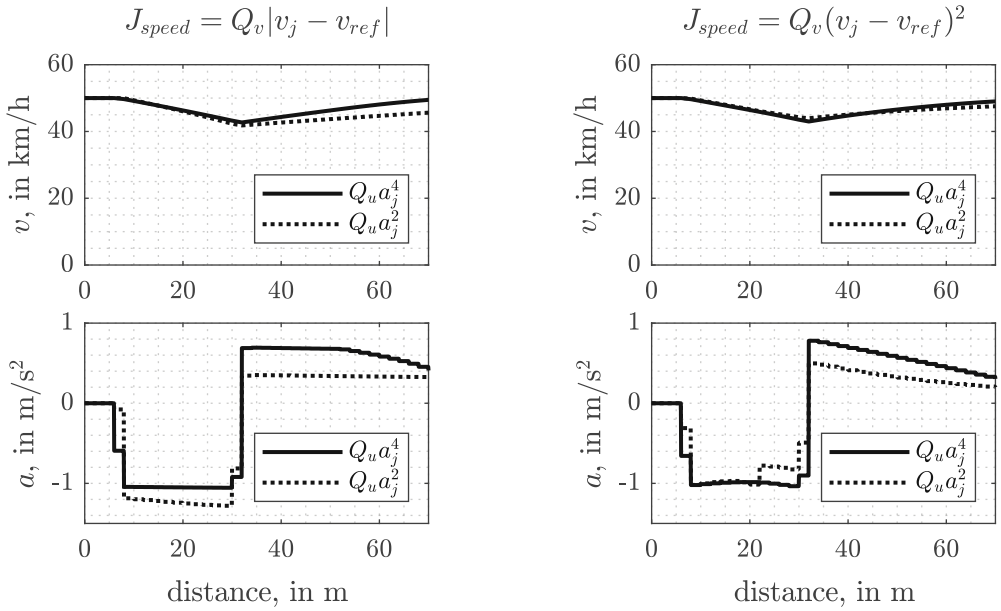

(a) $Q_v = 0.7$. (b) $Q_v = 0.4$.

Figure 4.8: Comparison of quadratic and quartic control input weighting given the speed weighting functions in (4.21) for the cosine bump scenario in Fig. 4.7. The parameters were chosen so that the magnitude of the deceleration phase remains comparatively constant: $Q_u = 1$ for $\tilde{u}^4_{k|j}$ and $Q_u = 2$ for $\tilde{u}^2_{k|j}$.

speed penalty produces a linear acceleration curve that drops off quickly, while the absolute penalty keeps the acceleration constant at first and later drops to zero when the reference speed is reached. Minor differences become apparent when considering the various input cost terms with quadratic or quartic functions. It seems that the quadratic weight restricts the acceleration phase more than the quartic one. In most cases, the quartic function will be used, since it allows an easier weighting between the comfort term and the input term, since both are accelerations in a given direction with similar magnitudes. Further, a look at the results shows which configuration best satisfies the key points for passing in a human fashion mentioned in Sec. 4.4: absolute speed and quartic vehicle control input weighting.

Terminal Cost: Long-Term vs. Short-Term Goals So far, only the final trajectory has been considered, which is calculated along the entire course of the road. At each step along the road, the driver model, the MPC, plans trajectories $\{\tilde{\mathbf{X}}^*_k, \tilde{\mathbf{U}}^*_k\}$ for the preview horizon. At each discrete step k, only the first computed input $\tilde{u}^*_{k|0}$ from the optimally planned trajectory $\tilde{\mathbf{U}}^*_k$ is used and at the next time $k+1$ the process is repeated. Have

Die approbierte gedruckte Originalversion dieser Diplomarbeit ist an der TU Wien Bibliothek verfügbar
The approved original version of this thesis is available in print at TU Wien Bibliothek.
TU Bibliothek Your knowledge hub WIEN

a closer look now at how the planned trajectories computed along the road at different positions look like. In Fig. 4.9 the cosine hump from the previous examples is traversed, but this time overlaid with the planned trajectories at each evaluation step k.

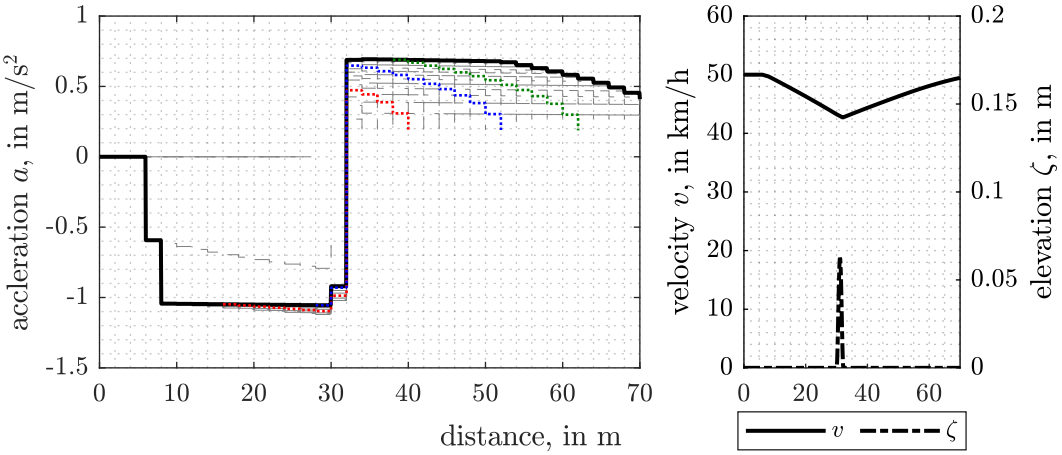

Figure 4.9: Illustrative example for a cosine bump with an absolute velocity v weight, quartic weight for acceleration a and comfort $\ddot{z}_B$. Superimposed in gray are the planned acceleration trajectories at each step. Highlighted in red, blue and green are planned trajectories at different positions along the road. Configuration: $Q_v = 0.7$, $Q_c = 0.3$, $Q_a = 1$, $\Delta l_s = 0.05\,\mathrm{m}$, $\Delta l_p = 2\,\mathrm{m}$, $l_{prev} = 25\,\mathrm{m}$.

In the deceleration phase, the trajectories are similar – most trajectories are close to each other. In a human context, this means that at the beginning of the braking maneuver, the driver is very confident about how to perform this maneuver. However, as the vehicle continues to approach and look over the bump, the driver model is uncertain about the acceleration phase after the bump. The uncertainty can be seen as a wide band of gray trajectories below the final acceleration trajectory in black. Compare the three highlighted trajectories in red, blue and green: the further the vehicle is traveling, the farther the driver model shifts the end of the acceleration phase to the right.

This uncertainty can be resolved by adding an additional cost term that places a greater stress on the long-term objective to the basic cost $J_0(\cdot)$ in (4.18). A terminal cost $J_{\text{terminal}}(\cdot)$ term is added as:

$$J(\tilde{\mathbf{X}}_k, \tilde{\mathbf{U}}_k) = J_0(\tilde{\mathbf{X}}_k, \tilde{\mathbf{U}}_k) + J_{\text{terminal}}(\tilde{\mathbf{X}}_k)\,, \tag{4.23a}$$

$$\text{with} \quad J_{\text{terminal}}(\tilde{\mathbf{X}}_k) = Q_t N_s (v_{ref} - \tilde{x}_{5,k|N_s-1})^2\,, \tag{4.23b}$$

$$= Q_t N_s (v_{ref} - v_{k|N_s-1})^2\,,$$

Die approbierte gedruckte Originalversion dieser Diplomarbeit ist an der TU Wien Bibliothek verfügbar
The approved original version of this thesis is available in print at TU Wien Bibliothek.
TU Bibliothek Your knowledge hub WIEN

where $Q_t \in \mathbb{R}_{>0}$ is the weight of the terminal cost term. To scale it properly, the cost is multiplied by the number of samples N_s. The original idea behind adding a terminal cost term is to shift the focus of the velocity weight to the end of the horizon and "unify" the trajectories along the road. This can be interpreted as the intention of the driver to have long- and short-term goals. The short-term goals along the prediction/preview horizon are to minimize the discomfort and vehicle input. The long-term goal is to place more emphasis on reaching the reference speed at the end of the prediction horizon. The result of such an additional terminal cost term is shown in Fig. 4.10.

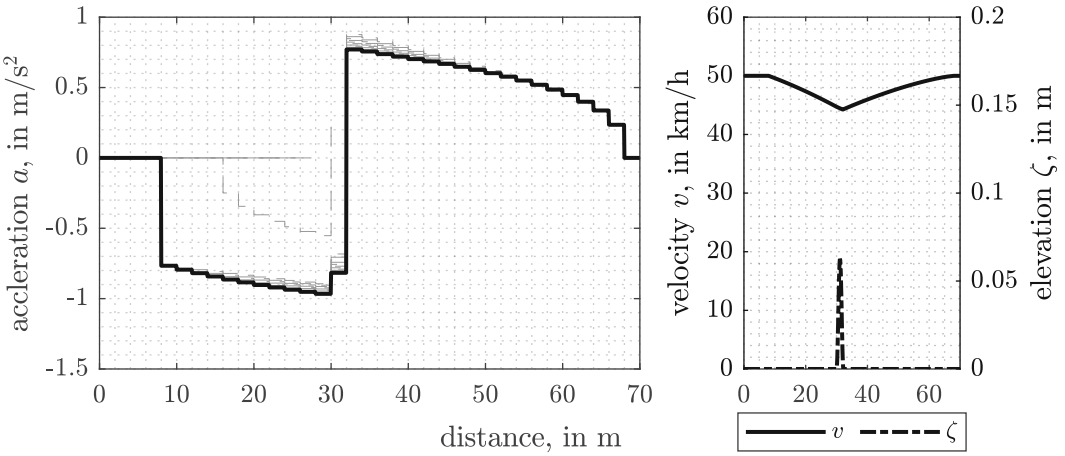

Figure 4.10: Illustrative example for a cosine bump with an absolute velocity weight, quartic weight for acceleration a and comfort $\ddot{z}_B$. Superimposed in gray are the planned acceleration trajectories at each step. Configuration: $Q_v = 0.7$, $Q_c = 0.3$, $Q_a = 1$, $\Delta l_s = 0.05\,\mathrm{m}$, $\Delta l_p = 2\,\mathrm{m}$, $l_{prev} = 25\,\mathrm{m}$ and $Q_t = 0.001$ which gives for the terminal cost $Q_t N_s \approx 0.5$.

With the addition of the terminal cost, the long term goal of reaching the reference velocity at the end of the horizon is enforced. It would also be possible to map the speed term only with the final cost, but this would remove the driver's short-term goal and would not penalize deviations along the trajectory in the prediction horizon. Applying the extended cost from (4.23) does not change the final acceleration trajectory significantly, but assists the driver model in planning along the route evident in that the gray trajectories are very close to each other.

Trajectory Holding As mentioned in the introduction of this work, a driver model should incorporate properties of a human driver, such as skill, reaction time, driving style and so on. Similarly, as the terminal cost term influences the "decision" process when crossing the obstacle, a trajectory holding can be understood as to keep the trajectory

Die approbierte gedruckte Originalversion dieser Diplomarbeit ist an der TU Wien Bibliothek verfügbar
The approved original version of this thesis is available in print at TU Wien Bibliothek.

as consistent as possible if once decided for one. Mathematically speaking, the optimal trajectory $\tilde{\mathbf{U}}^*_{k-1}$ from the previous step should be considered for optimization for the next trajectory $\tilde{\mathbf{U}}_k$. In a human context, this means that the driver tries to stay on the first chosen trajectory and only modifies it if it's really necessary. A skilled driver, for example, already knows how to approach such a road bump and won't really deviate from the first plan much. Given the previous designed trajectory $\tilde{\mathbf{U}}^*_{k-1}$ the total cost can then be advanced by adding a trajectory holding term $J_{\text{holding}}(\cdot)$:

$$J(\tilde{\mathbf{X}}_k, \tilde{\mathbf{U}}_k, \tilde{\mathbf{U}}^*_{k-1}) = J_0(\tilde{\mathbf{X}}_k, \tilde{\mathbf{u}}_k) + J_{\text{holding}}(\tilde{\mathbf{U}}_k, \tilde{\mathbf{U}}^*_{k-1})\,, \tag{4.24a}$$

$$\text{with} \quad J_{\text{holding}}(\tilde{\mathbf{U}}_k, \tilde{\mathbf{U}}^*_{k-1}) = \frac{1}{N_p - 1} \sum_{n=0}^{N_p-2} Q_h(n)(\tilde{u}_{k|n} - \tilde{u}^*_{k-1|n+1})^2\,, \tag{4.24b}$$

where $Q_h(n) \in \mathbb{R}_{>0}$ is the weight depending on the step n. Note, the input from the previous trajectory in the summation starts at one due to the car having advanced one step. Since it is not the intention to constrain the trajectory with these costs along the entire forecast horizon, but rather at the beginning and to give the planner some freedom towards the end, $Q_h(n)$ is designed so that the weight decreases to zero along the prediction horizon. This can be achieved, for example, by reducing the weight linearly along the prediction horizon.

How are different drivers mapped? It comes down to tuning or choosing the right weights for the comfort Q_c, speed Q_v, and input terms Q_u, respectively. For example, if the speed term is emphasized, a driver model can be built that both brakes late and does not lose much speed when crossing. The choice of the preview distance l_{prev} also plays a crucial role, because it determines how far in advance the driver is likely to react to the obstacle. If the driver model is given a shorter preview distance, the obstacle will be detected later and thus the driver model will have to brake harder to reach the comfort target. On the other hand, if the preview distance is longer, the driver is able to operate more conservatively by starting to brake earlier but not as hard. Of course, all this behavior also depends on how the terms are weighted relative to each other.

In Ch. 5 in Sec. 5.3, some variations of the driver model are discussed, which can be used to tune different driving styles.

Reaction Time Regarding human driver modeling, an essential issue is the time it takes for a driver to react to newly perceived road information. This reaction/response time of the driver model can be taken into account either directly in the optimization

Die approbierte gedruckte Originalversion dieser Diplomarbeit ist an der TU Wien Bibliothek verfügbar
The approved original version of this thesis is available in print at TU Wien Bibliothek.
TU Bibliothek Your knowledge hub WIEN

problem in (4.1) by constraining the input space or indirectly by either delaying the inputs to the trajectory optimization or delaying the generated trajectory in the control loop in Fig. 4.2:

1. Indirectly by
   a) feeding delayed states $\mathbf{x}_{k-d}$ and road information $\mathbf{Z}'_{k-d}$ the optimization problem at instant k,
   b) applying the delayed optimized input trajectory $\tilde{\mathbf{U}}^*_{k-d}$ or, in the sense of the receding horizon, the first input $\tilde{u}^*_{k-d|0}$ at instant k.
2. Directly accounting for reaction time in the trajectory optimization problem by constraining the input space $\mathcal{U}$.

Here $d \in \mathbb{Z}_{>0}$ is the number of shift samples in the spatial domain corresponding to the reaction time in the temporal domain. All three approaches are most easily explained by a number line. In Fig. 4.11, the correlation between the spatial and temporal domains is illustrated. The vertical dashed line in the figure represents the current position/time stamp of the vehicle. Based on the previous points on the road l_{k-1}, l_{k-2}, l_{k-3}, etc. the corresponding timestamps can be calculated. In the indirect case, the next smaller timestamp is sought from the current minus the reaction time (t_{k-3} in the figure). From there, either the input computed at that time stamp is used or delayed states and road information are fed to the MPC at the current time k. The direct approach with the input space constraint faces the problem that the corresponding timestamps are not known in advance, since the vehicle speed has not yet been determined. What is known, however, is the planned trajectory from the previous trajectory optimization at $k-1$. This information is used to calculate forward in time and find the appropriate points. Again, the time-delayed point is searched for (t_{k+2} in this case) and the input is bound in the new optimization problem to the previous trajectory up to this point.

For the indirect cases, the appropriate translation from reaction time to the spatial frame must first be found. For this, the corresponding timestamps up to $t_k \in \mathbb{R}_{\geq 0}$ must first be known, which can be calculated either analytically or numerically. The shift index d at instant k for case 1a and case 1b yields:

$$d = i^* = \arg\max_i \quad t_{k-i} \tag{4.25a}$$

$$\text{s.t.} \quad t_k - t_{k-i} \geq t_r\,, \quad \forall i = 0, 1, \ldots, k-1 \tag{4.25b}$$

Die approbierte gedruckte Originalversion dieser Diplomarbeit ist an der TU Wien Bibliothek verfügbar
The approved original version of this thesis is available in print at TU Wien Bibliothek.

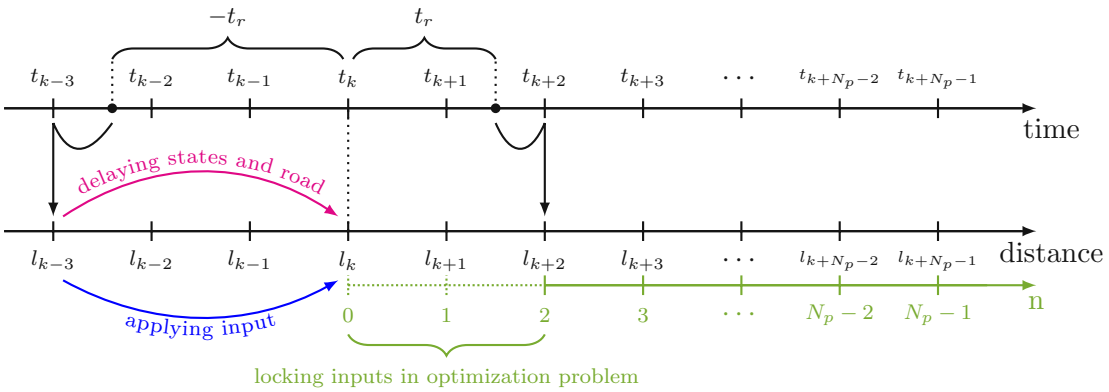

Figure 4.11: Interrelation between the spacial and time domain for a given reaction time t_r. This illustrative example shows that a given reaction time cannot be exactly achieved as the corresponding incremental time steps are not consistent as they vary with the vehicle velocity. In colors are the three approaches given.

where the index i maximizes the time t_{k-d} while still enforcing that the effective reaction time $t_k - t_{k-d}$ is greater or equal to the desired reaction time $t_r \in \mathbb{R}_{\geq 0}$. With the index determined, either the state $\mathbf{x}_{k-d}$ and road information $\mathbf{Z}'_{k-d}$ in case 1a are delayed for the optimization problem or the optimized input $\tilde{u}^*_{k-d|0}$ in case 1b is applied at step k. Note, due to the condition (4.25b) the effective reaction time will be most of the time greater than the desired one. Furthermore, the discrepancy depends on Δl_p as with smaller steps the spacing in space as well as in time is denser: $\lim_{\Delta l_p \to 0} t_k - t_r - t_{k-d} = 0$. The algorithm to calculate shift/delay samples d is given in the appendix in Alg. 1.

In case 2 the determination of the delay index is quite similar, but this time it is not calculated into the past but into the future. The previously optimized input trajectory $\tilde{\mathbf{U}}^*_{k-1}$ is used to calculate the future time steps $\mathbf{T} \in \mathbb{R}^{N_p}$, according to Alg. 2 in the appendix. Based on the time steps computed for further steps the index d is obtained by:

$$d = i^* = \arg\min_i \quad t_{k+i} \tag{4.26a}$$

$$\text{s.t.} \quad t_{k+i} - t_k \geq t_r\,, \quad \forall i = 1, \ldots, N_p - 1\,. \tag{4.26b}$$

After the index d has been determined, the input space can be constrained as follows:

$$\mathcal{U} = \left\{ \tilde{u}_{k|n} \in \mathbb{R} \;\middle|\; \tilde{u}_{k|n} = \tilde{u}^*_{k-1|n+1}\,, \forall n = 0, 1, \ldots, d-1 \right\}, \tag{4.27}$$

Die approbierte gedruckte Originalversion dieser Diplomarbeit ist an der TU Wien Bibliothek verfügbar
The approved original version of this thesis is available in print at TU Wien Bibliothek.
TU Bibliothek Your knowledge hub WIEN

which implies that the optimization steps up to $d-1$ are locked to the previously optimized trajectory $\tilde{\mathbf{U}}^*_{k-1}$.

What are the effects of the different approaches from the driver's point of view? For the indirect methods, the MPC has no knowledge of the response time. In the case of delayed states and road information, the driver-model simply perceives the situation with a time offset and therefore also reacts to it with an offset. In the case of the delay at the output, the driver perceives the situation correctly, but cannot react to it directly. In terms of control, however, both approaches lead to the same trajectory. In the first approach, the optimization problem at step k is solved with the information from step $k-d$, while in the second approach, the solution of the optimization problem at $k-d$ is simply applied at k. Thus, the applied $\tilde{u}^*_k$ is the same. This temporally shifted perception shifts the final planned trajectory in its entirety, as shown in Figure. 4.12.

In the direct method, on the other hand, the MPC receives the road information and the state of the vehicle without a time shift. However, the MPC is unable to react immediately to the new information because the first control steps are locked to the old trajectory. Yet, the MPC can react to the new road information with the unbound part of the control sequence $\tilde{\mathbf{U}}_k$. Thus, the information about the changed road conditions is not lost but encoded in the planned trajectory. This now leads to the fact that the final trajectory has a time delay at the beginning – the driver model cannot react immediately – but the rest of the trajectory is not simply shifted in time.

In the direct case, the MPC is aware of its reaction time and plans with it, while in the indirect case the driver model would simply perceive everything with a time delay or act with a time delay. In the driver's mind, this behavior could again be interpreted as skill and experience. An experienced driver is aware of his/her reaction time and can deal with it to some extent. A novice driver is perhaps overwhelmed with the overall situation and therefore reacts to the entire situation with a time delay. In short, we are digressing here to a very fundamental question of how humans process, store, and react to information, but this is far beyond the scope of this thesis and is thus not addressed in further detail.

In Fig. 4.12, the trajectory of the traversal was again planned for the cosine bump of the previous examples, but with the additional reaction time to the driver model. As previously stated, the indirect methods[7], which only delay either the input or the output of the optimization problem, do generate the same trajectories – both are superimposed in different colors. In the deceleration phase, all approaches have nearly the

[7] In the figure called *delay In.* and *delay Out.*.

Die approbierte gedruckte Originalversion dieser Diplomarbeit ist an der TU Wien Bibliothek verfügbar
The approved original version of this thesis is available in print at TU Wien Bibliothek.
TU Bibliothek Your knowledge hub WIEN

same behavior, trajectory and delayed braking as it was intended. For comparison there is a solution without any reaction time. The decisive differences between the approaches occur when driving over the bump and in the acceleration phase. In this phases the reaction time approach with the locked inputs closely reassembles the reference solution which has no reaction time. Compared to this, the indirect methods suffer here in such that the trajectory is shifted/delayed rightwards in time.

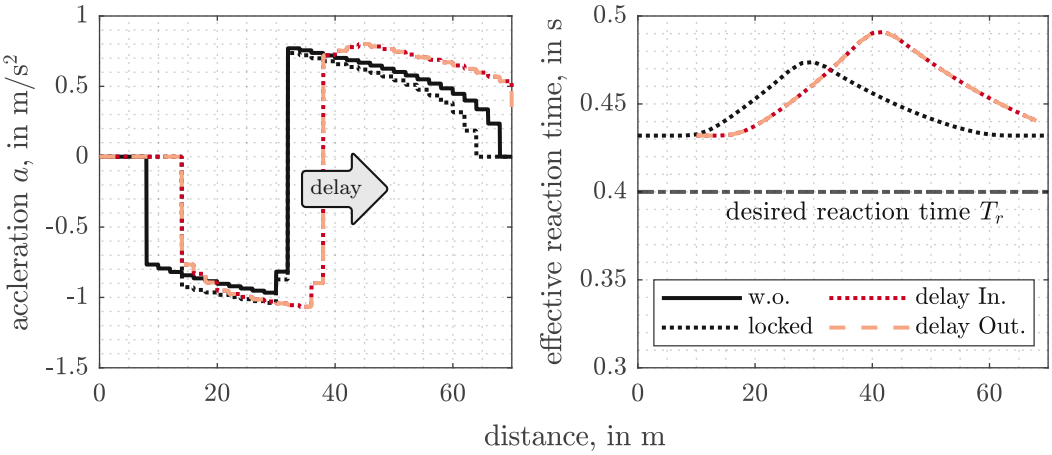

Figure 4.12: Trajectories and effective reaction times: The same cosine bump from the previous examples is used. In the right plot the effective reaction time is plotted. The horizontal line is the minimum required reaction time. For reference, the MPC is given without any response time.

In the right diagram of Fig. 4.12, the true/effective reaction times for the approaches are visualized. As mentioned earlier, due to the nature of discrete MPC, it is impossible to obtain exactly the desired reaction time. The direct approach with locking of the input space is chosen from here on.

Influence of Road Obstacle on the Design of the Cost Function The present cost function was developed based on a single cosine-shaped bump, but as shown in the previous chapter, there are a variety of different bumps, from potholes to raised crosswalks to curbs. Of particular interest are the various cosinusoidal bumps that are designed to excite the resonant frequencies of the vehicle.

As will be investigated in Ch. 5, a standard cost function is quite well suited to deal with all bumps. Yet, the tuning applied leads, for example, only to a small drop in speed for the small cosine bumps. Here, it may be useful to adjust the sensitivity of the driver model via the weighting factors and thus achieve an adaptive behavior for different obstacles. In addition, an obstacle was designed to stimulate human sensitivity

Die approbierte gedruckte Originalversion dieser Diplomarbeit ist an der TU Wien Bibliothek verfügbar
The approved original version of this thesis is available in print at TU Wien Bibliothek.
TU Bibliothek Your knowledge hub WIEN

to vertical acceleration. However, this sensitivity is not represented in the driver model itself. Therefore, it would make sense to strongly increase the weighting of the comfort term for this obstacle in order to represent an increased sensitivity.

Additional Constraints In Sec. 4.2 a reformulation of the state space model was introduced. The reformulation introduces a singularity at a full stop of the vehicle at $v \to 0$. This could be circumvented by switching back the system dynamics near the singularity and considering the optimization problem in the time domain. However, since it is the driver's task to drive over the hill, it can be assumed that a standstill is not desired. Therefore, a constraint is introduced in the optimization task:

$$\mathcal{X} = \left\{ \tilde{\mathbf{x}}_{k|j} \in \mathbb{R}^5 \;\middle|\; \tilde{x}_{5,k|j} \geq v_{min}\,, \quad \forall j = 0, 1, \ldots, N_s - 1 \right\}, \tag{4.28}$$

where v_{min} is an arbitrarily low speed limit that the vehicle should not fall below. The necessity of this constraint is visible in Fig. 4.7, since the simulation would not have been possible for this example, as the controller would have further reduced the speed to zero. In the example, a lower bound was set to 10 km/h. In the majority of the considered cases, the constraint is not active.

Recapitulation of full Driver-Model After writing the main points about the cost function, response time, and constraints in the previous sections, it is time to put everything into a final optimization problem:

$$\tilde{\mathbf{U}}_k^* = \underset{\tilde{\mathbf{U}}_k}{\arg\min} \quad J_0(\tilde{\mathbf{X}}_k, \tilde{\mathbf{U}}_k) + J_{\text{terminal}}(\tilde{\mathbf{X}}_k) \tag{4.29a}$$

$$\text{s.t.} \quad \tilde{\mathbf{x}}_{k|j+1} = \mathbf{f}(\tilde{\mathbf{x}}_{k|j}\,, z_{k|j}\,, \tilde{u}_{k|n}\,)\,, \quad \tilde{\mathbf{x}}_{k|0} = \mathbf{x}_k\,, \tag{4.29b}$$

$$\tilde{\mathbf{x}}_{k|j} \in \mathcal{X}\,, \quad z_{k|j} \in \mathbf{Z}_k^{'}\,, \quad \forall j = 0, 1, \ldots, N_s - 1 \tag{4.29c}$$

$$\tilde{u}_{k|n} \in \mathcal{U}\,, \quad \forall n = 0, 1, \ldots, N_p - 1 \tag{4.29d}$$

with reaction times accounted in $\mathcal{U}$ according to (4.27) and a lower bound for the velocity in $\mathcal{X}$ according to (4.28). In this optimization problem, trajectory holding is intentionally not incorporated, since locking inputs for reaction time to a previously planned trajectory and penalizing a deviation from the first inputs of a previously planned trajectory accomplish the same goal. The optimization task set here now contains the most important components for the driver model proposed in this thesis. For the remainder of this work, this optimization problem will be referred to as the *Basic-Cost-Function*. In the next step, the optimization problem is adapted for the half-car and, in particular,

Die approbierte gedruckte Originalversion dieser Diplomarbeit ist an der TU Wien Bibliothek verfügbar
The approved original version of this thesis is available in print at TU Wien Bibliothek.
TU Bibliothek Your knowledge hub WIEN

the inclusion of pitching effects to the cost function is addressed.

4.4.2 Half-Car

In this section, the trajectory optimization problem for the half-car is presented. Starting from the set of Eqs. (4.1), the corresponding optimization criterion $J(\cdot)$, the constrained sets $\mathcal{X}$, $\mathcal{X}_\mathcal{T}$ and $\mathcal{U}$ are required. The equations of motion have already been introduced in Ch. 3 in Sec. 3.2. In contrast to the quarter-car, the half-car not only captures the vertical motion of one axle, but as well maps the pitching of the vehicle. The focus of this section is therefore on integrating pitching motion in form of an additional cost term into the human driver model and studying its influence on the planned trajectories. There is no need to discuss all cost terms again from scratch, so based on the findings from the previous section, the cost function derived on the basis of the quarter-car is reused.

Trying the Basic-Cost-Function The optimization problem in (4.29) is written again, but adapted for the half-car[8]:

$$\tilde{\mathbf{U}}_k^* = \arg\min_{\tilde{\mathbf{U}}_k} \quad \overbrace{Q_t N_s (v_{ref} - \tilde{x}_{9,k|N_s-1})^2}^{J_{\text{terminal}}} + \underbrace{+ \frac{1}{N_s} \sum_{j=0}^{N_s-1} Q_c f_6^4(\tilde{\mathbf{x}}_{k|j}) + Q_v \left| v_{ref} - \tilde{x}_{9,k|j} \right| + Q_u \tilde{u}_{k|j}^4}_{J_0} \tag{4.30a}$$

$$\text{s.t.} \quad \tilde{\mathbf{x}}_{k|j+1} = \mathbf{f}(\tilde{\mathbf{x}}_{k|j}, \mathbf{z}_{k|j}, \tilde{u}_{k|n}), \quad \tilde{\mathbf{x}}_{k|0} = \mathbf{x}_k, \tag{4.30b}$$

$$\tilde{\mathbf{x}}_{k|j} \in \mathcal{X}, \quad \mathbf{z}_{k|j} \in \mathbf{Z}_k', \quad \forall j = 0, 1, \ldots, N_s - 1 \tag{4.30c}$$

$$\tilde{u}_{k|n} \in \mathcal{U}, \quad \forall n = 0, 1, \ldots, N_p - 1 \tag{4.30d}$$

where the road information in the half-car case $\mathbf{Z}_k' \in \mathbb{R}^{N_s \times 2}$ is defined as:

$$\mathbf{Z}_k' = \begin{bmatrix} \underbrace{\zeta_{r,k|0}'}_{\mathbf{z}_{k|0}} & \underbrace{\zeta_{r,k|1}'}_{\mathbf{z}_{k|1}} & \cdots & \underbrace{\zeta_{r,k|N_s-2}'}_{\mathbf{z}_{k|N_s-2}} & \underbrace{\zeta_{r,k|N_s-1}'}_{\mathbf{z}_{k|N_s-1}} \\ \underbrace{\zeta_{f,k|0}'}_{\mathbf{z}_{k|0}} & \underbrace{\zeta_{f,k|1}'}_{\mathbf{z}_{k|1}} & \cdots & \underbrace{\zeta_{f,k|N_s-2}'}_{\mathbf{z}_{k|N_s-2}} & \underbrace{\zeta_{f,k|N_s-1}'}_{\mathbf{z}_{k|N_s-1}} \end{bmatrix}^T. \tag{4.31}$$

In Fig. 4.13 the trajectory was planned with two driver models with different internal vehicle models. Both results are given superimposed. The reference is the dotted tra-

[8] Indexing for the vehicle model is omitted.

Die approbierte gedruckte Originalversion dieser Diplomarbeit ist an der TU Wien Bibliothek verfügbar
The approved original version of this thesis is available in print at TU Wien Bibliothek.
TU Bibliothek Your knowledge hub WIEN

jectory generated by the driver model in (4.29) with an internal quarter-car model. The simulation model matches the internal vehicle model. The second driver model uses a half-car as internal model in (4.30) and results in the solid black line. It is noticed clearly

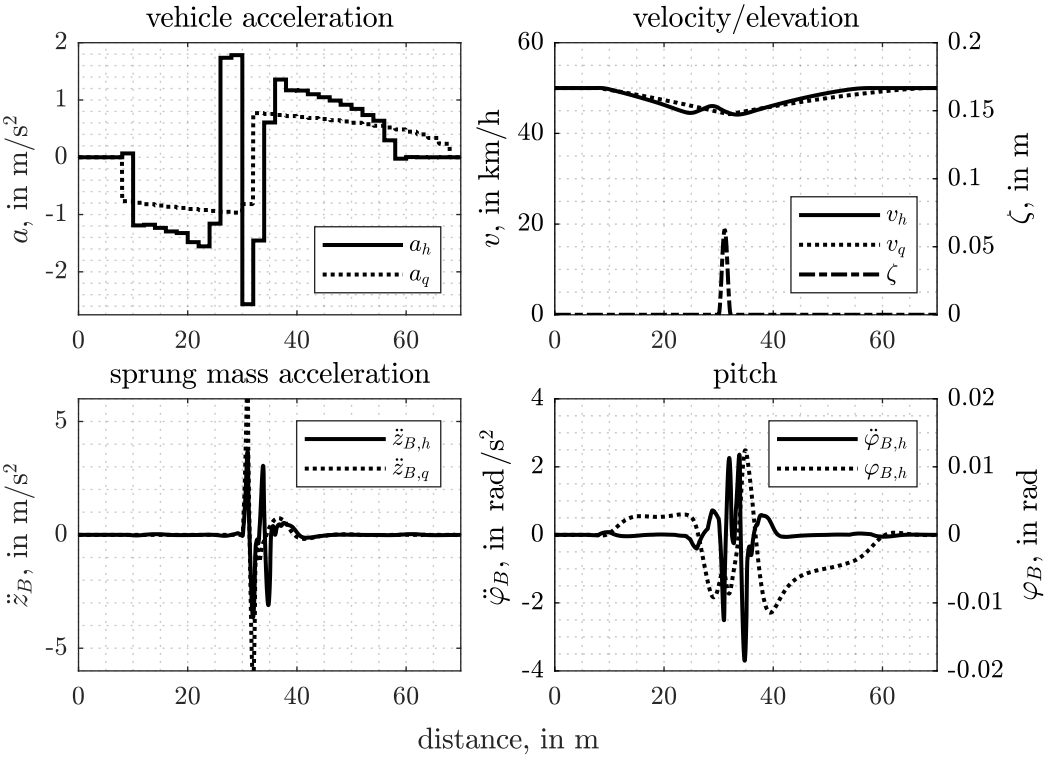

Figure 4.13: Comparison of the driver model based on the quarter-car (dashed) and half-car (solid). The inclusion of the pitching in the half-car lead to an acceleration and braking maneuver at the tip of the cosine bump. Note the subscript for the half-car (h) and quarter-car (q). The bottom right plot only shows the pitching motion for the driver model based on the half-car.

that the driver model based on the half-car acts similarly to the quarter-car driver in the braking and acceleration phase before and after the obstacle. However, the new driver model behaves differently in the middle section. The driver interrupts its braking phase with a short acceleration burst. In the following, the behavior will be further examined.

Longitudinal Jerk The first thing to be investigated is why the driver model tends to accelerate just before the bump. A major difference between the quarter-car reference solution and the half-car driver is, of course, the additional pitching motion in both the internal model and the simulation model. In the bottom right plot in Fig. 4.13, the pitch acceleration and angle of the sprung mass are displayed for the half-car driver.

Die approbierte gedruckte Originalversion dieser Diplomarbeit ist an der TU Wien Bibliothek verfügbar
The approved original version of this thesis is available in print at TU Wien Bibliothek.
TU Bibliothek Your knowledge hub WIEN

In the deceleration phase the pitch angle is positive meaning that the front suspension is compressed due to braking. When the vehicle hits the bump on the front axle the suspension would further compress and this would translate to higher sprung mass acceleration. Therefore, the driver-model tries to mitigate the influence of the bump by quickly accelerating before it, hence extending the front suspension – visible through the negative pitch angle shortly before the 30 m mark – and reducing the overall body acceleration experienced by the driver.

Currently, only the longitudinal acceleration as vehicle input is penalized in the cost function. This prevents longitudinal accelerations from becoming too large, but shapes the trajectory only to a certain extent. To get more control over the shape of the vehicle acceleration trajectory, the longitudinal jerk is additionally taken into account. Longitudinal jerk is understood as the derivative of the longitudinal acceleration, $r_k = \frac{da_k}{dt}$. A rapidly changing longitudinal acceleration corresponds to high jerk values. Thus, if the jerk is now penalized, the following cost function is obtained

$$J(\tilde{\mathbf{X}}_k, \tilde{\mathbf{U}}_k) = J_0(\tilde{\mathbf{X}}_k) + J_{\text{terminal}}(\tilde{\mathbf{X}}_k) + J_{\text{jerk}}(\tilde{\mathbf{U}}_k)\,, \tag{4.32a}$$

$$\text{with} \quad J_0(\tilde{\mathbf{X}}_k) = \frac{1}{N_s}\sum_{j=0}^{N_s-1} Q_c f_6^4(\tilde{\mathbf{x}}_{k|j}) + Q_v \left| v_{ref} - \tilde{x}_{9,k|j} \right| + Q_u \tilde{x}_{10,k|j}^4\,, \tag{4.32b}$$

$$J_{\text{terminal}}(\tilde{\mathbf{X}}_k) = Q_t N_s (v_{ref} - \tilde{x}_{9,k|N_s-1})^2\,,$$

$$J_{\text{jerk}}(\tilde{\mathbf{U}}_k) = \frac{1}{N_s}\sum_{j=0}^{N_s-1} Q_r r_{k|j}^2 = \frac{1}{N_s}\sum_{j=0}^{N_s-1} Q_r \tilde{u}_{k|j}^2\,.$$

The underlying system dynamics in (4.30b) have shifted to the jerk model given in (3.40) and the new input/optimization variable is the longitudinal jerk. Simulating the modified driver model with the jerk as input and comparing it to the previously one yields Fig. 4.14.

The weight of the jerk $Q_r \in \mathbb{R}_{>0}$ is responsible for the more rounded shape of the trajectory. At lower weights, the acceleration curve approaches that without jerk weighting and has a more trapezoidal shape. At larger values, the trajectory is rounder and more of a sinusoidal shape. Only minor differences in the sprung mass accelerations are evident from the plot. A deeper insight is given by plotting the optimal costs at each time k for the different terms, as shown in Fig. 4.15. A closer look at the comfort term $\ddot{z}_B$ reveals a higher comfort in the vertical direction for a driver model without jerk penalty.

Pitch-Dynamics So far, only the Basic-Cost-Function is considered with the adaption of longitudinal jerk to generate smoother trajectories. The intention behind this section

Die approbierte gedruckte Originalversion dieser Diplomarbeit ist an der TU Wien Bibliothek verfügbar
The approved original version of this thesis is available in print at TU Wien Bibliothek.
TU Bibliothek Your knowledge hub WIEN

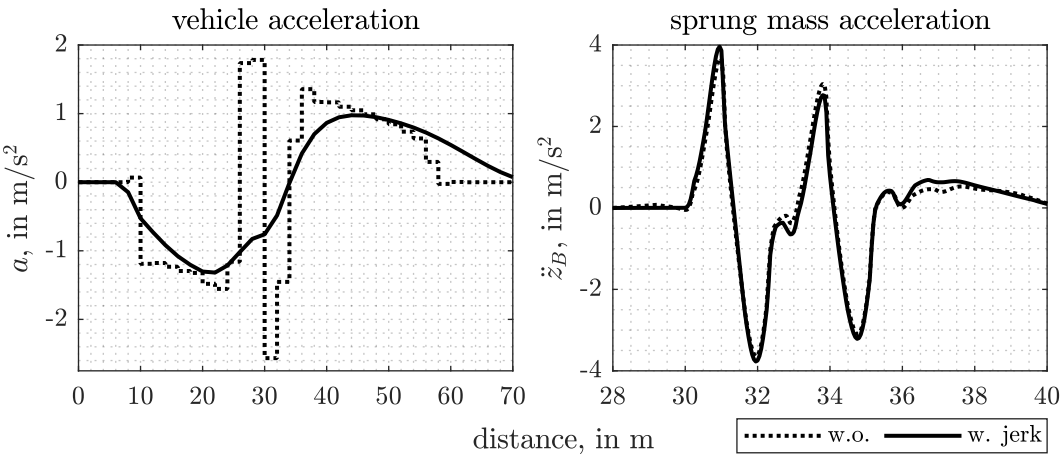

Figure 4.14: Basic-Cost-Function extended with jerk penalty: Adding vehicle jerk to the model and penalizing the jerk results in a smoother longitudinal vehicle acceleration. The solid line shows the driver model with jerk penalty, while the dashed line shows the driver model without jerk penalty. Simulated is the bump of Fig. 4.13.

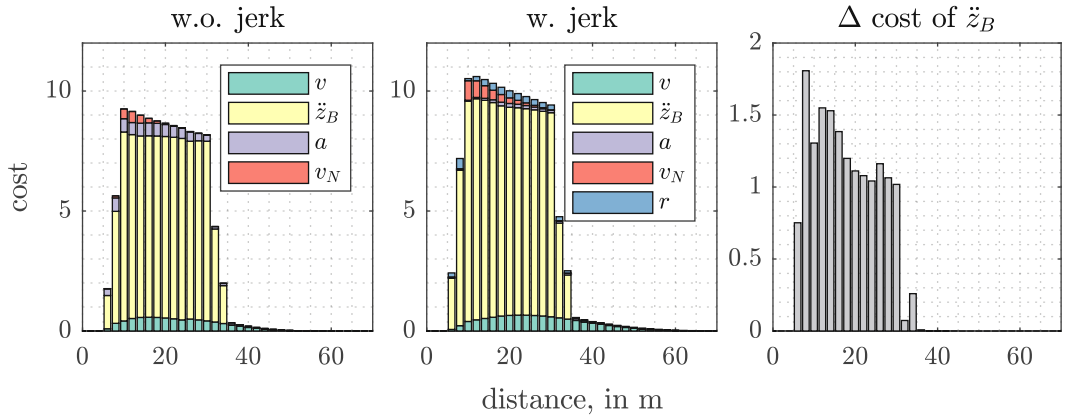

Figure 4.15: Individual costs at each step k along the road for a given cosine-shaped bump acting at 30 m. The smoother transition near the bump with the additional jerk terms in Fig. 4.14 comes at the cost of decreased ride comfort. The graph on the right plots the cost difference between the comfort terms: Positive values indicate that the driver model provides a smoother ride without the additional jerk term.

Die approbierte gedruckte Originalversion dieser Diplomarbeit ist an der TU Wien Bibliothek verfügbar
The approved original version of this thesis is available in print at TU Wien Bibliothek.

– as well as the half-car – is to improve the comfort and planning capabilities of the driver model by considering the pitching of the vehicle as well. The following paragraphs will investigate the pitch motion in the cost function with focus mainly on

- pitch acceleration $\ddot{\varphi}_B$ and
- pitch angle φ_B.

Pitch-Acceleration For the pitch acceleration, several different cost terms can be designed, e.g. in an absolute fashion, quadratic or quartic, similar to the sections for the quarter-car driver model. In the most straightforward case, the pitch acceleration is simply added as an additional term in the cost function:

$$J_{\text{pitch}}(\tilde{\mathbf{X}}_k) = \frac{1}{N_s} \sum_{j=0}^{N_s-1} Q_p f_8^4(\tilde{\mathbf{x}}_{k|j}) = \frac{1}{N_s} \sum_{j=0}^{N_s-1} Q_p \ddot{\varphi}_{B,k|j}^4 \,. \tag{4.33}$$

Here $Q_p \in \mathbb{R}_{>0}$ is used to weight the total influence of the pitch acceleration accordingly. The pitch acceleration is given by (3.40). In (4.33) a quartic weighting function is chosen without any special considerations, apart from the reasoning for a simpler weighting between the other accelerations in the previous sections.

In Fig. 4.16, the driver model advanced with the penalty for longitudinal jerk and pitch acceleration was simulated for the cosine bump of Fig. 4.13. The weight and therefore the importance of the pitch acceleration was gradually increased. With increasing weight the optimized vehicle acceleration trajectory shapes a similar behavior as in the case of the model without the penalty on the jerk. As can be seen in the right graph, the improvement of the pitch acceleration is marginal, and enhancements are only visible in the phase after the bump. In Fig. 4.16 a small weight of $Q_p = 1$ is advantageous in the acceleration phase, while the vehicle acceleration is still smooth in the transition phase over the bump. A small weight of the pitching acceleration can therefore be advantageous if the smoothness of the planned vehicle acceleration trajectory is not strongly disturbed. However, a higher weighting of the pitching acceleration penalty has a negative effect and again leads to undesirable behavior on the bump, as observed previously.

Another possibility to take pitch acceleration into account is to determine a mixed comfort criterion of pitch $\ddot{\varphi}_B$ and vertical acceleration $\ddot{z}_B$ derived from a virtual "headrest" position of the driver in Fig. 4.17. A virtual point, e.g., the driver's headrest – whereby seat dynamics were of course neglected here – is introduced into the model and used to evaluate comfort. For this purpose, the vertical and longitudinal accelerations

Die approbierte gedruckte Originalversion dieser Diplomarbeit ist an der TU Wien Bibliothek verfügbar
The approved original version of this thesis is available in print at TU Wien Bibliothek.
TU Bibliothek Your knowledge hub WIEN

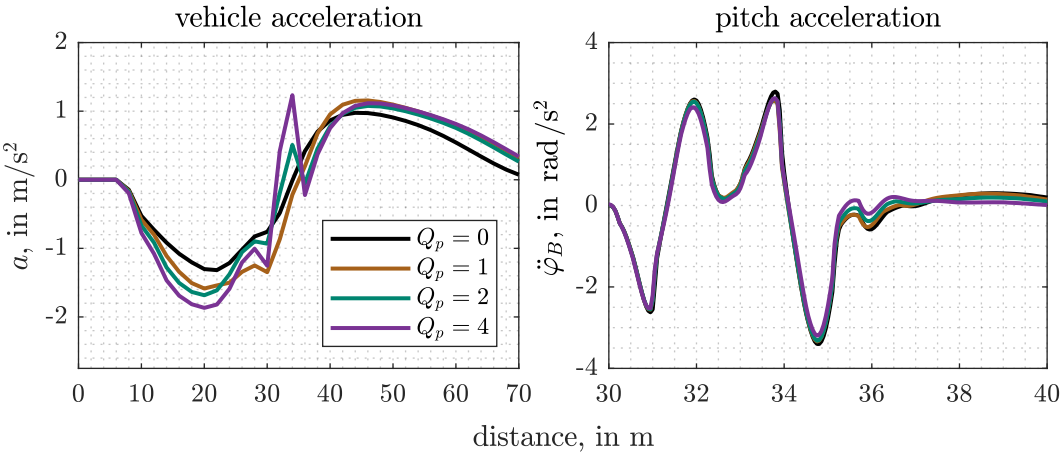

Figure 4.16: Basic-Cost-Function extended with jerk and pitch acceleration penalty: As can be seen in the left plot, the pitch acceleration penalty counteracts a smooth trajectory. To reduce the pitch acceleration, the driver model tries to accelerate near the hill to stretch the suspension and reduce the influence of the obstacle on the pitching. Cosine bump of Fig. 4.13 traversed.

are calculated, assuming linearized pitch dynamics:

$$a_{r,k|j} = a_{k|j} + h_r \ddot{\varphi}_{B,k|j} = \tilde{x}_{10,k|j} + h_r f_8(\tilde{\mathbf{x}}_{k|j}) \,, \tag{4.34a}$$

$$\ddot{z}_{r,k|j} = \ddot{z}_{B,k|j} - b_r \ddot{\varphi}_B = f_6(\tilde{\mathbf{x}}_{k|j}) + b_r f_8(\tilde{\mathbf{x}}_{k|j}) \,, \tag{4.34b}$$

where $h_r \in \mathbb{R}$ and $b_r \in \mathbb{R}$ are the vertical and horizontal distance from the center of mass to the virtual headrest. The accelerations in vertical and horizontal direction combine the old comfort criterion with the pitching motion, which then yields a new cost function $J_0(\cdot)$ as

$$J_0(\tilde{\mathbf{X}}_k) = \frac{1}{N_s} \sum_{j=0}^{N_s-1} Q_c \ddot{z}_{r,k|j}^4 + Q_v \left| v_{ref} - \tilde{x}_{9,k|j} \right| + Q_u a_{r,k|j}^4 \,. \tag{4.35}$$

Simulations using this approach give very similar results to those using the pitch acceleration term (4.33) and are therefore not shown.

Pitch-Angle There is also the question of the extent to which the driver reacts to the change in inclination caused by the vehicle pitching under various conditions. Extending the Basic-Cost-Function with the jerk penalty by an additional pitch angle penalty, e.g., using a quadratic weight function, yields the results shown in Fig. 4.18. To show only the influence of a pitch angle penalty, a pitch acceleration penalty was omitted.

In Fig. 4.18 the cost function was advanced with a penalty for the pitch angle with a

Die approbierte gedruckte Originalversion dieser Diplomarbeit ist an der TU Wien Bibliothek verfügbar
The approved original version of this thesis is available in print at TU Wien Bibliothek.
TU Bibliothek Your knowledge hub WIEN

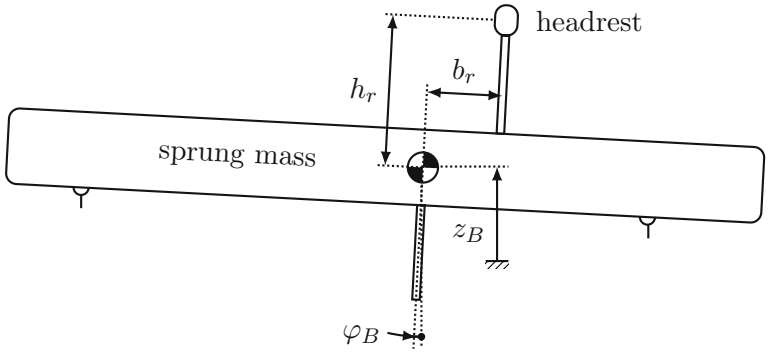

Figure 4.17: Half-Car model with headrest: Calculating the accelerations of a "virtual" headrest yields a new comfort criterion. The virtual headrest position is given by the distances h_r and b_r with respect to the center of mass of the sprung mass.

quadratic function. Since the magnitude of the pitch angle is small compared to the other quantities, large weights must be chosen so that the effect of the additional cost term becomes visible. Penalizing the pitch angle causes small changes in the braking phase, since the ride comfort term $\ddot{z}_B$ dominates here in the cost function. In the acceleration phase after the obstacle, on the other hand, the term has a large influence, which is mainly reflected in a reduced maximum longitudinal acceleration, resulting in smaller pitch angles during the phase (as shown starting at 40 m). However, the peak-to-peak value of the pitch angle while passing the bump (at about 30 meters in the figure) is slightly improved. Due to the restrictive behavior of the pitch angle penalty in the acceleration phase, the penalty is excluded from the final driver model.

Constraints and Reaction Time Similar to the driver model with an internal quarter-car model in Sec. 4.4.1, the reaction time can be introduced either by delaying the road information and vehicle states, by delaying the optimized control input, or by directly considering the reaction time in the optimization problem. Similarly, the direct approach has been adopted for the final half-car driver model. The input space $\mathcal{U}$ is constrained as described in (4.26) and (4.27) in Sec. 4.4.1.

In addition, a lower bound on the vehicle speed is implemented to intercept the singularity which is introduced through the reformulation of the equations of motion from temporal to space in Sec. 4.2:

$$\mathcal{X} = \left\{ \tilde{\mathbf{x}}_{k|j} \in \mathbb{R}^{10} \,\middle|\, \tilde{x}_{9,k|j} \geq v_{min} \,, \quad \forall j = 0, 1, \ldots, N_s - 1 \right\} . \tag{4.36}$$

Die approbierte gedruckte Originalversion dieser Diplomarbeit ist an der TU Wien Bibliothek verfügbar
The approved original version of this thesis is available in print at TU Wien Bibliothek.
TU Bibliothek Your knowledge hub WIEN

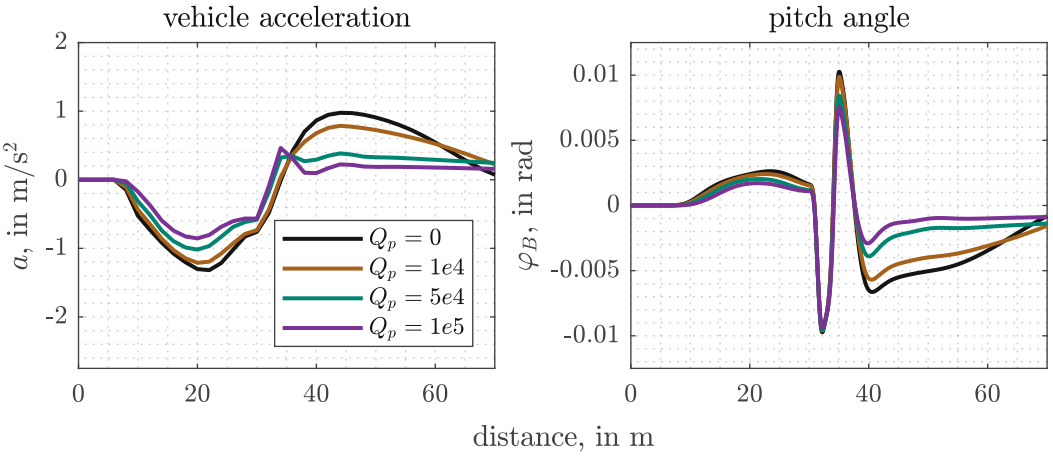

Figure 4.18: Basic-Cost-Function extended by jerk and pitch angle penalties: The pitch angle penalty leads to a limitation of the maximum acceleration after the obstacle and has a rather small influence in the braking phase. Cosine bump of Fig. 4.13 traversed.

In summary, the half-car driver model based on the jerk model in (3.40), the cost terms $J_0(\cdot)$, $J_{\text{terminal}}(\cdot)$ and $J_{\text{jerk}}(\cdot)$ in (4.32b) and the pitch cost $J_{\text{pitch}}(\cdot)$ in (4.33) is written as:

$$\tilde{\mathbf{U}}_k^* = \underset{\tilde{\mathbf{U}}_k}{\arg\min} \quad J_0(\tilde{\mathbf{X}}_k) + J_{\text{terminal}}(\tilde{\mathbf{X}}_k) + J_{\text{pitch}}(\tilde{\mathbf{X}}_k) + J_{\text{jerk}}(\tilde{\mathbf{U}}_k) \tag{4.37a}$$

$$\text{s.t.} \quad \tilde{\mathbf{x}}_{k|j+1} = \mathbf{f}(\tilde{\mathbf{x}}_{k|j}, \mathbf{z}_{k|j}, \tilde{u}_{k|n}), \quad \tilde{\mathbf{x}}_{k|0} = \mathbf{x}_k, \tag{4.37b}$$

$$\tilde{\mathbf{x}}_{k|j} \in \mathcal{X}, \quad \mathbf{z}_{k|j} \in \mathbf{Z}_k', \quad \forall j = 0, 1, \ldots, N_s - 1 \tag{4.37c}$$

$$\tilde{u}_{k|n} \in \mathcal{U}, \quad \forall n = 0, 1, \ldots, N_p - 1 \tag{4.37d}$$

The effect of reaction time on the planned trajectories was investigated. It turned out that the effects on the trajectory of longitudinal acceleration were similar to the findings for the quarter-car driver model described in Sec. 4.4.1: The trajectories are shifted to the right in time, and it was found that the direct approach, where the reaction time is considered in the optimization problem, gives the best results. Since the effect of reaction time in the driver model is qualitatively similar to that observed for the quarter-car driver model, it is refrained from discussing in detail here again.

Die approbierte gedruckte Originalversion dieser Diplomarbeit ist an der TU Wien Bibliothek verfügbar
The approved original version of this thesis is available in print at TU Wien Bibliothek.
TU Bibliothek Your knowledge hub WIEN

5 Simulation and Results

In this chapter, the driver model proposed in this work is tested on several obstacles as introduced in Sec. 3.6. To illustrate the influence of the internal vehicle model on the trajectory generation of the driver model, driver models with different internal vehicle models are compared. The resulting trajectories are qualitatively evaluated. It is also investigated to what extent the driver should be aware of nonlinearities in the vehicle model. Furthermore, this section deals with three short case studies dealing with driver model mismatch. This chapter concludes with a short section that focuses on modeling different driver behaviors.

5.1 Road Obstacles and Bumps

In the previous chapters, methodically on the basis of one obstacle, the driver model respectively the cost function of the underlying optimization problem was set up. For this purpose, a bump was chosen which, from the analysis of the transfer function and from [44], has the biggest impact in terms of discomfort $\ddot{z}_B$ on human drivers. This does not guarantee, however, that the driver model found in this way is suitable for all common road elevations and provides trajectories that meet the requirements defined in Sec. 4.4. Therefore, the driver models will now be tested on additional road obstacles. Furthermore, the behavior of the driver at different reference speeds will be studied.

Before delving deeper into the driver models, some parameters of the driver model are first defined, which – with some exceptions – apply to the upcoming simulations. The parameters are given in Tab. 5.1.

For the different driver models, the cost function $J(\cdot)$ is taken from the last section of the respective driver model, i.e., for the quarter-car driver model in (4.29) and for the half-car driver model in (4.37). It may be noted that in the previous chapter, the simulation model always matched the internal model with which the driver planned its trajectories, i.e., the quarter-car driver drove a quarter-car vehicle. In the following, the traversal of an obstacle is always simulated with the half-car model, regardless of the driver model. In addition to the half-car model, the simulation model features wheel

Die approbierte gedruckte Originalversion dieser Diplomarbeit ist an der TU Wien Bibliothek verfügbar
The approved original version of this thesis is available in print at TU Wien Bibliothek.
TU Bibliothek Your knowledge hub WIEN

lift-off if the dynamic tire force drops below the static one (total tire force vanishes).

General Parameters		
parameter	*value*	*unit*
l_{prev}	25	m
Δl_s	0.05	m
Δl_p	2	m
t_r	0.4	s
v_{min}	10	km/h
v_{ref}	50	km/h
N_s	500	1
N_p	12	1
Solver	fmincon interior-point	-

Weights for the optimality criterion $J(\cdot)$			
parameter	*Quarter-Car*	*Half-Car*	*unit*
Q_s	0.7	0.5	$\mathrm{s\,m^{-1}}$
Q_c	0.3	1.0	$\mathrm{s^{\,8}m^{-4}}$
Q_u	1.0	0.1	$\mathrm{s^{\,8}m^{-4}}$
Q_t	1×10^{-3}	1×10^{-3}	$\mathrm{s^2\,m^{-2}}$
Q_r	-	0.1	$\mathrm{s^{\,6}m^{-2}}$
Q_p	-	1.0	$\mathrm{s^{\,8}}$

Table 5.1: Parameters for the driver models: The left table contains the general parameters for the optimization problem. The right table contains the weights for the different terms in the cost function, given once for the quarter-car driver and the half-car driver.

5.1.1 Cosine Shaped Bumps

In this section, cosine shaped bumps are traversed. Cosine bumps are a commonly used obstacle as they closely resemble real-world obstacles on roads and the assumption of a single-point excitation of the underlying vehicle model is fulfilled [44]. To highlight the improvement of comfort and other values, two additional solutions are considered: a global optimization and a constant speed approach.

The global optimization (*GLOBAL*) considers the entire road at once and solves the same optimization problem as the driver model, but for the entire finite road path instead of a specific finite prediction horizon Δl_{prev}. Since the entire path is optimized at once, no driver reaction time is considered. The constant velocity (*INIT*) approach is introduced as a measure of improvement. In this approach, the obstacle is passed without any control intervention.

Bumps derived from Resonant Frequencies In Sec. 3.6 three cosine bumps were designed based around the resonant frequencies of the vehicle-model and the sensitivity of humans to vertical acceleration. The design parameters are given in Tab. 3.1.

Fig. 5.1 shows the behavior of the quarter-car and half-car driver models passing through all three road elevations in sequence. In the left column the responses of the

Die approbierte gedruckte Originalversion dieser Diplomarbeit ist an der TU Wien Bibliothek verfügbar
The approved original version of this thesis is available in print at TU Wien Bibliothek.
TU Bibliothek Your knowledge hub WIEN

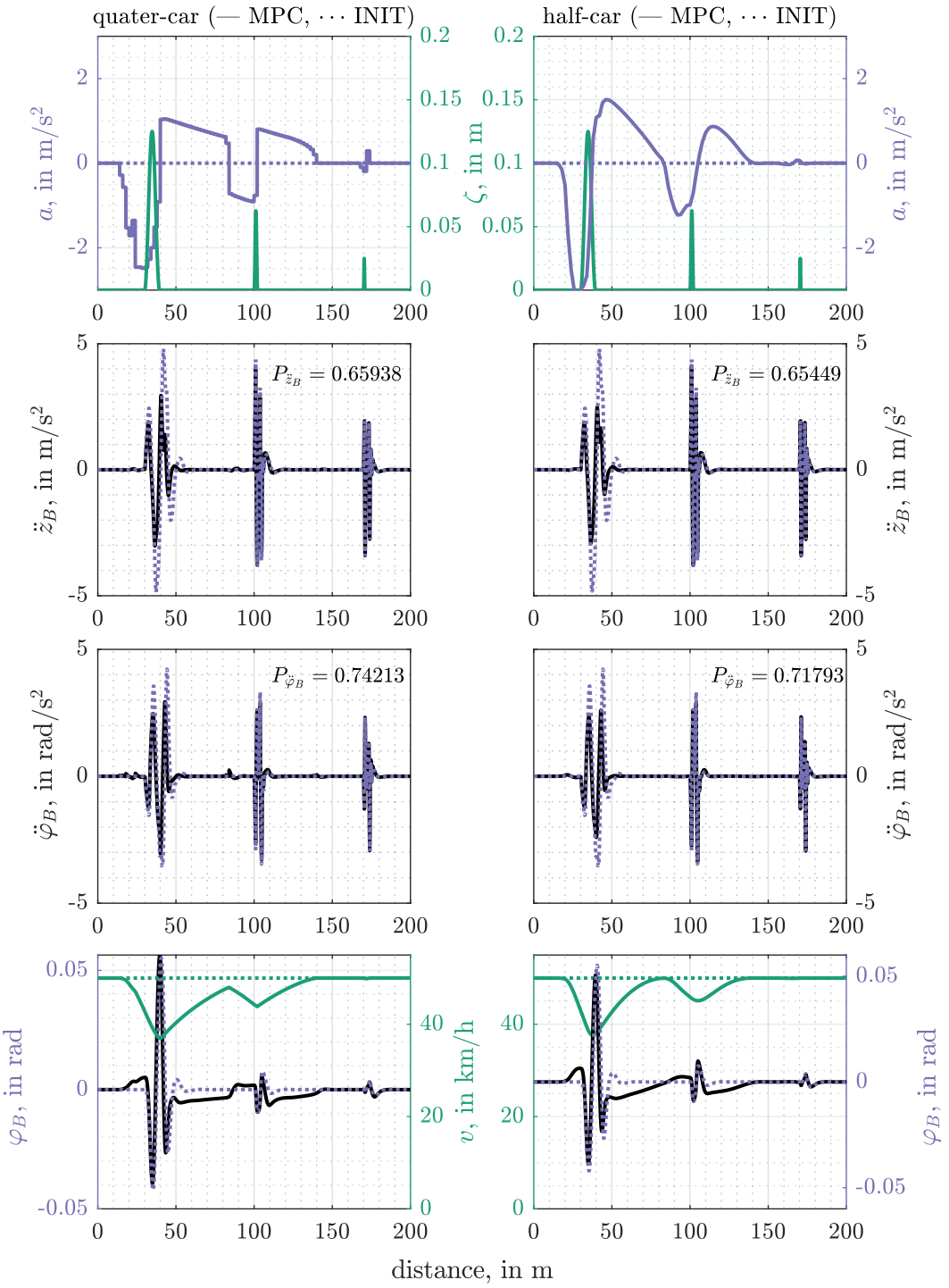

Figure 5.1: Simulation model response (left: driver with internal quarter-car; right: driver with internal half-car) when traversing a sequence of cosine bumps. Only slight differences are evident in the vertical and pitch acceleration curves between the driver models. Performance measures relative to the *INIT* simulation are given as well: $P_{\ddot{z}_B} = \frac{\mathrm{RMS}\left(\ddot{z}_B^{\mathrm{MPC}}\right)}{\mathrm{RMS}\left(\ddot{z}_B^{\mathrm{INIT}}\right)}$, $P_{\ddot{\varphi}_B} = \frac{\mathrm{RMS}\left(\ddot{\varphi}_B^{\mathrm{MPC}}\right)}{\mathrm{RMS}\left(\ddot{\varphi}_B^{\mathrm{INIT}}\right)}$.

Die approbierte gedruckte Originalversion dieser Diplomarbeit ist an der TU Wien Bibliothek verfügbar
The approved original version of this thesis is available in print at TU Wien Bibliothek.
TU Bibliothek Your knowledge hub WIEN

driver model with an internal quarter-car representation and similarly in the right column for a driver with an half-car representation are given. As a reference, the response of a vehicle traversing the obstacles with a constant velocity (*INIT*) is overlapped. The trajectories of both driver models depict a similar behavior. The planned trajectories of the half-car driver are smoother as the jerk penalty in the cost function enforces this. This is well reflected in the pitch angle φ_B and vehicle acceleration a. The quarter-car driver rapidly changes from accelerating to braking whereas the half-car driver model transitions smoothly. Both drivers barely react to the smallest elevation close to the end. By tuning, respectively, by shifting the sensitivity in the driver's sense, a more responsive behavior could be achieved for the smaller bump. For comparison, two numeric performance measures $P_{\ddot{z}_B}$ and $P_{\ddot{\varphi}_B}$ are introduced in Fig. 5.1. The performance measure $P_{\ddot{\varphi}_B}$ indicates that the half-car driver with its additional weight for the pitch acceleration performs better. In addition to the initial solution, the response of the driver is compared to an optimal solution for the whole trajectory. The global optimization for the quarter-car driver is given in Fig. 5.2.

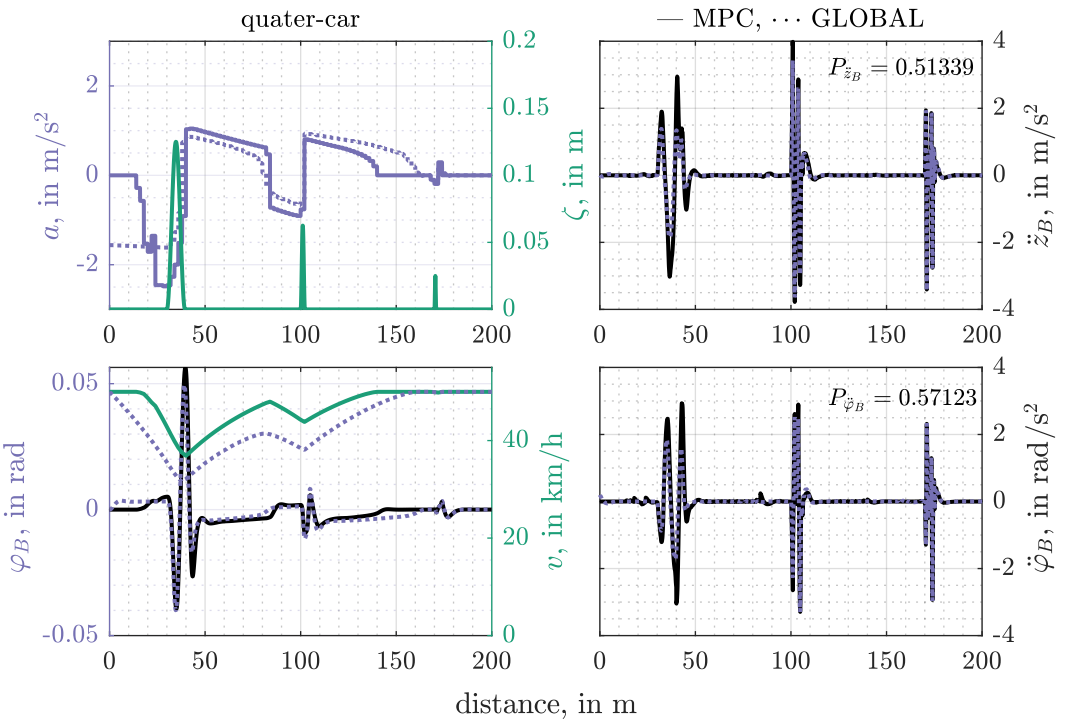

Figure 5.2: Global optimization for the quarter-car driver: The driver model is aware of the whole road and can therefore initiate the braking instantly. Performance measures $P_{\ddot{z}_B}$ and $P_{\ddot{\varphi}_B}$ are for the global trajectory and relative to the constant speed simulation in Fig. 5.1.

Die approbierte gedruckte Originalversion dieser Diplomarbeit ist an der TU Wien Bibliothek verfügbar
The approved original version of this thesis is available in print at TU Wien Bibliothek.
TU Bibliothek Your knowledge hub WIEN

In the case of global optimization, the driver model can initiate braking immediately and thus further reduce its speed and significantly improve comfort, as the performance measurements indicate. Of course, this means that the selected preview distance of 25 meters is not optimal for this situation and a higher value might be preferred. Depending on the obstacle ahead, an adaptive preview distance would be of interest to adjust. Especially at higher speeds, a larger preview distance is advantageous.

Severe Speed Bump Similar to the work in [25], a cosine speed bump is designed with a width of $W_b = 1\,\text{m}$ and a height of $H_b = 0.1\,\text{m}$. This bump has a height similar to the longest (first) bump in Fig. 5.1, but a width similar to the shortest (last) bump. This should lead to a more severe excitation.

In Fig. 5.3 the bump is traversed. The half-car driver shows a significant advantage in this scenario regarding the performance measures. The driver model is aware of the second excitation of the system coming from the rear axle. This driver model also reacts to the second peak at approx. 55 m, which is most clearly visible in the pitching acceleration $\ddot{\varphi}_B$ or the vertical sprung mass acceleration $\ddot{z}_B$. The improvements compared to the quarter-car model are achieved exactly at this point, see second peak of the vertical acceleration $\ddot{z}_B$ for the quarter-car.

The trajectory chosen by the quarter-car driver initially shows an acceleration spike, which in terms of human driving style is undesirable. The reason for this behavior is not entirely clear, but the author assumes that the solver of the optimization problem is stuck in a local minima (see Sec. 5.1.1 for a related discussion). A remedy and improvement could be to utilize trajectory-holding as explained in Sec. 4.4.1 or to penalize the jerk as it is done by the half-car driver as well.

Again, a global optimization in Fig. 5.4 of the entire path leads to a significant improvement in terms of performance measures. Subjectively speaking, the optimized acceleration trajectory does not correspond to a very human behavior, especially with regard to the abrupt change between braking and acceleration phases. Here, particularly the penalty of the jerk in the half-car model helps to produce a smooth transition between the two phases.

Low and High Velocity Approaches Up to this point, the reference speed v_{ref} was always set at 50 km/h. This reference was chosen because the obstacles which are primarily considered in this thesis potentially occur in urban traffic and no higher speeds are legally allowed. In this section, however, the case of lower and higher reference velocities is considered. Especially the high reference velocities are of interest. Let's look at how

Die approbierte gedruckte Originalversion dieser Diplomarbeit ist an der TU Wien Bibliothek verfügbar
The approved original version of this thesis is available in print at TU Wien Bibliothek.
TU Bibliothek Your knowledge hub WIEN

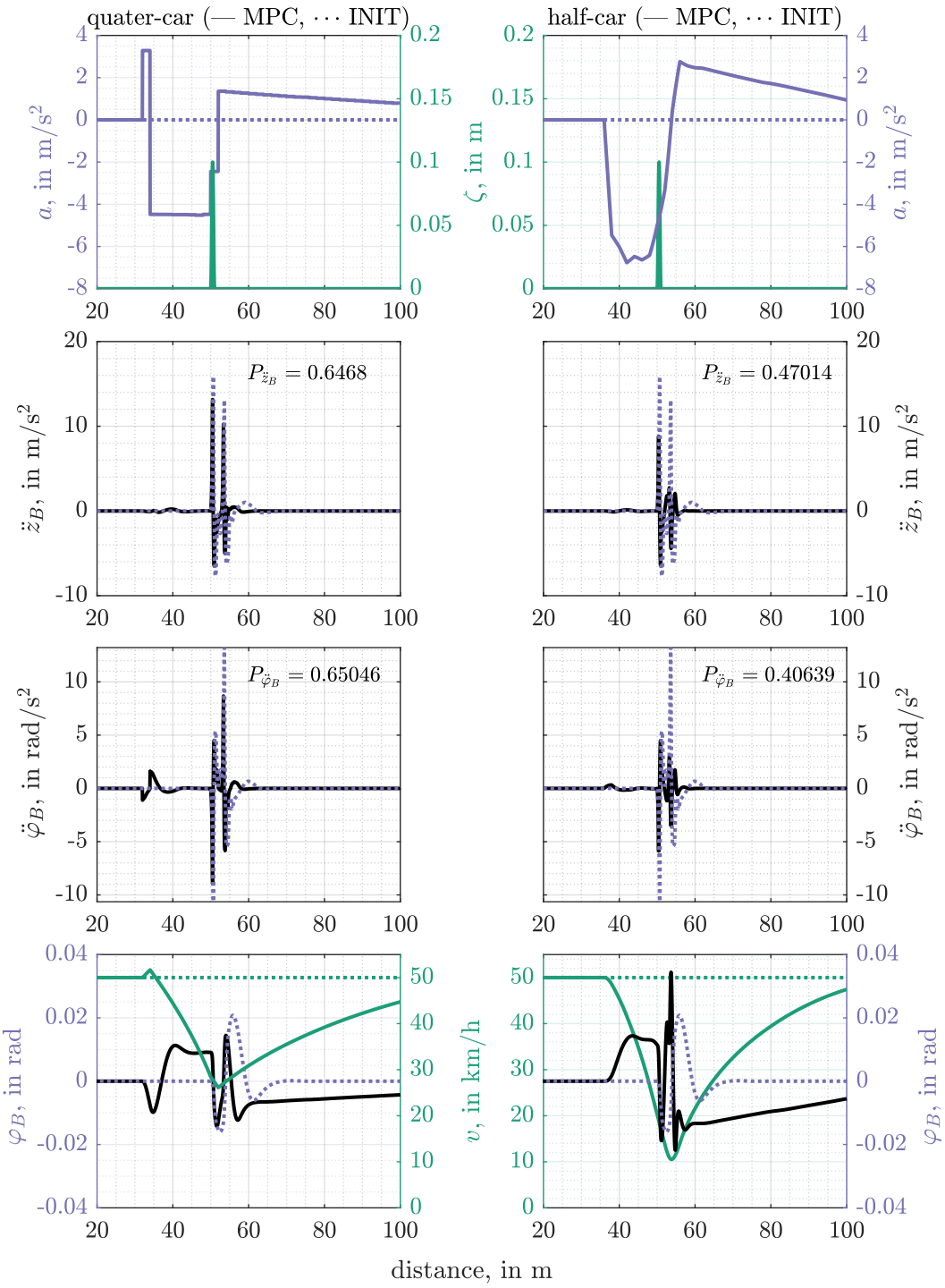

Figure 5.3: Simulation model response (left: driver with internal quarter-car; right: driver with internal half-car) when traversing the severe cosine speed bump. Compared to Fig. 5.1 in which both driver-models perform similarly, in this case the half-car-driver outperforms the quarter-car driver in both performance measures.

Die approbierte gedruckte Originalversion dieser Diplomarbeit ist an der TU Wien Bibliothek verfügbar
The approved original version of this thesis is available in print at TU Wien Bibliothek.

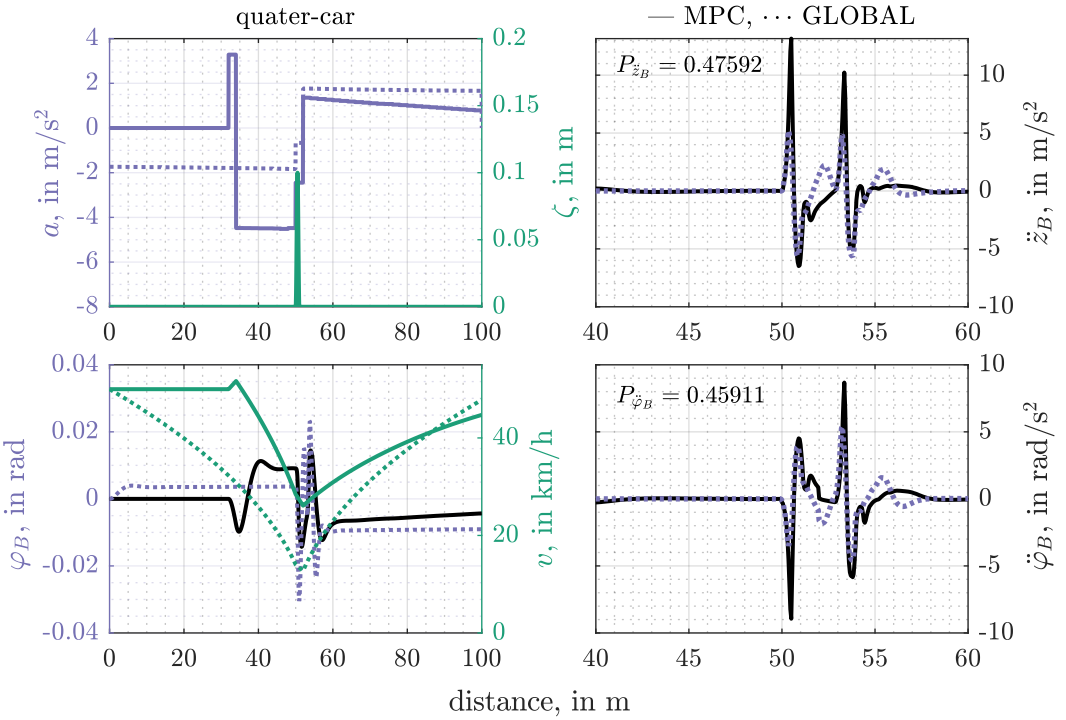

Figure 5.4: Global optimization trajectories when traversing the severe cosine bump: The globally planned trajectory was able to improve in terms of $P_{\ddot{z}_B}$ and $P_{\ddot{\varphi}_B}$ compared to the finite-horizon quarter-car MPC (compare indices with Fig. 5.3).

the half-car driver model behaves at different reference speeds. For this purpose, three different simulation runs were performed in Fig. 5.5 with v_{ref} equal 30 km/h, 50 km/h and 80 km/h.

Planning the optimal speed/acceleration trajectory for a given road obstacle can lead to surprising behavior at high speeds, i.e., the vehicle accelerates instead of braking, as shown in the figure in the upper right of Fig. 5.5 for the severe bump at 80 km/h. This raises the question why the driver model reacts in this way at higher speeds. It should be clarified whether the modeling of the driver by means of the chosen cost function is correct and advocates this behavior or if this behavior corresponds to the optimum of the optimization problem. A closer look at the cost function using global optimization shows that a trajectory where speed is increased instead of decelerated does not correspond to the global optimum. However, looking at the Fig. 4.6, one notices that towards high speeds the RMQ of the comfort term – the driving force for the speed reduction – flattens out and even slightly decreases. This gives rise to local minima for the nonlinear

Die approbierte gedruckte Originalversion dieser Diplomarbeit ist an der TU Wien Bibliothek verfügbar
The approved original version of this thesis is available in print at TU Wien Bibliothek.
TU Bibliothek Your knowledge hub WIEN

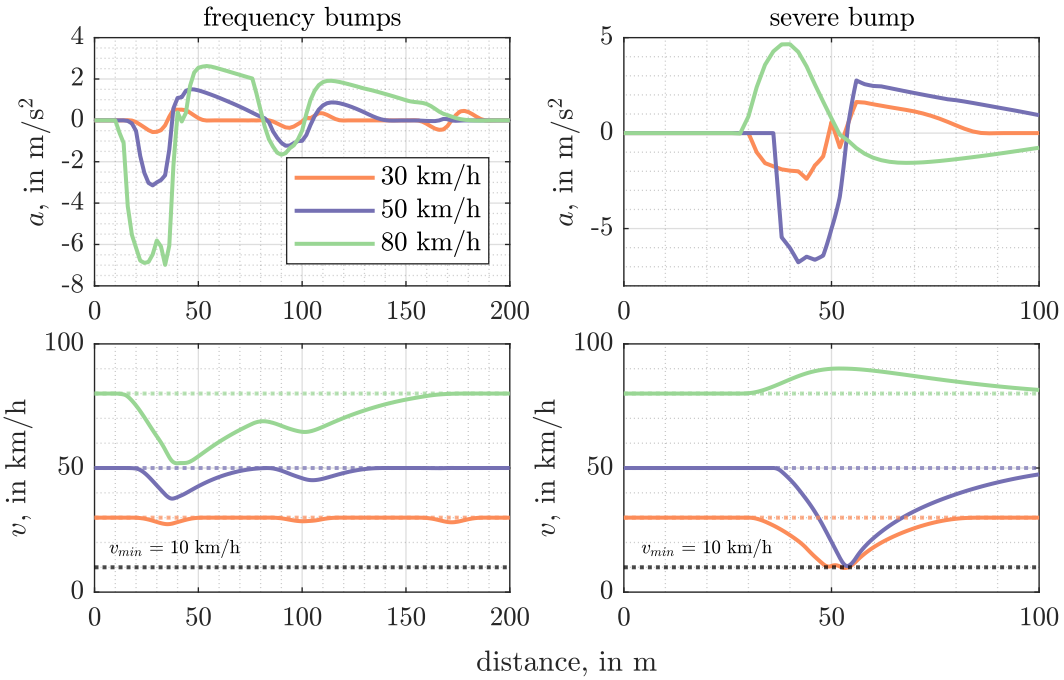

Figure 5.5: Simulations run with the half-car driver model at variations in the reference speed v_{ref}. For the high speed pass with $v_{ref} = 80\,\text{km/h}$ the preview distance l_{prev} is increased to 35 m.

optimization problem where the solver obviously ran into.

Without a more detailed investigation, it is claimed that this problem is mainly caused by the definition of the cost function and the solving procedure of the optimization problem. One could now argue that the range of application is to be found at lower speeds and that this is therefore not a problem. It is nevertheless interesting to know how to deal with the defined driver model at higher speeds.

Some approaches that have been developed to suppress this behavior are based on changing the behavior of the driver model to favor low speeds, or on helping the optimization problem to find the global minima with a better suited initial solution. To let the driver model prefer lower speeds and thus make the optimization problem more robust, the dynamic wheel contact force $F_{z,dyn}$ can be considered in the cost[1]. This is executed in Fig. 5.6. It was investigated also to support the optimization problem by better predefining the solver's initial solution. This can make the solving procedure more robust. The problem has not been addressed further in this thesis and is one of the follow-up tasks that should be addressed and solved in future work.

[1]This, however, raises the question to which extent a human driver is aware of the wheel force.

Die approbierte gedruckte Originalversion dieser Diplomarbeit ist an der TU Wien Bibliothek verfügbar
The approved original version of this thesis is available in print at TU Wien Bibliothek.
TU Bibliothek Your knowledge hub WIEN

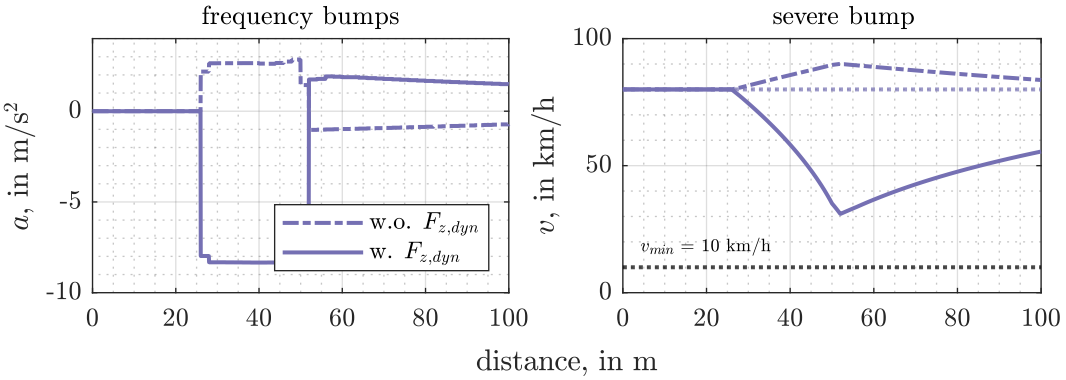

Figure 5.6: High velocity approach simulated with a quarter-car driver model with an additional penalty for the dynamic wheel contact force. Penalizing the wheel contact force $F_{z,dyn} = F_{k,T} + F_{k,S}$ forces a reduction in vehicle speed in the high velocity approach.

5.1.2 Raised Crosswalk

Of particular interest to the half-car are excitations from the road that excite both rear and front axles simultaneously. For this purpose, the case of a raised crosswalk was designed and simulated for both driver-models in Fig. 5.7. The ascent and descent ramps are cosine shaped. The total width is adjusted such that the width of the whole road bump is longer than the wheelbase of the vehicle: width of the crosswalk of 5 m and height of 0.1 m.

In this example, the half-car driver can also outperform the quarter-car driver in terms of the performance indices due to the additional knowledge about pitching motion. Most visible is here the decision from the half-car driver on top of the bump at around 50 m where the model does not immediately switch to the acceleration phase but rather just coasts over the bump and starts accelerating afterwards. In contrary, the quarter-car driver does as well accelerate after the bump but still breaks on top of it which impacts the pitching.

5.1.3 Pothole and Pavement-Curb

Inspired by the works of Čorić in [25], potholes are studied in this section. In addition, a pavement-curb was designed and studied. The assumption made for the simplified tire model (single-point excitation) is certainly no longer valid for the curb. The test case is sketched in Fig. 5.8.

The planned longitudinal acceleration and speed trajectories on this road are simulated

Die approbierte gedruckte Originalversion dieser Diplomarbeit ist an der TU Wien Bibliothek verfügbar
The approved original version of this thesis is available in print at TU Wien Bibliothek.
TU Bibliothek Your knowledge hub WIEN

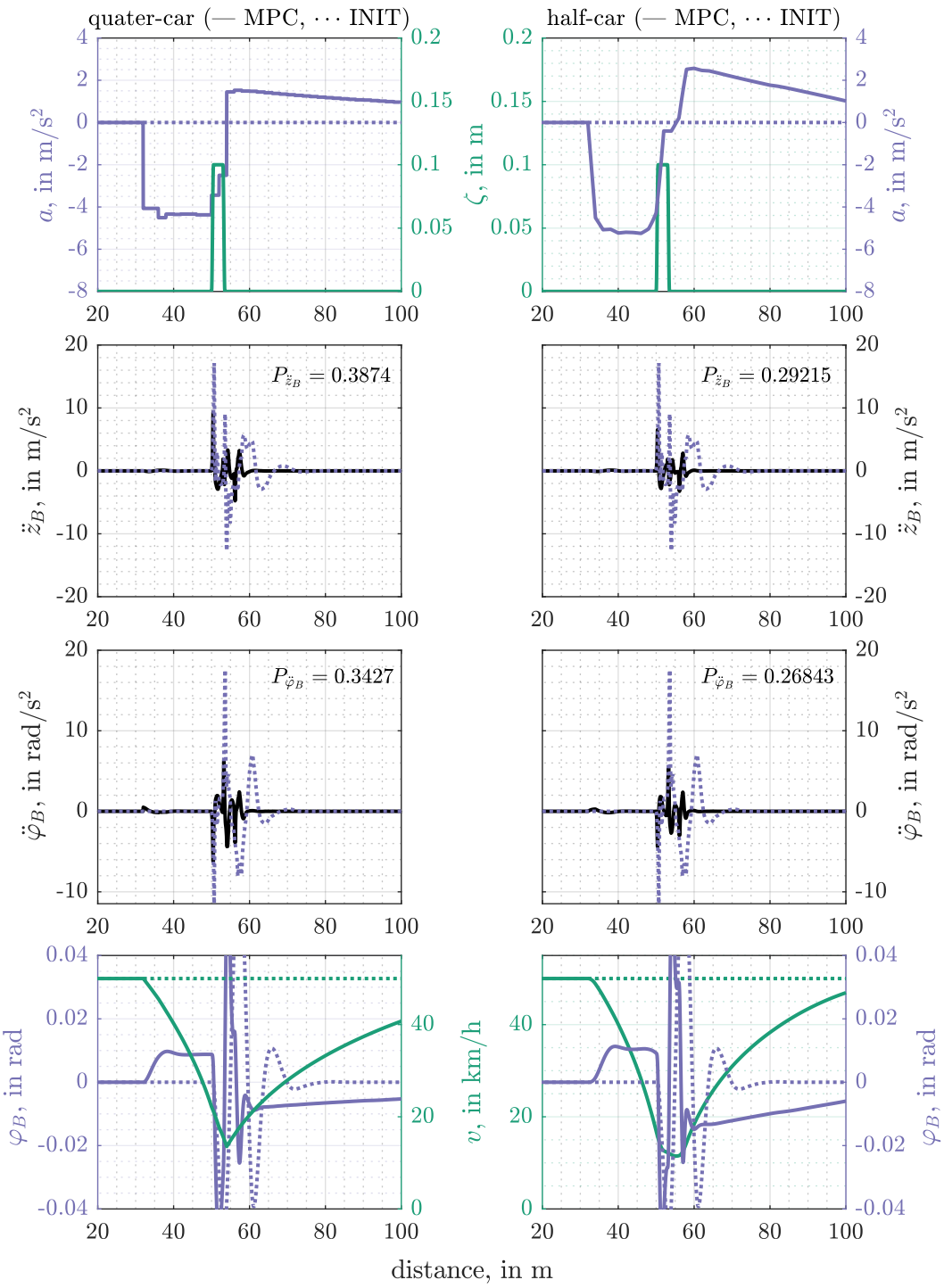

Figure 5.7: Simulation model response (left: driver with internal quarter-car; right: driver with internal half-car) when traversing an elevated pedestrian road crossing. Note the coasting between the braking and acceleration phase in the trajectory for the half-car driver.

Die approbierte gedruckte Originalversion dieser Diplomarbeit ist an der TU Wien Bibliothek verfügbar
The approved original version of this thesis is available in print at TU Wien Bibliothek.
TU Bibliothek Your knowledge hub WIEN

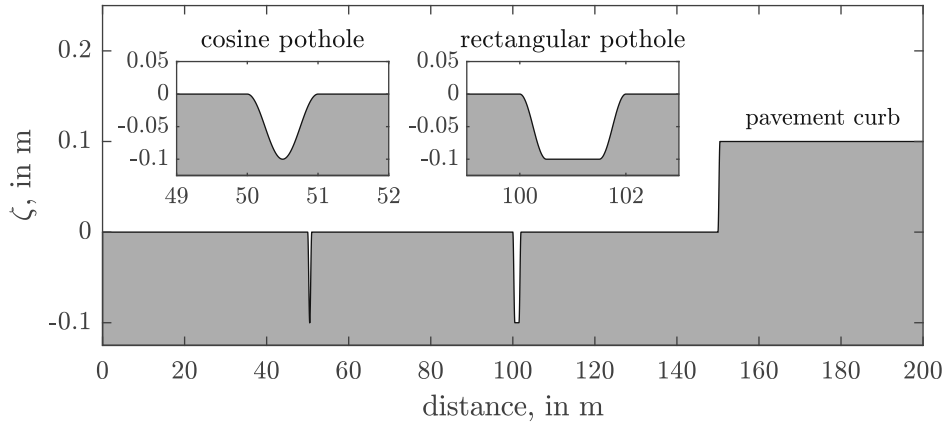

Figure 5.8: Road profile consisting of potholes and a curb. The potholes are inverted cosine shaped bumps similar to the realistic bump, road crossing case and the work in [25]. The curb is designed with a steep cosine on the ramp so that it can be continuously differentiated.

for both driver models in Fig. 5.9. Performance measures: $P_{\ddot{z}_B} = 0.52026$ and $P_{\ddot{\varphi}_B} = 0.3986$ for the half-car driver and $P_{\ddot{z}_B} = 0.6079$ and $P_{\ddot{\varphi}_B} = 0.5417$ for the quarter-car driver. In terms of the performance measures, the half-car driver model performs better. This can also be seen from the fact that the driver model with an internal half-car decelerates the vehicle slightly more at the first obstacle.

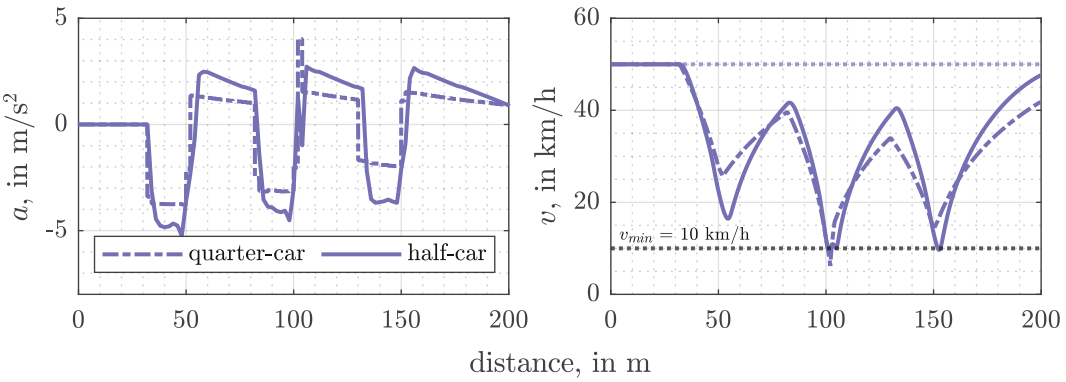

Figure 5.9: Results for traversing the road in Fig. 5.8 with both driver-models. The reference vehicle speed v_{ref} is set to 50 km/h. The quarter-car driver struggles more with the lower speed bound v_{min}.

Die approbierte gedruckte Originalversion dieser Diplomarbeit ist an der TU Wien Bibliothek verfügbar
The approved original version of this thesis is available in print at TU Wien Bibliothek.

5.2 Driver Model Mismatch

Until now, it has been assumed that the driver has a fairly accurate representation of the driving situation. In the previous section, primarily the abstraction level of the vehicle model was investigated, but each of the internal vehicle models for the driver were parameterized such that the dynamic behavior was well approximated with the simulation model: Once the driver knew the driving situation only in form of the simplified quarter-car and in the other variant the driver was given the full model of the half-car. Of course, the quarter-car driver model could already be interpreted as a driver model mismatch, since the driver's internal model does not match the simulation model. From the human's point of view, the driver can not only represent an abstraction of the vehicle in the mind, but can also estimate the parameterization through experience with the vehicle and thus has a good understanding of the dynamic process. In this section, however, it will be examined how a specific driver model deals with completely different conditions, e.g. a different or unknown vehicle. The model does not change, but the parameters of the vehicle do. The driver will now try to cope with the task with the false parameterization.

In the following section, three case studies will deal with this question. The first case study examines the importance for the driver to be aware of nonlinearities in the vehicle suspension, e.g., knowledge of compression and rebound stops. The second case study examines how the driver model changes the planned trajectories when different parameterized internal models are given for the same simulation model, e.g., when the driver is tuned for heavier or light and sporty vehicles. In the third case, an example is considered in which the simulation model has been modified with an additional payload that is not known to the driver in one case and is known in the second case. Of interest is how the driver reacts to the payload in both cases.

5.2.1 Linear Internal Vehicle Model

The first case study is still more concerned with the question of how the driver copes with a simplified internal vehicle model. A related question was already addressed in the previous section when the quarter-car driver was compared to the half-car driver in a simulation environment based on the half-car. In this section, however, the suspension of the half-car driver is modified so that the model in (3.36) is "linear".

For this purpose, the nonlinear spring forces are modified in (3.40). The spring force is relieved of the nonlinear components of the rebound and compression stop (the exponential components in Fig. 3.4a). Thus, the spring force is composed of only the static

Die approbierte gedruckte Originalversion dieser Diplomarbeit ist an der TU Wien Bibliothek verfügbar
The approved original version of this thesis is available in print at TU Wien Bibliothek.
TU Bibliothek Your knowledge hub WIEN

and linear components. A vehicle model with (piece-wise) linear differential equations in time is obtained[2]. The transformation in Sec. 4.2 and the discretization described in Sec. 4.3.1 still result in a nonlinear optimization problem as in (4.4.1), but with different vehicle dynamics.

In Fig. 5.10, the driver model based on the linear vehicle model was routed over the road bumps from the previous section. The cost function, weights, constraints, reaction times and simulation model remain unchanged to previous examples. Fig. 5.10a shows the planned trajectories for the bumps derived from the resonant frequencies and Fig. 5.10b for the severe cosine bump. The performance of the linear driver model when driving over the frequency-derived bumps deteriorates slightly for the vertical sprung mass acceleration indicated by $P_{\ddot{z}_B}$ as well for the pitch acceleration stated by $P_{\ddot{\varphi}_B}$ compared to the half-car driver from the previous section, see Fig. 5.1. In case of the severe bump, the nonlinear driver model is clearly outperforming the linear one in terms of ride comfort. Since the linear driver model is unaware of the end-stops in the suspension, it assumes that the selected speed reduction is sufficient to provide adequate ride comfort. However, as the nonlinear driver model has shown, comfort can be further increased by decelerating the vehicle to the speed limit v_{min}. The nonlinear driver model has shown that knowledge of the end-stops in the suspension is of great importance to achieve high ride comfort when severe obstacles are encountered.

5.2.2 Different Parameterized Internal Vehicle Models

In this section, the behavior of the driver model is investigated with different parameterized internal vehicle models. For comparison, a half-car is always used as the internal model. The first driver model uses the original parameterization (see Appx. A.2) and is referred to here as the *heavy vehicle*. Starting from the nonlinear half-car driver model, the parameterization of the internal vehicle in the driver model is changed to represent a sporty-light vehicle with a stiffer suspension, which is referred to here as a *light vehicle*:

- The sprung mass m_B of the vehicle is reduced to 500 kg,
- the new moment of inertia is given by $I_B \approx m_B l_r l_f$,
- the suspension stiffness is increased to $3.3 \times 10^4\,\mathrm{N\,m^{-1}}$ at the front and $2.5 \times 10^4\,\mathrm{N\,m^{-1}}$ at the rear and

[2]The question arises why only the spring forces were linearized and not also the piece-wise linear damper curve. In principle, this can also be done, but it is not straightforward to linearize the damping curve, since the gradients in the low-speed and high-speed stages are significantly different. Linearization would lead to completely different vehicle behavior.

Die approbierte gedruckte Originalversion dieser Diplomarbeit ist an der TU Wien Bibliothek verfügbar
The approved original version of this thesis is available in print at TU Wien Bibliothek.
TU Bibliothek Your knowledge hub WIEN

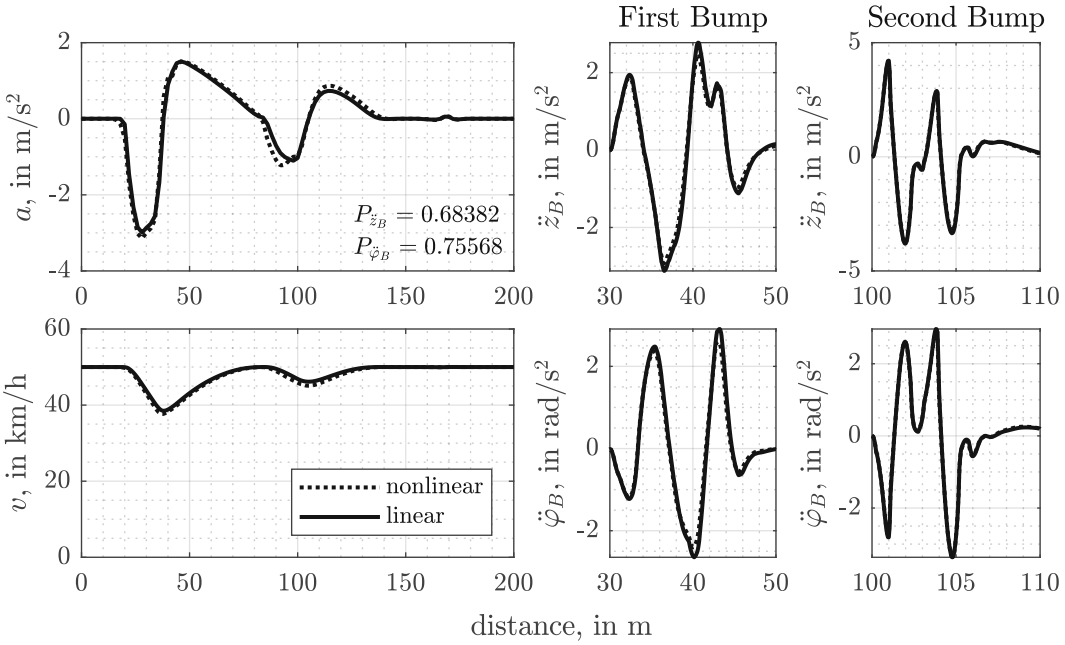

(a) Resonant Frequencies Bumps: The planned trajectories of the driver model with the linear internal vehicle model look very similar to the nonlinear one. In terms of performance indices $P_{\ddot{z}_B}$ and $P_{\ddot{\varphi}_B}$, the linear driver model performs slightly worse (compare indices from Fig. 5.1).

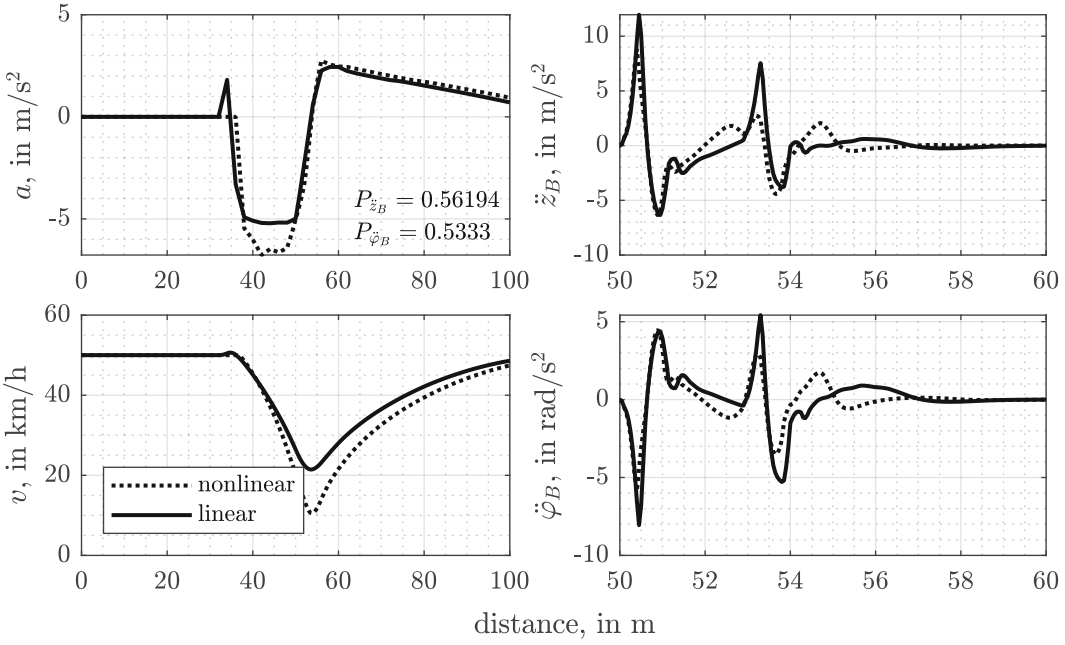

(b) Severe Bump: Here, the nonlinear version outperforms the linear one in the performance indices by a considerable amount (compare indices from Fig. 5.3). The nonlinear driver model decelerates down to the lower speed limit v_{min}, whereas the linear version does not.

Figure 5.10: Comparison of trajectories generated by the half-car driver with knowledge of nonlinearities (nonlinear, $\cdots$) and without (linear, -). Performance indices $P_{\ddot{z}_B}$ and $P_{\ddot{\varphi}_B}$ given for the linear model.

Die approbierte gedruckte Originalversion dieser Diplomarbeit ist an der TU Wien Bibliothek verfügbar
The approved original version of this thesis is available in print at TU Wien Bibliothek.
TU Bibliothek Your knowledge hub WIEN

- in the damper setup, the averaged low speed damping[3] D is increased to $4000\,\mathrm{N\,s\,m^{-1}}$ at the front axle and $3800\,\mathrm{N\,s\,m^{-1}}$ at the rear axle to obtain a stiffer chassis.

The wheel masses, tire parameters, geometric parameters of the half-car, and other parameters for suspension and damping settings are retained from the predecessor as specified in Tab. A.2.

It is investigated how the driver model behaves when the internal model is parameterized differently compared to the simulation model. In Fig. 5.11, the resonant frequency based cosine and the severe bump have been traversed. In one case, the driver's internal model is parameterized with the light vehicle data from above. In the other case, the internal model uses the heavier vehicle data, which is identical to the underlying simulation model.

Resonant Frequency Bumps Variations in the internal driver model can lead to significant changes in the planned trajectories as can be seen when traversing the middle/second bump of the frequency bump sequence. In case when the driver model assumes it's driving a light vehicle, it slows down the vehicle to lower speeds. In case of the driver with the internal heavy vehicle configuration, the driver does not brake as hard; this could be related to the fact that the increased vehicle mass reduces the amplitude of the vertical acceleration due to the increased inertia. When looking at the vertical and pitch acceleration plots below – shown are only the first and second bump – it's obvious that the the heavier driver model performs slightly better on the first bump. At the second bump it seems like that the lighter driver model performs better. One could think of this as a change in the vehicle model being similar to a change in weighting and therefore being more sensitive to the middle bump.

Severe Bump For the severe bump, only small differences in the planned longitudinal velocity and acceleration curves can be seen. This is most likely due to the severity of the bump and the preference to brake as close to the lower limit v_{min} as feasible. The differences in the vertical and pitch acceleration plots are most likely due to the maneuver around 50 m, where the light driver model brakes and accelerates quickly.

5.2.3 Vehicle with Additional Payload

In this section, a very similar case to the one above is considered, except that here the suspension is not modified, but the vehicle is given an additional load in form of an

[3] For explanation of the parameter D see Appx. A.1.

Die approbierte gedruckte Originalversion dieser Diplomarbeit ist an der TU Wien Bibliothek verfügbar
The approved original version of this thesis is available in print at TU Wien Bibliothek.
TU Bibliothek Your knowledge hub WIEN

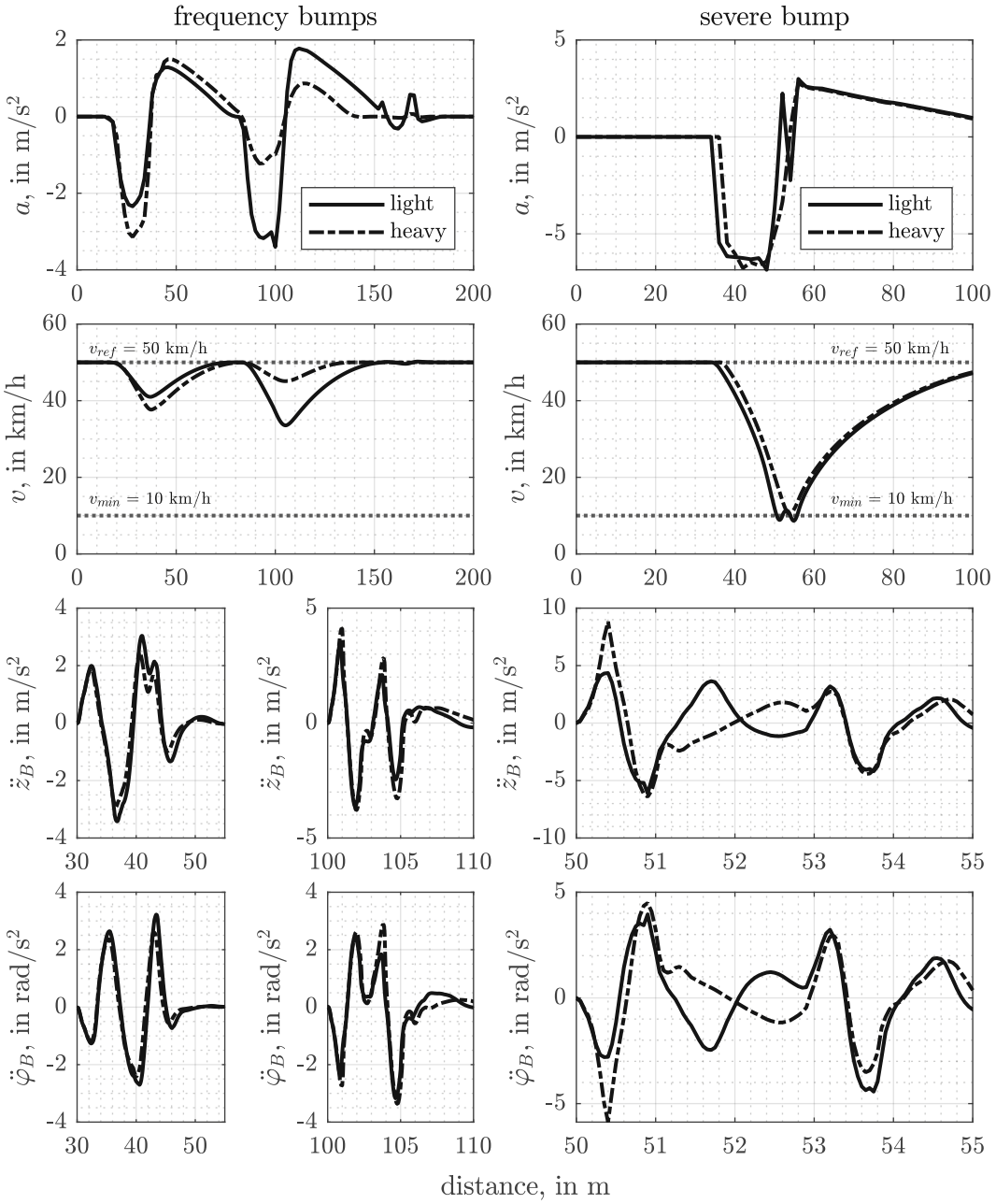

Figure 5.11: Comparison between driver models with either the light or heavy internal vehicle model: For each column, a case is compared in which both driver models pass through either the cosine bumps derived from the resonant frequencies or the severe bump. The simulation model calculates with the parameters from the heavy case.

Die approbierte gedruckte Originalversion dieser Diplomarbeit ist an der TU Wien Bibliothek verfügbar
The approved original version of this thesis is available in print at TU Wien Bibliothek.

increased sprung mass. The addition of a payload also results in a shift of the center of mass towards the rear axle which is captured by modifying the distances from rear and front to the center of mass. The following parameters from Tab. A.2 are modified:

- Sprung mass m_B is increased by 75 kg,
- distance l_r is set to $0.48 \cdot L$, distance l_f is set to $(1 - 0.48) \cdot L$, where L is the wheelbase, and
- the moment of inertia I_B is adjusted again with $I_B \approx m_B l_r l_f$.

Other parameters of the vehicle model remain unchanged, as do the cost function, the constraints, and the reaction time.

In Fig. 5.12, a similar behavior as in Fig. 5.11 is observed: Again, a heavier vehicle results in a smaller speed drop but only if the driver is aware of the additional payload. Without the knowledge of the additional load, the planned longitudinal acceleration trajectory takes a very similar shape to the nonlinear driver in Fig. 5.10a. The driver model cannot distinguish between a mass that is part of the vehicle and thus fixed, and an unsecured mass that could cause damage during heavy braking and acceleration maneuvers. This could be one aspect of improving the human driver model, for example, by retuning the weighting of the driver model's cost function in the presence of an unsecured mass to make crossing a road obstacle safer.

5.3 Modeling Different Driver Behaviors

Until now, the weighting parameters of the cost function in the driver model have never changed, and likewise, the same preview distance has always been presumed. By changing the weighting and thus shifting the driver's focus to either the speed or the comfort criterion, for example, a different behaving driver model can be created that either approaches the obstacle very conservatively or behaves aggressively just before and after the obstacle. In addition, the behavior of the driver and the effects on the developed trajectories can be studied at different preview distances, since a shorter or longer preview distance gives the driver model more or less time to react to the obstacle.

In Fig. 5.13 for the frequency bumps in the left column and for the severe bump in the right column, three different behaving driver models are exemplary simulated:

- A *basic* driver model that uses the already known cost function and weighting.
- A *conservative* driver model in which the preview distance l_{prev} is increased from 25 m to 35 m and the weighting of the comfort term Q_c is raised from 1.0 to 5.0.

Die approbierte gedruckte Originalversion dieser Diplomarbeit ist an der TU Wien Bibliothek verfügbar
The approved original version of this thesis is available in print at TU Wien Bibliothek.
TU Bibliothek Your knowledge hub WIEN

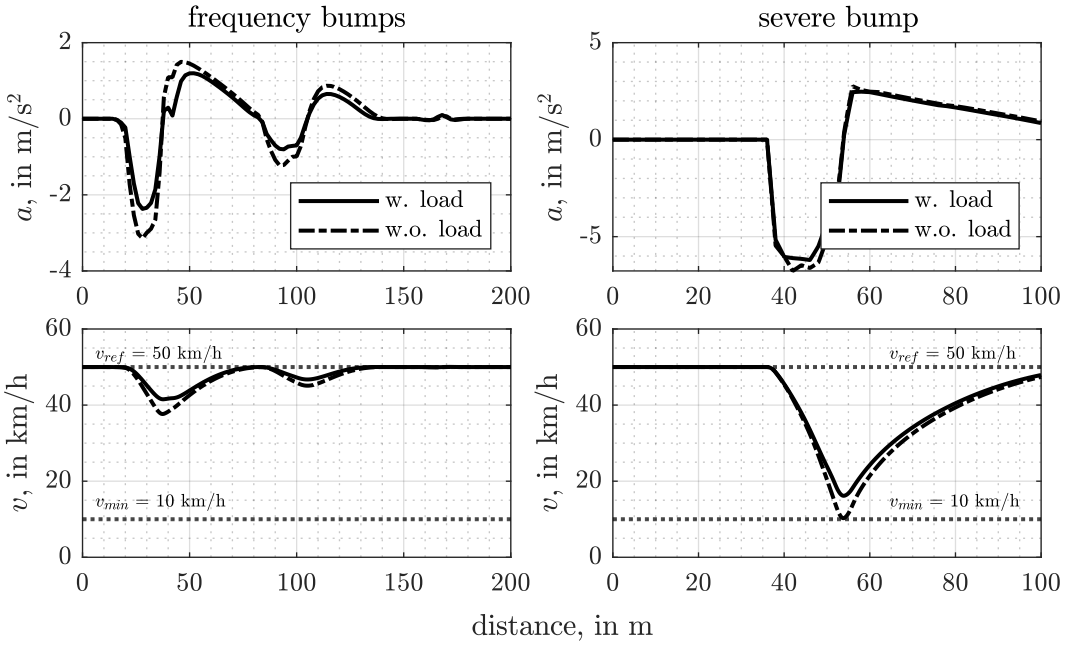

Figure 5.12: Comparison of the trajectories generated when the half-car driver drives over the frequency bumps and the severe bump. Compared cases: driver-model aware of the additional payload (w. load) and one where it is not (w.o. load).

- An *aggressive* driver model in which the preview distance is shortened to 20 m as well as the weight on the longitudinal Q_u and pitch acceleration Q_p is set to zero to focus on aggressive braking and acceleration.

It can be clearly observed that the aggressive driver brakes very late at the first obstacle in the left column and at the obstacle in the right column. The braking maneuver is stronger in terms of maximum deceleration. The driver is driving rather aggressively. Interestingly, at the middle/second bump in the left column, the aggressive driver opts for a small speed reduction and quickly passes the obstacle. However, this also corresponds to an aggressive driving style, as comfort is secondary for this driver model. In contrast, the conservative driver opts for a gentler braking maneuver over a longer time/distance. It is worth noting that the conservative driver model brakes the hardest on the second bump in the left column compared to the other drivers as a result of preferred driving comfort.

Die approbierte gedruckte Originalversion dieser Diplomarbeit ist an der TU Wien Bibliothek verfügbar
The approved original version of this thesis is available in print at TU Wien Bibliothek.
TU Bibliothek Your knowledge hub WIEN

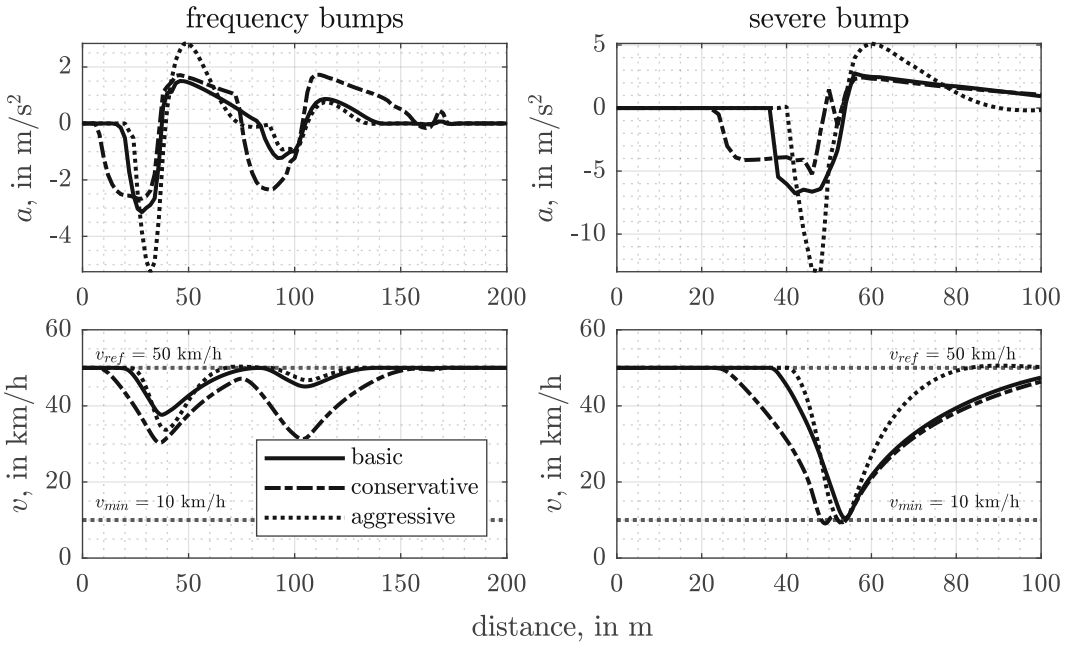

Figure 5.13: Comparison of different driver behaviors: By adjusting the weighting of the terms in the cost function and modifying the preview distance, different driver characteristics are obtained.

Die approbierte gedruckte Originalversion dieser Diplomarbeit ist an der TU Wien Bibliothek verfügbar
The approved original version of this thesis is available in print at TU Wien Bibliothek.
TU Bibliothek Your knowledge hub WIEN

6 Summary and Future Work

This work presented the development of a novel driver model which aims to represent the human driving behavior when crossing road obstacles with a vehicle. For this purpose, a MPC incorporating vertical and longitudinal vehicle dynamics was applied to generate human-like speed and acceleration trajectories on presented road obstacles.

6.1 Summary

The underlying internal representation of the vehicle dynamics plays a crucial role for the perception of comfort and further for the trajectory planning of vehicle speed and/or longitudinal acceleration profiles. Understanding how the vehicle behaves and reacts to obstacles on the road was the first step in creating a driver model. Thus, the first research question was how to use a versatile method from control theory, the model predictive controller, to create a driver model that can anticipate the impact of road obstacle and respond accordingly by adjusting the vehicle speed.

Research Question & Finding 1

How can human longitudinal vehicle control be modeled with a model predictive controller?

A mapping of the vehicle-road scenario is developed in Ch. 3 with two different vehicle models: A quarter-car and a half-car. The vehicle models presented are further developed in Sec. 4.2 for a constant preview distance to decouple the road excitation from the vehicle speed. Given this model, a MPC is designed in Sec. 4.1. The robustness and applicability of the different vehicle models as internal model of the driver model are validated in Ch. 5.

Anticipatory or predictive and feedback control are vital components of a driver model to respond to a given driving condition. An MPC was used to devise trajectories based on the developed vehicle models and a detailed cost function containing three important elements (vertical ride comfort, longitudinal comfort, vehicle forward speed) of a driver's

Die approbierte gedruckte Originalversion dieser Diplomarbeit ist an der TU Wien Bibliothek verfügbar
The approved original version of this thesis is available in print at TU Wien Bibliothek.
TU Bibliothek Your knowledge hub WIEN

decision process. Great importance is given to the shape of the generated trajectories as the behavior when traversing the bumps should be similar to those expected from a human driver. Therefore, the MPC cost function was exploited and its influence on the shape was analyzed. From this, the second research question stems and was addressed.

Research Question & Finding 2

How to determine suitable driving speed profiles from a human point of view for approaching, passing and departing different road obstacles (speed bumps, crosswalks, ...)?

Based on objective requirements defined in Sec. 4.1, a thorough and systematic study of how to design a cost function for the predictive controller is given in Sec. 4.4.1 for the quarter-car driver and in Sec. 4.4.2 for the half-car driver. This scalar function and the properties of the underlying vehicle are decisive for the resulting speed and acceleration profiles. In Sec. 4.1 it is shown how the behavior of the driver model can be influenced by the choice of the individual terms. The function was validated in Ch. 5 through various simulations.

From the literature review, it is known that a decent driver model should include some human properties like reaction times and driving styles. The last research question dealt with the driver's behavior during the formation of the trajectory.

Research Question & Finding 3

How can human properties such as dexterity, skill, driving style and reaction time be incorporated into the driver model?

In Sec. 4.1, the driver model has been enhanced to not react immediately to newly perceived road information in the planning horizon – reaction time has been added. In addition, the trajectory holding introduced in the same section can be used to constrain the planning capacity of the driver model such that the first trajectory selected is preferred and all subsequent trajectories should follow to some extent. To a certain degree, this allows for skill to be taken into account: A skilled driver will assess the obstacle first and then stick to the planned trajectory, while a novice driver will most likely adjust the course several times. In Sec. 5.3 it was shown that different driving styles can be represented by modifying weighting factors and/or different preview distances.

Die approbierte gedruckte Originalversion dieser Diplomarbeit ist an der TU Wien Bibliothek verfügbar
The approved original version of this thesis is available in print at TU Wien Bibliothek.
TU Bibliothek Your knowledge hub WIEN

6.2 Outlook

In the course of the elaboration, further questions have arisen. Thereof, possible directions for future work building on this thesis are derived:

- As shown in this thesis, the driver model is robust for low speeds, but has difficulties in dealing with high speeds. Two approaches towards a solution have been presented, but they are not entirely satisfactory. An improved cost function with respect to the comfort term could be considered.
- The question of computational effort was only briefly considered within this work (see Appx. B.2). For an application in the autonomous domain, the required computing time is of utmost interest.
- The degree of modeling in the vertical direction is more accurate than in the longitudinal direction. The model could be further developed by also taking the drive and brake dynamics into account.
- In this work, only road obstacles with symmetrical excitation of the vehicle were considered. Through this assumption, the vehicle model could be simplified. However, if real potholes need to be investigated, which only act in one road lane, this assumption no longer holds and a full vehicle would have to be applied.

Die approbierte gedruckte Originalversion dieser Diplomarbeit ist an der TU Wien Bibliothek verfügbar
The approved original version of this thesis is available in print at TU Wien Bibliothek.
TU Bibliothek Your knowledge hub WIEN

Bibliography

[1] World Health Organization, "Global status report on road safety 2018: Summary", Jun. 2018.

[2] CDC. (Dec. 14, 2020). "Road traffic injuries and deaths—a global problem", Centers for Disease Control and Prevention, [Online]. Available: https://www.cdc.gov/injury/features/global-road-safety/index.html (visited on 01/18/2021).

[3] European Commission. Directorate General for Mobility and Transport., *Road safety in the European Union: trends, statistics and main challenges, April 2018.* LU: Publications Office, 2018.

[4] F. Gustafsson, "Automotive safety systems", *IEEE Signal Processing Magazine*, vol. 26, no. 4, pp. 32–47, Jul. 2009, Conference Name: IEEE Signal Processing Magazine. DOI: 10.1109/MSP.2009.932618.

[5] A. Ziebinski, R. Cupek, H. Erdogan, and S. Waechter, "A survey of ADAS technologies for the future perspective of sensor fusion", in *Computational Collective Intelligence*, N. T. Nguyen, L. Iliadis, Y. Manolopoulos, and B. Trawiński, Eds., ser. Lecture Notes in Computer Science, Cham: Springer International Publishing, 2016, pp. 135–146. DOI: 10.1007/978-3-319-45246-3_13.

[6] European Commission. (Jun. 2020). "Road safety: Europe's roads are getting safer but progress remains too slow", European Commission - European Commission, [Online]. Available: https://ec.europa.eu/commission/presscorner/detail/en/IP_20_1003 (visited on 01/18/2021).

[7] European Transport Safety Council, *Prioritising the safety potential of automated driving in europe*, Apr. 2016.

[8] E. T. S. Council, *Ranking EU progress on road safety: 14th road safety performance index report*, Jun. 2020.

[9] SAE, *J3016c: Taxonomy and definitions for terms related to driving automation systems for on-road motor vehicles - SAE international*, Apr. 30, 2021.

Die approbierte gedruckte Originalversion dieser Diplomarbeit ist an der TU Wien Bibliothek verfügbar
The approved original version of this thesis is available in print at TU Wien Bibliothek.
TU Bibliothek Your knowledge hub WIEN

[10] S. Chen, M. Kuhn, K. Prettner, and D. E. Bloom, "The global macroeconomic burden of road injuries: Estimates and projections for 166 countries", *The Lancet Planetary Health*, vol. 3, no. 9, e390–e398, Sep. 1, 2019. DOI: 10.1016/S2542-5196(19)30170-6.

[11] P. A. M. Ruijten, J. M. B. Terken, and S. N. Chandramouli, "Enhancing trust in autonomous vehicles through intelligent user interfaces that mimic human behavior", *Multimodal Technologies and Interaction*, vol. 2, no. 4, p. 62, Dec. 2018, Publisher: Multidisciplinary Digital Publishing Institute. DOI: 10.3390/mti2040062.

[12] M. Plöchl and J. Edelmann, "Driver models in automobile dynamics application", *Vehicle System Dynamics*, vol. 45, no. 7, pp. 699–741, Jul. 2007. DOI: 10.1080/00423110701432482.

[13] J. Wu, H. Zhou, Z. Liu, and M. Gu, "Ride comfort optimization via speed planning and preview semi-active suspension control for autonomous vehicles on uneven roads", *IEEE Transactions on Vehicular Technology*, vol. 69, no. 8, pp. 8343–8355, Aug. 2020, Conference Name: IEEE Transactions on Vehicular Technology. DOI: 10.1109/TVT.2020.2996681.

[14] F. Walz and S. Hohmann, "Model predictive longitudinal motion control for low velocities on known road profiles", *Vehicle System Dynamics*, vol. 58, no. 8, pp. 1310–1328, Aug. 2, 2020, Taylor & Francis. DOI: 10.1080/00423114.2019.1618880.

[15] F. Klinger, "Kombinierte betrachtung passiver und (semi-)aktiver radaufhängungen mittels äquivalenter fahrwerksparameter", Ph.D. dissertation, Wien, 2018.

[16] C. Göhrle, A. Schindler, A. Wagner, and O. Sawodny, "Model predictive control of semi-active and active suspension systems with available road preview", in *2013 European Control Conference (ECC)*, Jul. 2013, pp. 1499–1504. DOI: 10.23919/ECC.2013.6669185.

[17] M. Čorić, J. Deur, J. Kasać, H. E. Tseng, and D. Hrovat, "Optimisation of active suspension control inputs for improved vehicle handling performance", *Vehicle System Dynamics*, vol. 54, no. 11, pp. 1574–1600, Nov. 1, 2016. DOI: 10.1080/00423114.2016.1222075.

[18] L. H. Csekő, M. Kvasnica, and B. Lantos, "Explicit MPC-based RBF neural network controller design with discrete-time actual kalman filter for semiactive suspension", *IEEE Transactions on Control Systems Technology*, vol. 23, no. 5, pp. 1736–

Die approbierte gedruckte Originalversion dieser Diplomarbeit ist an der TU Wien Bibliothek verfügbar
The approved original version of this thesis is available in print at TU Wien Bibliothek.
TU Bibliothek Your knowledge hub WIEN

1753, Sep. 2015, Conference Name: IEEE Transactions on Control Systems Technology. DOI: 10.1109/TCST.2014.2382571.

[19] E. Enders, G. Burkhard, and N. Munzinger, "Analysis of the influence of suspension actuator limitations on ride comfort in passenger cars using model predictive control", *Actuators*, vol. 9, no. 3, p. 77, Sep. 2020, Publisher: Multidisciplinary Digital Publishing Institute. DOI: 10.3390/act9030077.

[20] N. Giorgetti, A. Bemporad, H. E. Tseng, and D. Hrovat, "Hybrid model predictive control application towards optimal semi-active suspension", *International Journal of Control*, vol. 79, no. 5, pp. 521–533, May 1, 2006, Publisher: Taylor & Francis. DOI: 10.1080/00207170600593901.

[21] J. Theunissen, A. Sorniotti, P. Gruber, S. Fallah, M. Ricco, M. Kvasnica, and M. Dhaens, "Regionless explicit model predictive control of active suspension systems with preview", *IEEE Transactions on Industrial Electronics*, vol. 67, no. 6, pp. 4877–4888, Jun. 2020, Conference Name: IEEE Transactions on Industrial Electronics. DOI: 10.1109/TIE.2019.2926056.

[22] M. Nguyen, M. Canale, O. Sename, and L. Dugard, "A model predictive control approach for semi-active suspension control problem of a full car", in *2016 IEEE 55th Conference on Decision and Control (CDC)*, Dec. 2016, pp. 721–726. DOI: 10.1109/CDC.2016.7798353.

[23] M. Čorić, J. Deur, L. Xu, H. E. Tseng, and D. Hrovat, "Optimisation of active suspension control inputs for improved performance of active safety systems", *Vehicle System Dynamics*, vol. 56, no. 1, pp. 1–26, Jan. 2, 2018. DOI: 10.1080/00423114.2017.1340652.

[24] C. Göhrle, A. Wagner, A. Schindler, and O. Sawodny, "Active suspension controller using MPC based on a full-car model with preview information", in *2012 American Control Conference (ACC)*, ISSN: 2378-5861, Jun. 2012, pp. 497–502. DOI: 10.1109/ACC.2012.6314680.

[25] M. Čorić, J. Deur, L. Xu, H. E. Tseng, and D. Hrovat, "Optimisation of active suspension control inputs for improved vehicle ride performance", *Vehicle System Dynamics*, vol. 54, no. 7, pp. 1004–1030, Jul. 2, 2016. DOI: 10.1080/00423114.2016.1177655.

[26] R. S. Sharp and H. Peng, "Vehicle dynamics applications of optimal control theory", *Vehicle System Dynamics*, vol. 49, no. 7, pp. 1073–1111, Jul. 1, 2011, Publisher: Taylor & Francis. DOI: 10.1080/00423114.2011.586707.

Die approbierte gedruckte Originalversion dieser Diplomarbeit ist an der TU Wien Bibliothek verfügbar
The approved original version of this thesis is available in print at TU Wien Bibliothek.
TU Bibliothek Your knowledge hub WIEN

[27] D. A. Wilson, R. S. Sharp, and S. A. Hassan, "The application of linear optimal control theory to the design of active automotive suspensions", *Vehicle System Dynamics*, vol. 15, no. 2, pp. 105–118, Jan. 1, 1986, Publisher: Taylor & Francis. DOI: 10.1080/00423118608968846.

[28] Y. Hu, M. Z. Q. Chen, and Z. Hou, "Multiplexed model predictive control for active vehicle suspensions", *International Journal of Control*, vol. 88, no. 2, pp. 347–363, Feb. 1, 2015, Publisher: Taylor & Francis. DOI: 10.1080/00207179.2014.953589.

[29] R. S. Prabakar, C. Sujatha, and S. Narayanan, "Optimal semi-active preview control response of a half car vehicle model with magnetorheological damper", *Journal of Sound and Vibration*, vol. 326, no. 3, pp. 400–420, Oct. 9, 2009. DOI: 10.1016/j.jsv.2009.05.032.

[30] F. Yakub and Y. Mori, "Model predictive control for car vehicle dynamics system - comparative study", in *2013 IEEE Third International Conference on Information Science and Technology (ICIST)*, ISSN: 2164-4357, Mar. 2013, pp. 172–177. DOI: 10.1109/ICIST.2013.6747530.

[31] D. J. Cole, "Occupant–vehicle dynamics and the role of the internal model", *Vehicle System Dynamics*, vol. 56, no. 5, pp. 661–688, May 4, 2018, Publisher: Taylor & Francis. DOI: 10.1080/00423114.2017.1398342.

[32] M. Plöchl and P. Lugner, "A 3-level driver model and its application to driving simulations", *Vehicle System Dynamics*, vol. 33, pp. 71–82, sup1 Jan. 1, 1999, Publisher: Taylor & Francis. DOI: 10.1080/00423114.1999.12063071.

[33] I. I. Delice and S. Ertugrul, "Intelligent modeling of human driver: A survey", in *2007 IEEE Intelligent Vehicles Symposium*, ISSN: 1931-0587, Jun. 2007, pp. 648–651. DOI: 10.1109/IVS.2007.4290189.

[34] C. C. Macadam, "Understanding and modeling the human driver", *Vehicle System Dynamics*, vol. 40, no. 1, pp. 101–134, Aug. 1, 2003, Publisher: Taylor & Francis. DOI: 10.1076/vesd.40.1.101.15875.

[35] J. Edelmann, M. Plöchl, W. Reinalter, and W. Tieber, "A passenger car driver model for higher lateral accelerations", *Vehicle System Dynamics*, vol. 45, no. 12, pp. 1117–1129, Dec. 1, 2007, Publisher: Taylor & Francis. DOI: 10.1080/00423110701203644.

Die approbierte gedruckte Originalversion dieser Diplomarbeit ist an der TU Wien Bibliothek verfügbar
The approved original version of this thesis is available in print at TU Wien Bibliothek.
TU Bibliothek Your knowledge hub WIEN

[36] T. A. Johns and D. J. Cole, "Measurement and mathematical model of a driver's intermittent compensatory steering control", *Vehicle System Dynamics*, vol. 53, no. 12, pp. 1811–1829, Dec. 2, 2015, Publisher: Taylor & Francis. DOI: 10.1080/00423114.2015.1100748.

[37] E. Donges, "A two-level model of driver steering behavior", *Human Factors: The Journal of the Human Factors and Ergonomics Society*, vol. 20, no. 6, pp. 691–707, Dec. 1978. DOI: 10.1177/001872087802000607.

[38] C. J. Nash, D. J. Cole, and R. S. Bigler, "A review of human sensory dynamics for application to models of driver steering and speed control", *Biological Cybernetics*, vol. 110, no. 2, pp. 91–116, Jun. 1, 2016. DOI: 10.1007/s00422-016-0682-x.

[39] T. Glück, A. Kugi, and A. Steinböck, "Fortgeschrittene Methoden der nichtlinearen Regelung - Wintersemester 2020/2021", 2020.

[40] S. Jakubek, A. Schirrer, and O. König, "Adaptive and predictive control", TU Wien, Aug. 2019.

[41] A. Steinböck, "Optimierung", TU Wien, 2021.

[42] K. Murali Madhavan Rathai, "Synthesis and real-time implementation of parameterized NMPC schemes for automotive semi-active suspension systems", Issue: 2020GRALT052, Theses, Université Grenoble Alpes, Nov. 2020.

[43] MathWorks. (2021). "Constrained nonlinear optimization algorithms - MATLAB & simulink", Constrained Nonlinear Optimization Algorithms, [Online]. Available: https://de.mathworks.com/help/optim/ug/constrained-nonlinear-optimization-algorithms.html (visited on 02/12/2021).

[44] M. Mitschke and H. Wallentowitz, *Dynamik der Kraftfahrzeuge*, 5th ed., ser. VDI-Buch. Springer Vieweg, 2014. DOI: 10.1007/978-3-658-05068-9.

[45] R. N. Jazar, *Vehicle Dynamics: Theory and Application*, 2nd ed. New York: Springer-Verlag, 2014. DOI: 10.1007/978-1-4614-8544-5.

[46] Richter, *Schwerpunkte der Fahrzeugdynamik*. Verlag TÜV Reinland.

[47] F. Klinger, J. Edelmann, M. Plöchl, S. Jeindl, and B. Angrosch, "Virtual chassis tuning with emphasis on the damper characteristics – a method for optimal integrative damper adjustment by means of vertical and lateral dynamics simulation and evaluation criteria", in *6th International Munich Chassis Symposium 2015*, P. Pfeffer, Ed., ser. Proceedings, Wiesbaden: Springer Fachmedien, 2015, pp. 325–346. DOI: 10.1007/978-3-658-09711-0_22.

Die approbierte gedruckte Originalversion dieser Diplomarbeit ist an der TU Wien Bibliothek verfügbar
The approved original version of this thesis is available in print at TU Wien Bibliothek.
TU Bibliothek Your knowledge hub WIEN

[48] MathWorks. (2021). "Solve nonstiff differential equations — medium order method - MATLAB ode45 - MathWorks deutschland", [Online]. Available: https://de.mathworks.com/help/matlab/ref/ode45.html (visited on 04/19/2021).

[49] S. Jakubek, C. Hametner, and A. Schirrer, "Digital control", TU Wien, 2020.

[50] MathWorks. (2021). "Quadratic programming - MATLAB quadprog - MathWorks deutschland", [Online]. Available: https://de.mathworks.com/help/optim/ug/quadprog.html (visited on 06/06/2021).

[51] J. B. Rawlings, D. Q. Mayne, and M. M. Diehl, *Model Predictive Control: Theory, Computation, and Design*. Nob Hill Publishing, 2009.

Die approbierte gedruckte Originalversion dieser Diplomarbeit ist an der TU Wien Bibliothek verfügbar
The approved original version of this thesis is available in print at TU Wien Bibliothek.
TU Bibliothek Your knowledge hub WIEN

A Models

This chapter includes the parameters used – with exceptions mentioned in the thesis – for all simulations given. Further, for the half-car model, the jerk-model matrices are given as well as an estimated transfer function.

A.1 Quarter-Car: Parameters

parameter	*value*	*unit*	*description*
m_B	465.7	kg	sprung mass (car body)
m_W	50.4	kg	unsprung mass (car wheel)
c_T	500	$\mathrm{N\,s\,m^{-1}}$	tire damping coefficient
k_T	262 200	$\mathrm{N\,m^{-1}}$	tire stiffness
k_S	2.7922×10^4	$\mathrm{N\,m^{-1}}$	suspension stiffness; linear part
D	3530	$\mathrm{N\,s\,m^{-1}}$	averaged low speed damping
A	1/2	1	asymmetry parameter
s_d	0.25	1	degression factor rebound stage ($s_d < 1$)
s_z	0.40	1	degression factor compression stage ($s_z < 1$)
v_d	0.20	$\mathrm{m\,s^{-1}}$	transition velocity compression stage
v_z	0.20	$\mathrm{m\,s^{-1}}$	transition velocity rebound stage
$f_{1,cmp}$	1/3	1	nonlinear spring progression factor
$f_{2,cmp}$	4	1	curvature of progressive rise
$f_{1,rbd}$	1	1	nonlinear spring progression factor
$f_{2,rbd}$	8	1	curvature of progressive rise
Δz_{cmp}	0.02	m	clearance of progressive compression part
Δz_{rbd}	0.08	m	clearance of progressive rebound part
$F_{k_S,nlin,max}$	1×10^5	N	maximum nonlinear spring force

Table A.1: Parameters of the quarter-car model.

The damper model in this text uses slopes z_1, z_2, d_1, and d_2 for the low and high section of the damper. These can be calculated from the parameters in the table above by the following relationships:

- averaged low damper speed $D = \frac{d_1+z_1}{2}$ in $\mathrm{N\,s\,m^{-1}}$,

Die approbierte gedruckte Originalversion dieser Diplomarbeit ist an der TU Wien Bibliothek verfügbar
The approved original version of this thesis is available in print at TU Wien Bibliothek.
TU Bibliothek Your knowledge hub WIEN

- asymmetry parameter $A = \frac{d_1}{z_1}$,
- degrading factor for the compression stage $s_d = \frac{d_1}{d_2} < 1$ and
- degrading factor for the rebound stage $s_z = \frac{z_1}{z_2} < 1$.

A.2 Half-Car: Parameters

parameter	*value*	*unit*	*description*
m_B	803	kg	sprung mass (car body)
I_B	1430	$\mathrm{kg\,m^2}$	moment of inertia (car body)
h_T	0.600	m	acceleration force leverage
h_B	0.222	m	breaking force leverage
l_f	1.206	m	distance front contact point to CoM
l_r	1.664	m	distance rear contact point to CoM

parameter	*front value*	*rear value*	*unit*	*description*
$m_{W,i}$	50.4	50.4	kg	unsprung mass (car wheel)
$c_{T,i}$	262 200	262 200	$\mathrm{N\,s\,m^{-1}}$	tire damping coefficient
$k_{T,i}$	500	500	$\mathrm{N\,m^{-1}}$	tire stiffness
$k_{S,i}$	2.7915×10^4	2.0231×10^4	$\mathrm{N\,m^{-1}}$	suspension stiffness; linear part
D_i	3530	3515	$\mathrm{N\,s\,m^{-1}}$	averaged low speed damping
A_i	1/2	1/2	1	asymmetry parameter
$s_{d,i}$	0.25	0.25	1	degression factor cmp. stage ($s_{d,i} < 1$)
$s_{z,i}$	0.40	0.40	1	degression factor rbd. stage ($s_{z,i} < 1$)
$v_{d,i}$	0.20	0.20	1	transition velocity cmp. stage
$v_{z,i}$	0.20	0.20	1	transition velocity rbd. stage
$f_{1,cmp,i}$	1/3	1/3	1	nonlinear spring progression factor
$f_{2,cmp,i}$	4	4	1	curvature of progressive rise
$f_{1,rbd,i}$	1	1	1	nonlinear spring progression factor
$f_{2,rbd,i}$	8	8	1	curvature of progressive rise
$\Delta z_{cmp,i}$	0.02	0.02	m	clearance of prog. cmp. part
$\Delta z_{rbd,i}$	0.08	0.08	m	clearance of prog. rbd. part
$F_{k_S,nlin,max,i}$	1×10^5	1×10^5	N	maximum nonlinear spring force

Table A.2: Parameters of the half-car model. The index $i \in \{r, f\}$ indicates values for either the rear or front axle. The abbreviations *rbd.* and *cmp.* denote rebound and compression, respectively.

Die approbierte gedruckte Originalversion dieser Diplomarbeit ist an der TU Wien Bibliothek verfügbar
The approved original version of this thesis is available in print at TU Wien Bibliothek.
TU Bibliothek Your knowledge hub WIEN

A.3 Half-Car: Jerk-Model

System advanced by an additional integrator state and jerk defined as new input:

$$\mathbf{x}_h = \begin{bmatrix} x_{h,1} \\ x_{h,2} \\ x_{h,3} \\ x_{h,4} \\ x_{h,5} \\ x_{h,6} \\ x_{h,7} \\ x_{h,8} \\ x_{h,9} \\ x_{h,10} \end{bmatrix} = \begin{bmatrix} \zeta_r - z_{W,r} \\ \dot{z}_{W,r} \\ \zeta_f - z_{W,f} \\ \dot{z}_{W,f} \\ z_{W,r} - \varphi l_r - z_B \\ \dot{z}_B \\ z_{W,f} + \varphi l_f - z_B \\ \dot{\varphi} \\ v \\ a \end{bmatrix}, \quad \text{(A.1a)} \qquad \dot{\mathbf{x}}_h = \begin{bmatrix} \dot{\zeta}_r - x_{h,2} \\ \ddot{z}_{W,r} \\ \dot{\zeta}_f - x_{h,4} \\ \ddot{z}_{W,f} \\ x_{h,2} - x_{h,8} l_r - x_{h,6} \\ \ddot{z}_B \\ x_{h,4} + x_{h,8} l_f - x_{h,6} \\ \ddot{\varphi} \\ \dot{v} \\ \dot{a} \end{bmatrix}, \quad \text{(A.1c)}$$

$$u_h = r\,, \quad \text{(A.1b)} \qquad \mathbf{z}_h = \begin{bmatrix} \dot{\zeta}_r \\ \dot{\zeta}_f \end{bmatrix}. \quad \text{(A.1d)}$$

$$\mathbf{A}_{h,1} = \begin{bmatrix} 0 & -1 & 0 & 0 & 0 & 0 & 0 & 0 & 0 & 0 \\ \frac{k_{T,r}}{m_{W,r}} & -\frac{c_{T,r}}{m_{W,r}} & 0 & 0 & -\frac{k_{S,r}}{m_{W,r}} & 0 & 0 & 0 & 0 & 0 \\ 0 & 0 & 0 & -1 & 0 & 0 & 0 & 0 & 0 & 0 \\ 0 & 0 & \frac{k_{T,f}}{m_{W,f}} & -\frac{c_{T,f}}{m_{W,f}} & 0 & 0 & -\frac{k_{S,f}}{m_{W,f}} & 0 & 0 & 0 \\ 0 & 1 & 0 & 0 & 0 & -1 & 0 & -l_r & 0 & 0 \\ 0 & 0 & 0 & 0 & \frac{k_{S,r}}{m_B} & 0 & \frac{k_{S,f}}{m_B} & 0 & 0 & 0 \\ 0 & 0 & 0 & 1 & 0 & -1 & 0 & l_f & 0 & 0 \\ 0 & 0 & 0 & 0 & \frac{l_r k_{S,r}}{I_B} & 0 & -\frac{l_f k_{S,f}}{I_B} & 0 & 0 & 0 \\ 0 & 0 & 0 & 0 & 0 & 0 & 0 & 0 & 0 & 1 \\ 0 & 0 & 0 & 0 & 0 & 0 & 0 & 0 & 0 & 0 \end{bmatrix} \quad \text{(A.2)}$$

Die approbierte gedruckte Originalversion dieser Diplomarbeit ist an der TU Wien Bibliothek verfügbar
The approved original version of this thesis is available in print at TU Wien Bibliothek.
TU Bibliothek Your knowledge hub WIEN

$$\mathbf{B}_h = \begin{bmatrix} 0 \\ 0 \\ 0 \\ 0 \\ 0 \\ 0 \\ 0 \\ -\frac{m_B}{I_B} \\ 0 \\ 0 \end{bmatrix}, \tag{A.3a}$$

$$\mathbf{E}_h = \begin{bmatrix} 1 & 0 \\ \frac{c_{T,r}}{m_{T,r}} & 0 \\ 0 & 1 \\ 0 & \frac{c_{T,f}}{m_{W,f}} \\ 0 & 0 \\ 0 & 0 \\ 0 & 0 \\ 0 & 0 \\ 0 & 0 \\ 0 & 0 \end{bmatrix}, \tag{A.3b}$$

$$\mathbf{A}_{h,2} = \begin{bmatrix} 0 & 0 \\ -\frac{1}{m_{W,r}} & 0 \\ 0 & 0 \\ 0 & -\frac{1}{m_{W,f}} \\ 0 & 0 \\ \frac{1}{m_B} & \frac{1}{m_B} \\ 0 & 0 \\ \frac{l_r}{I_B} & -\frac{l_f}{I_B} \\ 0 & 0 \end{bmatrix} \tag{A.3c}$$

A.4 Half-Car: Transfer Function Estimate

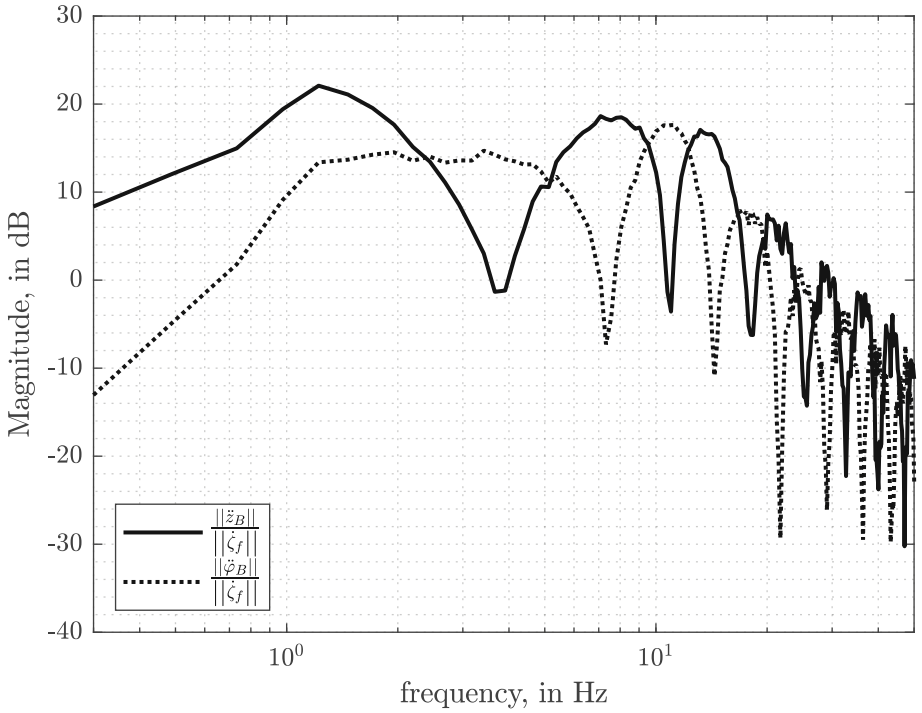

Figure A.1: Half-car transfer function estimated at $v = 75\,\mathrm{km/h}$ derived from a stochastic road excitation.

Die approbierte gedruckte Originalversion dieser Diplomarbeit ist an der TU Wien Bibliothek verfügbar
The approved original version of this thesis is available in print at TU Wien Bibliothek.

B Model Predictive Control

The idea of this chapter is to give a rough understanding of how a model predictive control (MPC) works by looking at a simple linear example. A second section of this text deals with the computational effort for the novel MPC presented in this paper. The last section contains the algorithms to compute the shift index d for the reaction time in the novel driver model.

B.1 Reference Velocity Tracking: Linear Example

This small example should only be a short introduction to how MPC works. Imagine the following tracking problem: A vehicle is to follow a reference speed trajectory. Calculate the optimal traction force required to achieve this in an optimal way.

For the vehicle model, a simplified point mass model is assumed:

$$\underbrace{\begin{bmatrix}\dot{s}\\ \dot{v}\end{bmatrix}}_{\dot{\mathbf{x}}} = \underbrace{\begin{bmatrix}0 & 1\\ 0 & 0\end{bmatrix}}_{\mathbf{A}}\underbrace{\begin{bmatrix}s\\ v\end{bmatrix}}_{x} + \underbrace{\begin{bmatrix}0\\ \frac{1}{m}\end{bmatrix}}_{\mathbf{B}}\underbrace{F}_{u}, \tag{B.1}$$

$$y = \underbrace{\begin{bmatrix}0 & 1\end{bmatrix}}_{\mathbf{C}} x\,, \tag{B.2}$$

where m is the vehicle mass, s is the distance traveled and v is the speed of the vehicle. The input u is the driving force F.

This system can be discretized exactly to obtain a difference equation of the fashion:

$$\mathbf{x}_{k+1} = \mathbf{A}_d x_k + \mathbf{B}_d u_k\,, \tag{B.3}$$

$$y_k = \mathbf{C} x_k\,, \tag{B.4}$$

where the zero-order-hold assumption for the input was used. The optimal control

Die approbierte gedruckte Originalversion dieser Diplomarbeit ist an der TU Wien Bibliothek verfügbar
The approved original version of this thesis is available in print at TU Wien Bibliothek.
TU Bibliothek Your knowledge hub WIEN

problem is given as:

$$\tilde{\mathbf{U}}_k^* = \arg\min_{\tilde{\mathbf{U}}_k} \quad J_k = \sum_{n=1}^{N_p} (y_{ref,k} - \tilde{y}_{k|n}) Q (y_{ref,k} - \tilde{y}_{k|n}) + \sum_{n=0}^{N_p-1} \tilde{u}_{k|n} R \tilde{u}_{k|n} \tag{B.5a}$$

$$\text{s.t.} \quad \tilde{\mathbf{x}}_{k|n+1} = \mathbf{A}_d \tilde{\mathbf{x}}_{k|n} + \mathbf{B}_d \tilde{u}_{k|n} \,, \quad \tilde{\mathbf{x}}_{k|0} = \mathbf{x}_k \,, \tag{B.5b}$$

$$\tilde{y}_{k|n} = \mathbf{C} \tilde{\mathbf{x}}_{k|n} \,, \tag{B.5c}$$

$$\tilde{\mathbf{x}}_{k|n} \in \mathcal{X} \,, \quad \tilde{u}_{k|n} \in \mathcal{U} \,, \quad \forall n = 0, 1, \ldots, N_p - 1 \tag{B.5d}$$

where $y_{ref,k} \in \mathbb{R}$ is the reference velocity, the output weight $Q \in \mathbb{R}$ and the input weight $R \in \mathbb{R}$. This problem is a quadratic-programming (QP) problem which is convex and can be further simplified by inserting the linear constraint into the cost function. By looking at the evolution over the prediction horizon:

$$\tilde{y}_{k|1} = \mathbf{C} \tilde{\mathbf{x}}_{k|1} = \mathbf{C}\mathbf{A}_d \tilde{\mathbf{x}}_{k|0} + \mathbf{C}\mathbf{B}_d \tilde{u}_{k|0} \,, \tag{B.6a}$$

$$\tilde{y}_{k|2} = \mathbf{C} \tilde{\mathbf{x}}_{k|2} = \mathbf{C}\mathbf{A}_d \tilde{\mathbf{x}}_{k|1} + \mathbf{C}\mathbf{B}_d \tilde{u}_{k|0} = \mathbf{C}\mathbf{A}_d^2 \tilde{\mathbf{x}}_{k|0} + \mathbf{C}\mathbf{A}_d\mathbf{B}_d \tilde{u}_{k|1} + \mathbf{C}\mathbf{B}_d \tilde{u}_{k|0} \,, \tag{B.6b}$$

$$\tilde{y}_{k|3} = \mathbf{C} \tilde{\mathbf{x}}_{k|3} = \mathbf{C}\mathbf{A}_d^3 \tilde{\mathbf{x}}_{k|0} + \mathbf{C}\mathbf{A}_d^2\mathbf{B}_d \tilde{u}_{k|2} + \mathbf{C}\mathbf{A}_d\mathbf{B}_d \tilde{u}_{k|1} + \mathbf{C}\mathbf{B}_d \tilde{u}_{k|0} \,, \tag{B.6c}$$

$$\vdots$$

$$\tilde{y}_{k|N_p} = \mathbf{C} \tilde{\mathbf{x}}_{k|N_p} = \mathbf{C}\mathbf{A}_d^{N_p} \tilde{\mathbf{x}}_{k|0} + \mathbf{C}\mathbf{A}_d^{N_p-1} \mathbf{B}_d \tilde{u}_{k|N_p-1} + \ldots + \mathbf{C}\mathbf{A}_d^0 \mathbf{B}_d \tilde{u}_{k|0} \,, \tag{B.6d}$$

which can be further simplified in matrix form:

$$\underbrace{\begin{bmatrix} \tilde{y}_{k|1} \\ \tilde{y}_{k|2} \\ \tilde{y}_{k|3} \\ \vdots \\ \tilde{y}_{k|N_p} \end{bmatrix}}_{\tilde{\mathbf{Y}}_k} = \underbrace{\begin{bmatrix} \mathbf{C}\mathbf{A}_d \\ \mathbf{C}\mathbf{A}_d^2 \\ \mathbf{C}\mathbf{A}_d^3 \\ \vdots \\ \mathbf{C}\mathbf{A}_d^{N_p} \end{bmatrix}}_{\mathbf{F}} \tilde{\mathbf{x}}_{k|0} + \underbrace{\begin{bmatrix} \mathbf{C}\mathbf{B}_d & \mathbf{0} & \mathbf{0} & \ldots & \mathbf{0} \\ \mathbf{C}\mathbf{A}_d\mathbf{B}_d & \mathbf{C}\mathbf{B}_d & \mathbf{0} & \ldots & \mathbf{0} \\ \mathbf{C}\mathbf{A}_d^2\mathbf{B}_d & \mathbf{C}\mathbf{A}_d\mathbf{B}_d & \mathbf{C}\mathbf{B}_d & \ldots & \mathbf{0} \\ \vdots & & & & \\ \mathbf{C}\mathbf{A}_d^{N_p-1}\mathbf{B}_d & \mathbf{C}\mathbf{A}_d^{N_p-2}\mathbf{B}_d & \mathbf{C}\mathbf{A}_d^{N_p-3}\mathbf{B}_d & \ldots & \mathbf{C}\mathbf{B}_d \end{bmatrix}}_{\mathbf{\Phi}} \underbrace{\begin{bmatrix} \tilde{u}_{k|0} \\ \tilde{u}_{k|1} \\ \tilde{u}_{k|2} \\ \vdots \\ \tilde{u}_{k|N_p-1} \end{bmatrix}}_{\tilde{\mathbf{U}}_k} . \tag{B.7}$$

The cost function J_k can then be given as:

$$J = (\mathbf{Y}_k - \mathbf{Y}_{ref,k})^T \mathbf{Q} (\mathbf{Y}_k - \mathbf{Y}_{ref,k}) + \tilde{\mathbf{U}}_k^T \mathbf{R} \tilde{\mathbf{U}}_k \,. \tag{B.8}$$

The optimization problem can now be solved analytically for the case of no constraints by substituting the prediction equation (B.7) into the cost function and solving for the minimum:

$$\tilde{\mathbf{U}}_k^* = \left(\mathbf{\Phi}^T \mathbf{Q} \mathbf{\Phi} + \mathbf{R} \right)^{-1} \mathbf{\Phi}^T \mathbf{Q} (\mathbf{Y}_{ref,k} - \mathbf{F}\mathbf{x}_k) \,. \tag{B.9}$$

Die approbierte gedruckte Originalversion dieser Diplomarbeit ist an der TU Wien Bibliothek verfügbar
The approved original version of this thesis is available in print at TU Wien Bibliothek.
TU Bibliothek Your knowledge hub WIEN

If constraints are involved, the optimal control sequence $\tilde{\mathbf{U}}_k^*$ is obtained by a QP-solver e.g. QUADPROG [50]. Therefore, the hessian $\mathbf{H}$ and the gradient $\mathbf{f}_k$ are defined:

$$\mathbf{H} = 2\left(\mathbf{\Phi}^T\mathbf{Q}\mathbf{\Phi} + \mathbf{R}\right) , \tag{B.10}$$

$$\mathbf{f}_k = 2\mathbf{\Phi}^T\mathbf{Q}\left(\mathbf{F}\mathbf{x}_k - \mathbf{Y}_{ref,k}\right) . \tag{B.11}$$

Finally, let's compare the solution of an unconstrained case with one where the input drive force form (B.1) is constraint to a maximum of 200 N in Fig. B.1.

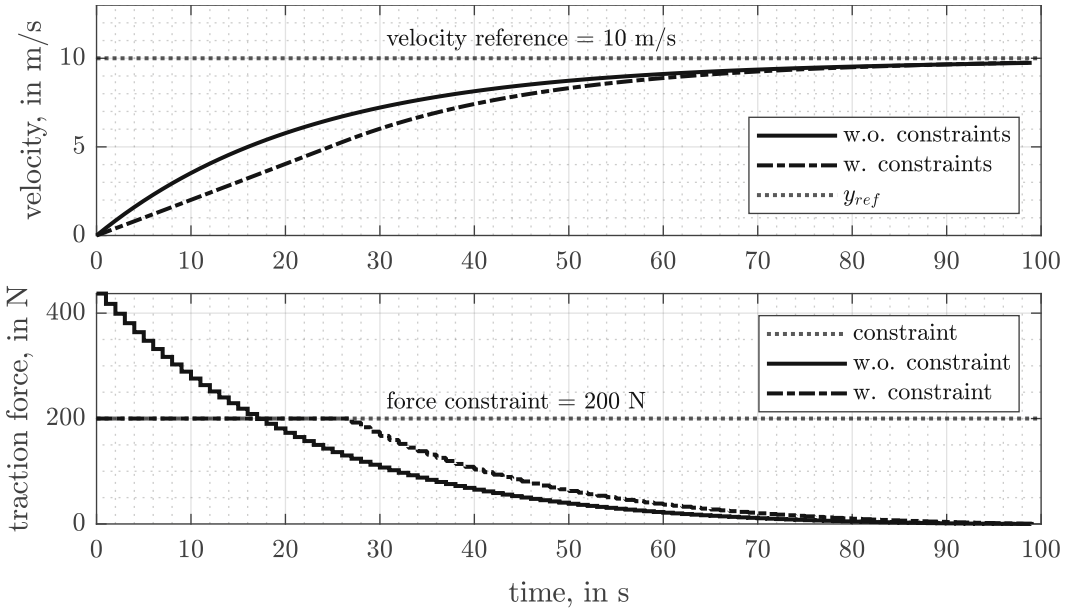

Figure B.1: Velocity reference tracking comparing a solution with constraints and one without. Through the variation of the weights Q and R the behavior of the MPC can be tuned. Higher Q would yield a faster response time but violate the constraints further in the unconstrained case as well. Higher R reduces the magnitude of the input force. $T_s = 1\,\text{s}$, $N_p = 100$, $m = 1000\,\text{kg}$, $R = 1/10$, $Q = 200$.

For more information, I recommend to look at [39]–[41], [51].

B.2 Computational Cost of the Novel Driver Model

In this section, a brief overview of the calculation costs for the novel MPC is given in tabular form. It should be noted that the cost strongly depends on the length of the prediction horizon as well as the number of control interventions in this horizon.

Die approbierte gedruckte Originalversion dieser Diplomarbeit ist an der TU Wien Bibliothek verfügbar
The approved original version of this thesis is available in print at TU Wien Bibliothek.
TU Bibliothek Your knowledge hub WIEN

Therefore, reducing l_{prev}, while helpful in reducing the computation time, also reduces the ability of the driver model to react earlier to the road disturbance. For the case shown in Fig. 5.1, the following averaged computation times are achievable:

driver model	*Gradient Approximation* [43]	*Reduced Gradient Method* [41]
quarter-car	0.2549 s	0.1090 s
half-car	0.7436 s	-

Table B.1: With the solver MATLAB provided by FMINCON with its standard gradient approximation method, the computation times shown in the second column are achievable. By providing the gradient by the Reduced Gradient Method as described in [41] to the solver, the computation times shown in the third column are achievable. The controller was called every 2 m on a path with a total length of 200 m, resulting in 100 controller calls.

B.3 Reaction Time Algorithms

Algorithm 1 Example of the calculation of d for the quarter-car in case 1

Input: $\mathbf{U}_k = [u_0, u_1, \dots u_{k-1}]^T$, $\mathbf{x}_0$, Δl_p, t_r ▷ $\mathbf{U}_k \in \mathbb{R}^k$ applied inputs up to index k
Output: d ▷ Returns d according to Eq. (4.25)

```
v ← x_{5,0}
T ← zeros(k + 1, 1)
for i ← 0 to k − 1 do
    if u_i = 0 then
        T_{i+1} ← T_i + Δl_p/sqrt(v^2)
    else
        T_{i+1} ← T_i + (sqrt(v^2 + 2Δl_p u_i) − sqrt(v^2)) /u_i
    end if
    v ← sqrt(v^2 + 2Δl_p u_i)
end for
t_previous ← interp1(T, T, T_k − t_r, previous)
i_previous ← min(abs(T − t_previous))
return d = k − i_previous
```


Die approbierte gedruckte Originalversion dieser Diplomarbeit ist an der TU Wien Bibliothek verfügbar
The approved original version of this thesis is available in print at TU Wien Bibliothek.
TU Bibliothek Your knowledge hub WIEN

Algorithm 2 Example of the calculation of d for the quarter-car in case 2

Input: $\tilde{\mathbf{U}}^*_{k-1} = \begin{bmatrix} \tilde{u}^*_{k-1|0} & \tilde{u}^*_{k-1|1} & \dots & \tilde{u}^*_{k-1|N_p-1} \end{bmatrix}^T$, $\mathbf{x}_k$, Δl_p, t_r
Output: d ▷ Returns the d according to Eq. (4.26)

$v \leftarrow x_{5,k}$
$\mathbf{T} \leftarrow \text{zeros}(N_p, 1)$
for $i \leftarrow 1$ to $N_p - 1$ **do**
  if $\tilde{u}^*_{k-1|i} = 0$ **then**
    $T_i \leftarrow T_{i-1} + \Delta l_p / \text{sqrt}(v^2)$
  else
    $T_i \leftarrow T_{i-1} + \left(\text{sqrt}(v^2 + 2\Delta l_p \tilde{u}^*_{k-1|i}) - \text{sqrt}(v^2) \right) / \tilde{u}^*_{k-1|i}$
  end if
  $v \leftarrow \text{sqrt}(v^2 + 2\Delta l_p \tilde{u}^*_{k-1|i})$
end for
$t_{\text{next}} \leftarrow \text{interp1}(\mathbf{T}, \mathbf{T}, T_0 + t_r, \text{next})$
$i_{\text{next}} \leftarrow \min(\text{abs}(\mathbf{T} - t_{\text{next}}))$
return $d = k - i_{\text{next}}$

Die approbierte gedruckte Originalversion dieser Diplomarbeit ist an der TU Wien Bibliothek verfügbar
The approved original version of this thesis is available in print at TU Wien Bibliothek.
TU Bibliothek Your knowledge hub WIEN